
# The Development of a Pipeline for the Analysis of Polymeric Nanoparticle Interactions with Protein-Containing Media

**Karim Daramy**

Strathclyde Institute of Pharmacy and Biomedical Sciences

University of Strathclyde

Glasgow, UK

A thesis presented in fulfilment of the requirements for the degree of Doctor of Philosophy.

June 2024

**Declaration**

This thesis is the result of the author's original research. It has been composed by the author and has not been previously submitted for examination which has led to the award of a degree.

The copyright of this thesis belongs to the author under the terms of the United Kingdom Copyright Acts as qualified by University of Strathclyde Regulation 3.50. Due acknowledgement must always be made of the use of any material contained in, or derived from, this thesis.

This thesis was written by the author using original research conducted by author in between 1st October 2020 until 31st March 2024. This thesis hasn't been previously submitted for examination or led to an award.

Signed:

Date: 3rd June 2024

**Acknowledgements**

Funding from the Engineering and Physical Sciences Research Council (EPSRC) Doctoral Training Partnership is acknowledged, which supported this studentship. I would also like to extend my thanks to Malvern Panalytical for allowing me to beta test their Nanosight Pro technology for my project, and PostNova Analytics for supporting method optimisation.

I would also like to thank my supervisors Dr Zahra Rattray and Prof Yvonne Perrie for their continued support throughout my PhD studies. My thanks also go to Dr Yiwen Pei and Dr Caterina Minelli of the National Physical Laboratory as my supervisory team for their guidance and support throughout my studies, and the National Physical Laboratory for including me in the Postgraduate Institute (PGI).

I would like to thank my supervisor Dr Zahra in particular for her guidance, and wisdom over my studies. Your mentorship, kindness, and constant encouragement over the years have made this journey very special and have given me a strong foundation for the future within science and life.

Special thanks to the Rattray Translational Pharmaceutics lab, particularly to Panida Punnabhum for her support in accessing the EPSRC multiscale metrology suite for optimizing and method development on the field flow fractionation setup.

I wanted to also acknowledge and thank my all my colleagues within the Rattray lab for playing an important part of my academic journey and for all the important lessons, and cherished memories. Particularly Abdullah for his constant friendship over the years, Layla for her kindness, and Domenica for her support.

I wanted to thank my parents Olivier, and Hania for their encouragement and constant support over the years and my younger sisters Nour for our constant chats, and Yara who also started her own scientific journey.

## COVID-19 Impact Statement

I started my PhD in October 2020, which was during restricted accessibility to the laboratories. This delayed the start of my training and laboratory studies within the first year of my PhD studies, limiting the amount of laboratory-based research activities I could carry out during this period. This meant that I was unable to optimise the laboratory work associated with the latter two chapters of the thesis within the timeframe of my PhD studies to the best.

**Abstract**

Nanoparticles are increasingly implemented in biomedical applications, including the diagnosis and treatment of disease. When exposed to complex biological media, nanoparticles spontaneously interact with their surrounding environment, leading to the surface-adsorption of small and bio-macromolecules- termed the “corona”. Corona composition is governed by nanoparticle properties and incubation parameters. While the focus of most studies examining nanoparticle interactions with biological systems is on the protein signature of the nanoparticle corona, the impact of experimental protocols on nanoparticle size in the presence of complex biological media, and the impact of nanoparticle recovery from biological media remains under reported in the literature.

Therefore, the principal hypothesis of this thesis is that the methods used to isolate nanoparticles during the screening of bio-nano interactions in biological media, can significantly alter the results obtained from these studies. To further probe this hypothesis, in this thesis polystyrene latex nanoparticles were used as a robust and non-biodegradable model to investigate the impact of different nanoparticle isolation pipelines on subsequent nanoparticle physical parameters. To validate this hypothesis, I examined the routinely implemented pipeline for nanoparticle isolation, which is the centrifugation-resuspension protocol for nanoparticle isolation from biological media.

In Chapter 2 [1] , I showed that the commonly used centrifugation-wash protocol leads to a significant increase in the mean particle size, of nanoparticle-protein samples when compared with *in-situ* samples analysed using Particle Tracking Analysis. This is likely due to protein aggregation, and particle agglomeration caused by high-speed centrifugation. The centrifugation-wash protocol was typically accompanied by a significant decrease in sample concentration. Furthermore, nanomedicines are typically intended for intravenous administration (IV). Therefore, it was crucial to understand the impact of physiologically-relevant shear flow conditions on protein corona formation. Results showed that there were significant differences in measured parameters following incubation at shear flow rates which mimicked the

median cubital vein, and arteries compared to static incubation conditions with SDS-PAGE analysis further showing changes in protein corona composition.

Subsequently, I explored the use of asymmetric flow field flow fractionation multiplexed with a range of multiple inline optical inline detectors (AF4-MD) to optimise the separation of model polystyrene latex nanoparticles from bulk incubation protein media, following exposure to physiologically-relevant temperature conditions and protein composition mimicking cell culture conditions. I studied the impact of AF4 flow parameters and decay profiles on the quality of fractogram obtained and applied these design principles to the analysis of polystyrene latex nanoparticles exposed to media containing 10% vol FBS for 2 and 24 hours (Chapter 3).

Results from this chapter indicate that AF-MD offers a potential promising tool for both the separation of nanoparticles from the bulk protein content in the media, and inline analysis of physical changes occurring in nanoparticle systems following exposure to biological media. An added benefit of using AF4-MD as a technique for studying nano-bio interactions is that it is possible to simultaneously study the physical properties of different intermediates formed during the sample elution step. There is also the scope for downstream recovery of pooled fractions collected from different elution peaks for offline analysis using other techniques such as liquid chromatography-mass spectrometry-based proteomics analysis of the nanoparticle protein corona composition. In Chapter 3, I also found that through combining inline multiangle light scattering with dynamic light scattering measurements, the shape factor can be determined for particles- an indicator of nanoparticle morphology. Peaks eluting at later timepoints were found to have altered morphology from a spherical shape to more extended elongated shapes following incubation with protein-containing media, with the extent being more pronounced for samples incubated for up to 24 hours.

Findings from chapter 3 overall showed that frit-inlet based AF4 was more appropriate for the resolution and analysis of nanoparticle-protein corona complexes and the signal quality was consistently low across all three polystyrene latex nanoparticle types studied. Therefore, the use of additional

AF4 based methodologies based on charge separation was explored in later chapters to examine whether better efficiency of resolution and mass recovery could be achieved.

In chapter 4, I further explored the utility of simultaneous diffusion and charge-based separation through the implementation of electric flow-field flow fractionation (EAF4) multiplexed with online light scattering, UV and fluorescence detectors. In addition to simultaneous separation and online analysis *via* multiple detectors, I demonstrate the resolution of different charged species in response to incubation with protein-containing media, where I also compared the different approaches used in this thesis in terms of their ability to resolve nanoparticle from complex biological media use to screen nano-bio interactions in drug discovery efforts. EAF4 demonstrated more significant promise for the resolution of nanoparticles from bulk protein content in comparison to conventional and frit-inlet AF4, and the simultaneous inline analysis of nanoparticle-protein complex surface electrostatic properties (zeta potential) and changes occurring in particle size and geometry (shape factor) in response to incubation with media containing protein.

Overall, this thesis has examined the current state of the art in the separation and physical analysis of nanoparticles from biological media. For future efforts, I recommend that pipelines studying bio-nano interactions during early nanomedicine development consider more biologically relevant shear flow conditions and media composition that can significantly alter nanoparticle physical parameters and subsequent conclusions from these studies. Moreover, in this thesis I demonstrate the need for case-by-case optimisation of AF4 based protocols, an area which at the time of this thesis remains underreported in the literature.

## Research Outputs

### Publications

**Daramy, K.**, P. Punnabhum, M. Hussain, C. Minelli, Y. Pei, N. J. W. Rattray, Y. Perrie and Z. Rattray (2023). "Nanoparticle Isolation from Biological Media for Protein Corona Analysis: The Impact of Incubation and Recovery Protocols on Nanoparticle Properties." Journal of Pharmaceutical Sciences, https://doi.org/10.1016/j.xphs.2023.12.021.

### Pre-prints

Cunningham, M. R., Rattray, N.J.W, McFadden, Y., Berardi, D., **Daramy, K.**, Kelly, P.E., Galbraith, A., Lochiel, I., Mills, L., Scott, Y., Chalmers, S., Lannigan, A., and Rattray, Z. (2023). "A roadmap for patient-public involvement and engagement (PPIE): Recounting the untold stories of breast cancer patient experiences." medRxiv: 2023.2006.2019.23291192.

### Conference contributions

### Oral presentations

**Daramy, K.**, Pei, Y., Minelli, C., Perrie, Y. & Rattray, Z., (2023) “Investigating the Impact of Shear Flow on Nanoparticle-Protein Interactions.” SciX 2023, Reno, Sparks, Nevada, October 2023.

**Daramy, K.**, Walker, J., Pei, Y., Minelli, C., Perrie, Y. & Rattray, Z., (2022) “Investigating the Impact of Shear Flow on Nanoparticle-Protein Interactions.”, British Journal of Pharmacy 7(2). doi: https://doi.org/10.5920/bjpharm.1131. Academy of Pharmaceutical Sciences 2022 Pharm Sci Conference, Belfast, UK, September 2022.

### Poster presentations

**Daramy, K.**, Punnabhum, P., Perrie, Y., Rattray, Z. “The Development of an AF4 Characterization Pipeline for Polymeric Nanoparticle-Protein Interactions.” British Journal of Pharmacy. 2023. https://doi.org/10.5920/bjpharm.1367. Academy of Pharmaceutical Sciences 2023 Pharm Sci Conference, University of Reading, Reading UK, September 2023.

**Daramy, K.**, Punnabhum, P., Perrie, Y., Rattray, Z. “The development of a novel pipeline for polymeric nanoparticle characterization following incubation under shear flow conditions.” 2023. National Physical Laboratory Postgraduate Institute Conference: Postgraduate Institute for Measurement Science Symposium, University of Strathclyde, Glasgow, UK, June 2023. (**Runner up poster prize winner**)

**Daramy, K.**, Perrie, Y., Rattray, Z. “Understanding protein corona formation under shear flow conditions”. 2022. JPAG Pharmaceutical Analysis Research Awards and Careers Fair 2022, Royal Society of Chemistry, London, UK, November 2022.

**Daramy, K.**, Punnabhum, P., Walker, J., Bindhu Syammohan, S., Rattray, Z. “The application of field-flow fractionation to the analysis of nanomedicines.” British Journal of Pharmacy 7(2). doi: https://doi.org/10.5920/bjpharm.1132. Academy of Pharmaceutical Sciences 2022 Pharm Sci Conference, Belfast, UK, September 2022.

**Daramy, K.**, Minelli, C., Perrie, Y., Rattray, Z. “Characterization of polymeric nanoparticle-protein interactions.” JPAG Pharmaceutical Analysis Research Awards and Careers Fair 2021, virtual event, November 2021. (**Runner up poster prize**)

**Daramy, K.**, Minelli, C., Perrie, Y., Rattray, Z. “Characterization of polymeric nanoparticle-protein interactions.” American Academy of Pharmaceutical Sciences Annual Pharm Sci Conference 2021, virtual event, October 2021.

**Table of Contents**

**List of Figures**

**List of Tables**

## List of Abbreviations

| | |
|---|---|
| AF4 | Asymmetric Flow Field Flow Fractionation |
| AF4-MD | Asymmetric Flow Field Flow Fractionation-Multi Detector |
| BCA | Bicinchoninic Acid Assay |
| CD | Circular Dichroism |
| CDE | Clathrin-dependent Endocytosis |
| CME | Caveolae-mediated Endocytosis |
| DLS | Dynamic Light Scattering |
| DLVO | Derjaguin-Landau-Verwey-Overbeek |
| EAF4 | Electrical Asymmetric Flow Field Flow Fractionation |
| ELISA | Enzyme-Linked Immunosorbent Assay |
| ELS | Electrophoretic Light Scattering |
| FBS | Fetal Bovine Serum |
| FTIR | Fourier Transform Infrared Spectroscopy |
| ICP-MS | Inductively-Coupled Plasma Mass Spectrometry |
| ITC | Isothermal Titration Calorimetry |
| LC | Liquid Chromatography |
| LC-MS | Liquid Chromatography Mass-Spectrometry |
| MALS | Multiangle Light Scattering |
| MPS | Mononuclear Phagocyte System |
| MS | Mass Spectrometry |
| NP | Nanoparticle |
| NMR | Nuclear Magnetic Resonance |
| NTA | Nanoparticle Tracking Analysis |
| PBS | Phosphate-buffered Saline |
| PLGA | Poly(lactic-co-glycolic acid) |
| PTA | Particle Tracking Analysis |
| PS | Phosphate-buffer |
| QCM | Quartz Crystal Microbalance |
| ROS | Reactive Oxygen Species |

| | |
|---|---|
| SDS-PAGE | Sodium dodecyl sulfate-polyacrylamide gel electrophoresis |
| SEC | Size-Exclusion Chromatography |
| FE-SEM | Field Emission Scanning Electron Miscopy |
| TEM | Transmission Electron Microscopy |

# Chapter 1 Introduction

This chapter introduces the topics of nanomedicine, the nanoparticle protein corona and methods that have been employed for the analysis of the nanoparticle protein corona to-date by reviewing research within these fields. Initially, the concept of nanomedicine and physicochemical properties dictating the quality, safety and efficacy of this therapeutic modality are explored. This section is concluded with an introduction to the model nanoparticles used for the purposes of this thesis. Current gaps in the existing literature and areas requiring further consideration in researching the nanoparticle protein corona are highlighted.

This is followed by the necessity for comprehensive analysis of bio-nano interactions is highlighted, which is followed by the concept of the protein corona and existing knowledge of the processes underpinning protein corona formation and factors that impact the formation and composition of the protein corona.

Next, the analytical processes including protocols for the isolation and recovery of nanoparticles from biological media and their relative merits are reviewed and discussed. Finally, the hypothesis, aims and objectives of this thesis are defined.

### 1.1 What are nanoparticles?

In recent years the use of nanocarriers for biomedical applications rose to the global public health challenge of the COVID-19 pandemic, where lipid nanoparticle vaccines were developed by Pfizer/BioNTECH and Moderna for the global immunization of the world population against this deadly virus.[2] Since 1995, over 50 nanoparticle-based medicinal products have been approved by regulators for clinical use.[3] There has been a steady increase in the approval of novel nanocarrier-based products for clinical applications with the recent approval of three key formulations (Onpattro, Hensify and Vyxeos) and > 400 nanoparticle products are currently under clinical evaluation in ongoing trials with an estimated 65% of these products being developed for the diagnosis and treatment of cancer.[4] Recent developments in nanomedicine research have enabled scientists to treat diseases such as cancer with enhanced safety and efficacy profiles compared to conventional medicines.[5]

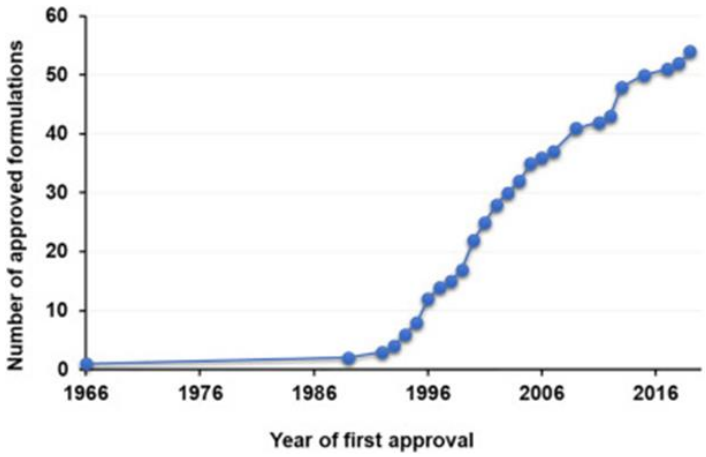


**Figure 1.1** Trends in the number of approved nanomedicine products for clinical use. Adapted from (Germain, M. et al. 2020).[4]

Nanotechnology is a multidisciplinary field, which combines biology, chemistry, physics and material science for the design of materials and objects with at least one dimension on the nanoscale (1-100 nm), which can interact with cells and molecules at the molecular level for specialised functions such as drug

delivery, imaging and diagnosis. The implementation of nanotechnology for medicinal purposes in known as nanomedicine.[6]

Nanoparticles are small colloidal particles which typically have at least one dimension in the 1-100 nm size range. They have become an increasingly popular therapeutic and diagnostic tool due to their versatile properties such as a large surface area to volume ratio, their flexibility for drug delivery applications through encapsulation or adsorption of drug onto the nanoparticle surface, and changes in drug properties when reformulated at the nanoscale.[7] The physiochemical properties of a nanoparticle will determine its biological fate, and these include nanoparticle characteristics such as size (diameter), shape, surface area to volume ratio, surface chemistry, their colloidal stability (aggregation, dispersion and agglomeration) under formulation conditions and physiological conditions.[8] Comprehensive knowledge of nanoparticle physical and chemical properties and disease pathophysiology is vital for the design of new safe and effective nanoparticles for targeted drug delivery in areas of unmet clinical need.[9]

### 1.2 Physiochemical properties of nanocarriers dictating biological fate

This section focuses on how different physical (e.g., size, shape, curvature) and chemical properties (e.g., surface charge, roughness, hydrophobicity) of nanoparticles impact their biological performance and subsequent biological fate.

**Particle Size and polydispersity**

Nanoparticle size plays a crucial role in determining the biological fate of a nanoparticle and its therapeutic cargo. Nanoparticle size affects cellular interactions, cytotoxicity, cellular uptake, biodistribution and drug release, which are overall crucial for nanomedicine safety and efficacy.[10-12]

Nanoparticle internalisation takes place predominantly via endocytosis, which is a cellular function used to maintain homeostatic conditions.[13] There different mechanisms of endocytosis that are classified as receptor-mediated or non-receptor-mediated endocytosis. Endocytic internalisation of nanoparticles takes place following adsorption (passive or receptor-mediated) of the

nanoparticles to cellular membranes, which is followed by invagination of the membrane into endocytic vesicles. Internalised endocytic vesicles are sequestered to the early endosome, from which they are sorted. Late endosomes are subsequently formed, where further breakdown of the cargo may take place, or transport to lysosomes where under acidic pH and hydrolytic enzyme conditions further breakdown of the cargo takes place.[14]

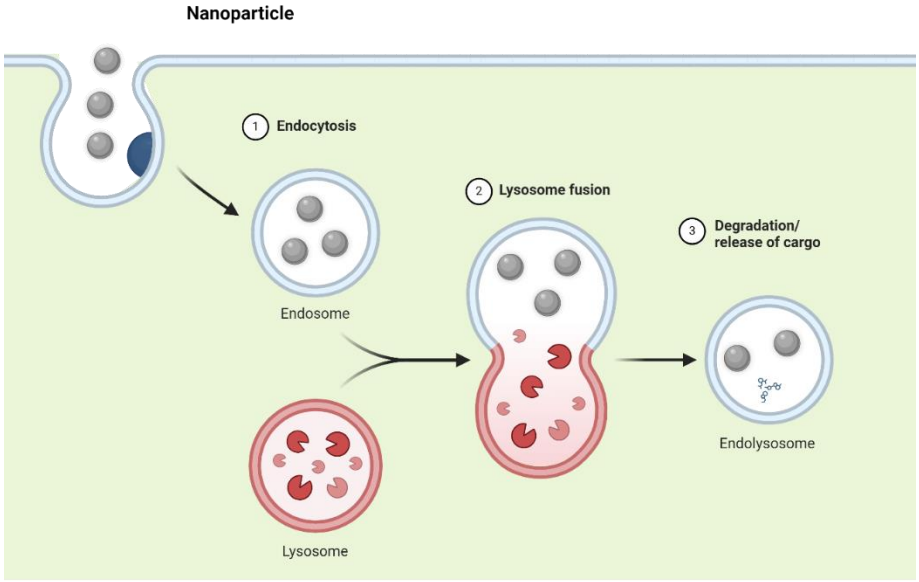


**Figure 1.2** A simplified schematic illustrating the internalisation of nanoparticles by cells *via* endocytosis. Created in Biorender.

Nanoparticle internalisation may occur *via* one or more endocytic internalisation routes, namely clathrin- and caveolae- mediated endocytosis, and macropinocytosis.[14]

There are three general mechanisms of nanoparticle cellular uptake, that include i) phagocytosis, ii) pinocytosis and iii) receptor-mediated endocytosis. The uptake of nanoparticles in tumour cells is determined by nanoparticle size and shape.[15] A study compared a range Poly(lactic-co-glycolic acid) (PLGA) nanoparticles at various sizes including (~70, ~100, and ~200 nm) with results showing an increased tumour uptake with a decrease in particle size.[16]

Recent studies have suggested transmembrane penetration, electroporation and cytoplasmic microinjections as alternate endocytosis pathways; however, the two main endocytic pathways recruited for internalisation are caveolin-

dependent endocytosis and clathrin-mediated endocytosis. The caveolin-dependent pathway is initiated by the formation of flask-shaped caveolae, which are 50-80 nm in size and has shown certain advantages in gene delivery due to opportunistic escape of caveolae from lysosomal degradation.[17] Clathrin-mediated endocytosis is the primary mechanism for nanocarrier internalisation and the most widely studied, being the most effective internalisation mechanism for particles in the 100-120 nm size range and one of the main strategies for nanoparticle drug delivery.[17] This occurs initially through the binding of ligands on the nanoparticle surface to cell surface receptors, which leads to the formation of clathrin-coated pits which forms a vesicle for nanoparticle internalization with studies suggesting the occurs within (30-120 seconds) of ligand binding.[18,19] A previous study using coumarin-6-loaded PLGA nanoparticles (100-200 nm) shows that PLGA nanoparticles were mainly internalised using the caveolin, and clathrin-mediated pathways.[20]

Corresponding mechanisms of cellular uptake used by nanoparticles are governed by their size, which is summarised in **Table 1.1**.

**Table 1.1** The impact of nanoparticle size on route of cellular internalisation

| Nanoparticle Size | Uptake Mechanism |
|---|---|
| **50-80 nm** | Caveolin-dependant endocytosis [17] |
| **100-120 nm** | Clathrin-mediated endocytosis [17] |
| **200-500 nm** | Pinocytosis [21] |
| **>500 nm** | Phagocytosis [22] |

Nanoparticles show increased cellular uptake when compared to larger micron-sized particles (1,000-10,000 nm) due to showing the same uptake mechanisms of absorptive endocytosis.[23] When developing new nanoparticles it is crucial to optimise size for the intended therapeutic indication and target biology, as this will subsequently play a major role in determining the efficacy and mechanism of cellular uptake in target tissues, off-target organs and tumour cells.[11]

Particle size impacts nanoparticle circulation time (half-life), with nanoparticles < 10 nm in diameter being cleared rapidly by the kidneys, reducing the efficacy of these nanocarriers for drug delivery due to glomerular filtration. Furthermore, nanoparticles with a diameter > 200 nm activate the complement system, which results in their accumulation in either the spleen or the liver.[11] This occurs due to the opsonization of nanoparticles upon exposure to a biological system, opsonin proteins will bind to the nanoparticle surface and are components of the protein corona composition. Opsonin protein increase binding to phagocytes which leads to internalization.[11,24]

The multinuclear phagocytic system determines the site of accumulation of engineered nanoparticles by size, with nanoparticles in the 200-500 nm diameter size range accumulating in the spleen. This is due to the size of the inter-endothelial cell slits in the spleen, which allow for nanoparticles to permeate the endothelial barrier. Nanoparticles in the 50-100 nm size range have predominantly been shown to accumulate in the liver.[25]

Phagocytosis is the predominant mechanism for the efficient cellular uptake of nanoparticles >500 nm in diameter. Previous studies in mice have shown that for polystyrene particles in the 1-2 μm size range, phagocytosis is the optimal uptake pathways.[22] Pinocytosis is an actin-mediated mechanism and the main uptake pathway for particles in the 0.2- 5 μm size range, and is non-specific pathway for large particles, pathogens and macromolecules.

**Nanoparticle Morphology**

The transport of nanoparticles in biological systems is dependent on their size and morphology, which must be taken into consideration when designing a new nanoparticle based delivery system.[26] Some of the key characteristics affected by nanoparticle morphology, include degradation and drug release kinetics due to changes occurring in the particle surface area to volume ratio.[27] The morphology of nanoparticles has also been shown to directly impact the extent of their cellular uptake, through altered contact-based interactions between the nanoparticle and cell membrane ligands. It is important to account for both nanocarrier morphology and size for cellular uptake, since optimal sizes for cellular uptake are based on different morphologies and material types.[28]

Nanoparticle morphology has also been shown to impact nanomedicine circulation times due to alterations in the immune response, interactions with vascular endothelial cells (adherence), and behaviour under haemodynamic flow conditions.[29,30]

The large variability in nanoparticle morphology and its definition has led to challenges in achieving consensus on particle geometry within the community due to similar nanoparticle morphologies being given different names by other scientists. Therefore, a quantitative framework for nanoparticle morphological classification is being developed to improve methodologies and allow for replication. The current four primary morphological descriptors used for nanomaterials are nanospheres, nanorods, nano-urchins and nano-stars.[31,32]

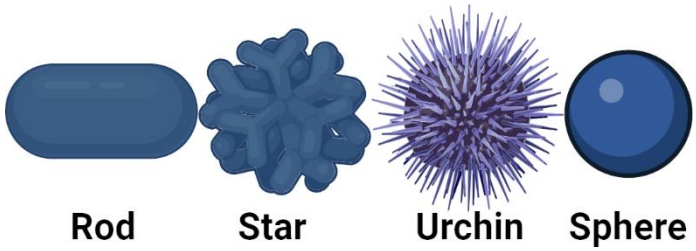


**Figure 1.3** Schematic representation of different nanoparticle morphological descriptors. Created in Biorender.

With smaller-sized nanomedicines the extent of particle surface curvature increases, leading to alterations in the particle surface area available for interactions with its surrounding environment. Nanoparticle curvature is crucial as it combines both particle size and shape to regulate interaction forces (e.g., van der Waals).[32] The curvature of a nanoparticle in combination with its shape play a significant role in determining the biological fate of nanocarriers in the context of surface area available for ligands and proteins to interact with, and adsorb on to the nanocarrier surface, which in turn dictates the range and types of interactions with biomolecules.[32] For example, studies using silicon oxide nanoparticles at different sizes and curvatures showed that particles in the 50-100 nm size range, which would have a curvature between 0.02-0.04 nm show a higher level of target receptor activation as opposed to nanoparticles with shallower or sharper curvatures.[33] Furthermore, a previous study compared three different shapes of gold nanoparticles (nanostars, nanorods, and nanotriangles) with nanotriangles showing the greatest cellular uptake followed by nanorods, and then stars.[34]

Knowledge of the interplay between nanoparticle size, polydispersity, shape and curvature parameters and their relationship with cellular internalisation mechanisms and organ biodistribution in biological systems (*in vitro* and *in vivo*) is critical for the clinical translation of novel nanoparticle-based therapies.

## Surface characteristics

### Surface Charge

The surface charge of nanocarriers plays a key role in their cellular uptake, biodistribution and how they interact with biological systems (e.g., cellular uptake into tumours and interactions with the circulatory system). For example, nanomedicines with a cationic surface charge (zeta potential >+10 mV) have been shown to be cytotoxic, interacting with blood constituents, inducing haemolysis, and undergoing rapid clearance by the multinuclear phagocytic system in the circulation, overall resulting in systemic toxicity and a short half-life under circulation.[35,36]

Nanomedicines with native charges (zeta potential < – 10 mV), have a lower extent of cellular uptake in comparison to cationic nanomedicines and also cause rapid clearance *via* the mononuclear phagocytic system, leading to a low circulation half-life. Rapid hepatic clearance of nanomedicines has been observed for nanocarriers with a zeta potential below -40 mV.[35] Therefore, nanomedicines with a near neutral zeta potential of approximately ± 10 mV are preferred for the longest circulation time. However, a challenge with such systems is poor colloid stability, requiring formulation design efforts using steric stabilisers.[36] This can be explained due to the Derjaguin-Landau-Verwey-Overbeek (DLVO) theory, with higher colloidal stability achieved with an increasing surface charge *via* electrostatic repulsion.[37] With colloidal nanoparticle formulations showing (±30 mV) being considered stable.[38]

The surface charge of nanocarriers also impacts the composition of proteins and biomolecules that adsorb on the nanoparticles surface in complex biological media. Studies have shown that negatively-charged liposomes showed higher levels of fibrinogen adsorption as opposed to neutral or positively-charged liposomes. Furthermore, positively-charged domains in immunoglobulin G have also shown higher levels of protein adsorption on to more negatively-charged nanoparticles.[39] The adsorption of proteins on nanoparticle surface, leads to the formation of a multilayered complex referred to as the protein corona (PC), which plays a crucial role in the biological interactions of nanoparticles.

Some general trends in nanocarrier surface charge association with biological fate can be seen across nanoparticles. For example, positively-charged nanoparticles are internalised more extensively in comparison to neutral or negatively-charged nanoparticles. However, positively-charged nanoparticles also have a higher chance of accumulating in the liver. This is similar to the clearance rates typically seen with cationic macromolecules.[40] A study by [41] showed that positively-charged nanoparticles are internalised more extensively in proliferating cancer cells showing both higher uptake and dissociation, while negatively-charged nanoparticles show higher rates of diffusion which may make them more ideal for deep tissue drug delivery.[40]

A further study suggested that that higher nanoparticle surface charge density will lead to an increase the quantity of proteins adsorbed unto the nanoparticles cell surface however there are other properties which relate to protein adsorption include hydrophobicity.[42]

**Surface Hydrophobicity**

Nanocarrier surface hydrophobicity plays a crucial role in nanoparticle biological interactions, especially with the cell membrane and cell surface receptors. Prior work has shown that hydrophobic nanoparticles tend to create inclusions in the target cell membrane which allow nanocarriers to spontaneously embed themselves in the hydrophobic core and be internalised. Conversely, hydrophilic nanoparticles will adsorb on the target cell surface and are then wrapped and internalised into the membrane.[43]

For example, increasing the hydrophobicity of N-isopropylacrylamide:N-tert-butylacrylamide (NIPAM:BAM) copolymers resulted in significant changes in the type and extent of proteins that adsorbed onto nanoparticle surfaces following exposure to protein-containing medium. Increasing the ratio of BAM monomer, which is hydrophobic, was found to increase the quantity of surface-bound proteins by five-fold.[44]

The hydrophobicity of nanoparticles impacts nanoparticle-protein interactions, with a direct positive correlation between nanoparticle hydrophobicity and the quantity of protein adsorbed as a general trend. Hydrophilic nanoparticles adsorb proteins to a much lesser extent, but only under highly favourable

charge conditions, which drive electrostatic interactions with proteins. These results suggest that surface charge and hydrophobicity both play a role in protein adsorption onto the nanoparticles surface.

Therefore, a strategy in the design of nanomedicines to reduce protein binding and adsorption interactions, has included the use of surface functionalisation to render the nanoparticle surface more hydrophilic. Functionalisation with hydrophilic groups drives the formation of hydration shells around the nanoparticle, making the surface less available for interactions with protein molecules.[29] Overall, these strategies result in reduced surface adsorption of proteins, which stealth nanomedicines from immune recognition by the multinuclear phagocytic system and increases their circulation half-life.[45]

For example, poly(ethylene glycol) (PEG) coating is the most well-characterised surface motif that has been used, the incorporation of which can control nanoparticle properties based on molecular weight chain length and branching properties of the PEG used in nanoparticle stealthing.[46]

**Surface roughness**

Surface characteristics of nanocarriers impact their nanoparticle-protein interactions, with the surface roughness influencing the identity and quantity of surface-adsorbed proteins. General trends have shown that nanoparticles with a smooth surface preferably adsorb proteins in the 120-310 kDa and 30-70 kDa molecular weight range. Nanoparticles with a rough surface preferably adsorb proteins in the 10-30 kDa and 70-120 kDa molecular weight range, which include proteins such as albumin, fibrinogen and clusterin. Furthermore, nanoparticles with a rough surface typically show lower zeta potential (surface charge) when compared to smooth nanoparticles of the same material composition.[47,48]

Overall, the early characterisation of nanoparticle physical and chemical properties is critical for the late-stage success of these drug delivery systems. Poorly designed nanoparticles in terms of properties and colloid stability can limit the safety (e.g., toxicity resulting from off-target accumulation of nanoparticles) and efficacy (e.g., insufficient cellular uptake) of nanocarrier based delivery systems. Moreover, the scope exists to engineer nanoparticles

so that the composition of the proteins binding to nanoparticles are altered, with the ultimate goal of controlling circulation half-life and minimising off-target accumulation of nanocarriers. In the next section of this introduction, I will give an overview of nanoparticle interactions occurring with proteins and how these are characterised for nanoparticle-based systems.

### 1.3 The Nanoparticle Biomolecular Corona

Most nanomedicines are intended for administration via the intravenous injection route into the body, meaning that all injected nanoparticles will immediately be surrounded by cells and biomolecules under blood flow.

Upon entering a biological system, nanoparticles will interact with their surrounding environment and circulating biomacromolecules including proteins will spontaneously adsorb onto the nanoparticle surface- a concept referred to as the nanoparticle biomolecular corona- a term coined by Dawson and co-workers.[49] The high surface energy of nanoparticles gives rise to the spontaneous adsorption of free circulating proteins.

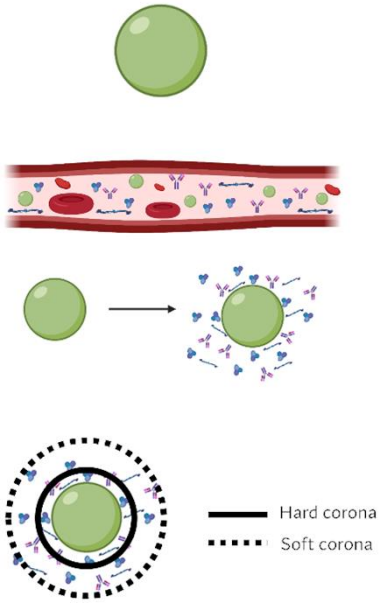


**Figure 1.4** Schematic representing the exposure of administered nanoparticle to blood protein components and surface adsorption of biomolecules. Created in Biorender.

The focus of this thesis is on studying the development of protocols for examining the protein corona, so the remainder of this thesis introduction will discuss nanoparticle-protein interactions. Since the discovery of the biomolecular (protein) corona in 2007, there have been >100 reviews concerning the nanoparticle protein corona and its impact on nanoparticle biological fate.[50]

The protein corona is dynamic in nature and its composition changes over time because of continuous protein interactions (**Figure 1.4**). As aforementioned earlier in this introduction, nanomedicines have various different physical and chemical characteristics, which dictate their affinity for various types of proteins and biomolecules following administration.

During the initial stages of exposure to biological media (e.g., serum) following injection, the proteins occurring at high abundance in serum such as albumin and apolipoproteins, will adsorb on the nanoparticle surface and form the soft protein corona. These proteins do not necessarily bind at a high affinity to the nanomedicine. However, during extended exposure to the circulatory system and interstitial fluids under shear flow, higher affinity proteins occurring at a lower abundance will adsorb onto the nanoparticle surface to form the hard protein corona as described by the Vroman effect (**Figure 1.5**).[51] The high abundance low affinity proteins will be replaced by higher affinity proteins over time until an equilibrium state is achieved. This is the reason why the protein corona composition often does not reflect the naturally occurring abundance of proteins in circulation. Moreover, as the nanomaterial under circulation undergoes organ biodistribution and experiences different fluid shear flow rates and protein compositions, the composition of the protein corona will be continually altered.[52]

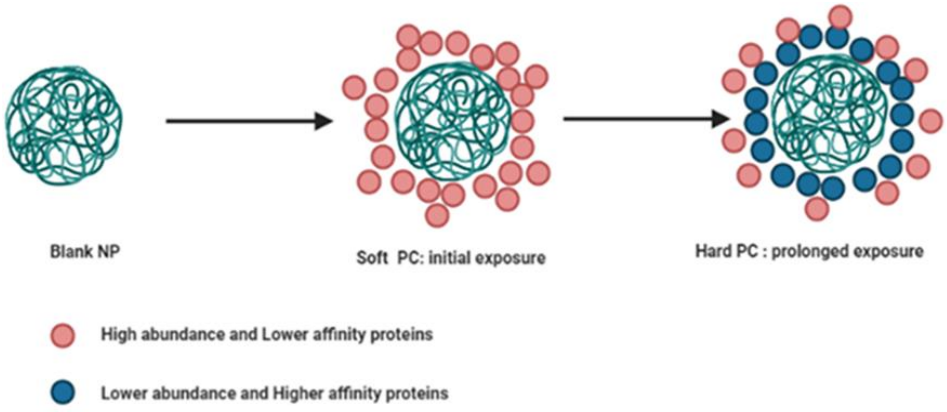


**Figure 1.5** The dynamics of protein corona formation during initial (soft) and late (hard) exposure of nanoparticles to biological media (Created in Biorender).

The biological identity of nanoparticles changes in response to protein corona formation, which in turn dictates their biological fate. Following protein corona formation, many nanoparticle physicochemical properties such as size, shape, and surface chemistry are altered. These changes subsequently impact the cellular uptake, drug release and biodistribution profiles of nanoparticles.[53] The interactions between nanoparticles and proteins, and protein-protein interactions may induce protein misfolding and aggregation, which increases the immunogenicity risk of nanoparticles and a reduced circulation time for nanoparticles due to increased elimination by the MPS and may elicit an immune response and damage healthy tissues. There is a concern that surface ligands present in actively targeted nanoparticles will have their function eliminated or reduced following protein corona formation.[54]

The composition of the protein corona is primarily proteins, however there are other biomolecules present including sugars, lipids and nucleic acids.[55] Analysis of the protein corona and its impact on nanoparticle physical and compositional properties is crucial to developing our understanding of the biological interactions of nanoparticles and their subsequent fate.

## 1.4 Factors influencing the nanoparticle protein corona beyond nanoparticle properties

### Blood Flow

Most nanomedicines are intended for intravenous administration; therefore, it is of paramount importance during the development of a new nanomedicine to profile the interactions taking place between nanoparticles and blood protein components. While many studies have profiled the protein corona in response to incubation with blood plasma and serum components, very few studies to date have considered how these interactions occur under hemodynamic conditions, and in the presence of blood flow.

A nanoparticle injected intravenously, will experience a high degree of shear resulting from blood velocities it will encounter throughout the circulatory systems. For example, blood velocities of 0.85 cm/s and 8.5 cm/s have been reported for veins (median cubital vein) and arteries, respectively.[56]

In considering haemodynamic effects on nanoparticles, the following assumptions can be made:

Vasculature is cylindrical and based on rigid tubes, despite compliance resulting from the presence of elastic smooth muscle layers. Blood is assumed to be a Newtonian fluid, though the presence of blood cells and biomacromolecules renders it essentially non-Newtonian. The blood flow to which a nanoparticle is subjected is constant, not accounting for heartbeats, pulses, or entrance to capillary beds within the vascular tree. Based on these assumptions the Haagen-Poisseuille's law[57] can be applied to estimate the shear stress to which a nanoparticle is being subjected in the circulatory system.

$$\boldsymbol{\tau = 8.\mu.\frac{u}{d}} \qquad \textbf{Equation 1.1}$$

Where $\tau$ is the shear stress, $\mu$ the viscosity of blood, $u$ the velocity of blood flow, and $d$ the diameter of the vessel.

The Haagen-Poisseuille equation shows that shear stress is directly proportional to the diameter of the blood vessel and the reciprocal of the vessel

diameter. For example, based on this model, the shear stress experienced in the aorta will be up to ~10 dyn/cm, while in the capillaries the shear stress will increase up to 55 dyn/cm.[58]

Recent studies investigating nanoparticle interactions with biological media have considered the introduction of flow into experiments to compare how flow and shear stress impacts the range and extent of protein corona formation with nanocarriers.[59] Though the role of flow in protein corona composition has been increasingly recognised; however, only a limited number of studies have adopted these conditions.[59,60]

In recent years the increased availability of commercial lab on a chip-based microfluidics systems has offered the scope to study the interactions occurring between nanoparticles and biomolecules under flow in systems mimicking haemodynamic conditions. However, studies using such approaches in the literature are currently lacking.

**Composition of the biological media and environmental parameters**

Several environmental parameters are known to play a key role in mediating nanoparticle interactions with cellular and biological systems, particularly the formation of the nanoparticle protein corona during in vitro screening experiments.[61]

Screening cellular uptake of nanoparticles is a routine experiment performed during the early evaluation of prototype nanoparticulate delivery systems prior to their preclinical evaluation. Prior studies have reported that the exposure of nanoparticles to fetal bovine serum enhances the cellular uptake of chitosan nanoparticles and alters their biodistribution due to the presence of proteins such as lipoproteins in serum that interact with and adsorb onto nanoparticle surfaces.[62]

Partikel et al demonstrated that the composition of human serum and concentration used in protein corona studies has significant potential to impact the nanoparticle protein corona for poly(lactic-co-glycolic) acid nanoparticles.[63] Beyond the effects of serum protein composition and protein concentration-dependency, they also showed that the physiological

environment to which the nanoparticle is exposed, significantly impacts nanoparticle cellular interactions.[63]

Environmental pH has been shown to influence the surface adsorption of BSA in silicone oxide nanoparticles, concluding that electrostatic contributions can be significantly altered by pH of the test medium explored.[64] These findings overall have implications for screening nanoparticle biological interactions in media mimicking blood or the tumour microenvironment, since the tumour pH is slightly acidic in nature, which may alter the range of electrostatic interactions occurring between nanoparticle systems and tumour cells under acidic pH (pH 6-7).[65] Variations in incubation temperature conditions in combination with media pH alterations regulate interactions between nanoparticles and biological media, through altered protein conformations resulting in different charge distribution profiles on protein molecule surfaces.[66]

Temperature conditions under which nanoparticles are incubated with biological media, will also impact the protein corona content. A survey of the nanomedicine protein corona analysis literature reported that the use of physiologically relevant temperature was reported in up to 75% of studies within the field, whereas no incubation temperature was reported in 10% of the literature.[67]

With the composition of the nanoparticle protein corona being impacted to such a large extent by variables during incubation with protein containing media, there is a critical need within the field to define gold standard incubation conditions for evaluating the nanoparticle protein corona. Defining such approaches requires a consideration of the composition of the incubation media, pH, temperature and total protein concentration. This becomes particularly relevant in the context of the biology being targeted by the nanomedicine and the use of systems that adequately simulate the biological system to which the nanomedicine will be exposed.

## 1.5 Techniques used to isolate the nanoparticle protein corona from biological media

Since understanding the protein corona range and concentration of surface-adsorbed proteins is essential, comprehensive analysis of the nanoparticle protein corona needs be performed. This may be achieved through:

i) physical separation of the nanoparticles from biological incubation media, or
ii) the *in-situ* separation and analysis of the nanoparticle protein corona.

A key challenge in the development and implementation of approaches for nanoparticle isolation/resolution from biological media, is balancing the alterations in the corona composition during the process of separation against background matrix effects during *in situ* measurements of the protein corona.

Generally, any separation-based technique will result in alterations in the protein corona, particularly since all approaches can alter the equilibrium of free unbound and adsorbed proteins. Most separation techniques will result in the soft corona being removed, which has significantly restricted the existing body of knowledge on the composition and characteristics of the soft corona to-date. Most existing knowledge on the nanoparticle protein corona at present is based on the analysis of the hard protein corona.

The importance of the protein corona in determining the biological fate of nanoparticles has been established in the previous sections of this report. Therefore, it is also crucial to understand the advantages and limitations of existing techniques used for the isolation of nanoparticles from biological media, for the downstream characterisation and analysis of the protein corona.

Current methods for nanoparticle recovery following incubation with biological media include i) centrifugation-wash, ii) magnetic isolation, iii) size exclusion chromatography (SEC), and iv) flow field-flow-fractionation (AF4) modes.

Centrifugation-wash recovery is the most widely used technique because it can be optimised for many different nanoparticles (centrifugation times and speed) and is the most widely accessible approach for nanoparticle isolation for most labs worldwide. However, there are limitations associated with

centrifugation-based recovery, which need to be considered. These may include the loss of the soft protein corona and false negatives resulting from the dissociation of proteins from nanoparticles due to the centrifugation speed. Further limitations include the possibility of false positives caused by long centrifugation times and high speeds, which may cause protein aggregation and nanoparticle agglomeration. Centrifugation based isolation is also not ideal for low density nanoparticles since the lack of density differences with the bulk protein media may lead to low recovery yields. However, the development of a sucrose cushioning gradient has been explored as an approach, which allows for the isolation of different nanoparticle -protein corona components based on size.[50]

Magnetic-based isolation is another method for the recovery of nanoparticles from biological media and is typically used for magnetic iron oxide nanoparticles. While this method is considered to cause less damage to the protein corona in comparison to centrifugation-resuspension and reduces the risk of protein aggregation from high gravitational forces, there is still an increased risk of agglomeration, which correlates with nanoparticle size. Therefore, magnetism is preferable for smaller-sized nanoparticles (< 10 nm). This technique is overall quite limited in its use and may interfere with other analytical techniques.[68]

Size-Exclusion Chromatography (SEC) is considered a gentler technique for the recovery of nanoparticles from biological media and causes minimal damage to the protein corona. In SEC, nanoparticles are typically too large to enter the pores in the stationary phase; thus, only the proteins enter this phase which allows for the separation. This method of separation allows for the determination of the association rate of proteins to the nanoparticle surface, to measure protein corona thickness and to separate nanoparticle-protein complexes into fractions which can be further analysed using multiple inline detectors (typically UV and light scattering) or for downstream offline analyses. The main limitation of SEC use, is the loss of materials resulting from protein and nanoparticle interactions with the stationary phase, dilution effects from the mobile phase and the pressure applied to the column, which can each

reverse the protein corona composition or nanoparticle agglomerates formed.[22]

Asymmetric Flow Field Flow Fractionation (AF4) is a technique which separates nanoparticle -protein complexes from bulk protein media through the presence of a crossflow which takes place between a non-porous plate and a porous plate covered in a membrane which allows eluted proteins to pass the membrane, and the nanoparticles are retained. This technique can separate nanoparticle-protein complexes with very little to no damage to the protein corona and is able to analyse complex nanoparticulate systems. With a recent study showing AF4-based separation techniques are able to retain the weakly associated soft corona proteins, which can then be collected for further downstream analysis. [69] A wide range of techniques such as multi-parametric surface plasmon resonance are currently being explored for soft corona protein characterization but this remains underreported in the literature at the time of this thesis.[70]

Furthermore, AF4 can be coupled to additional inline detectors and can measure key nanoparticle characteristics including size, density and shape (critical quality attributes). The main limitation of AF4 as a technique is that the equipment is costly, method development is time-consuming, and AF4 run parameters must be optimised for each analyte type prior to data acquisition.[71]

The concept of AF4 based separation is illustrated as follows:

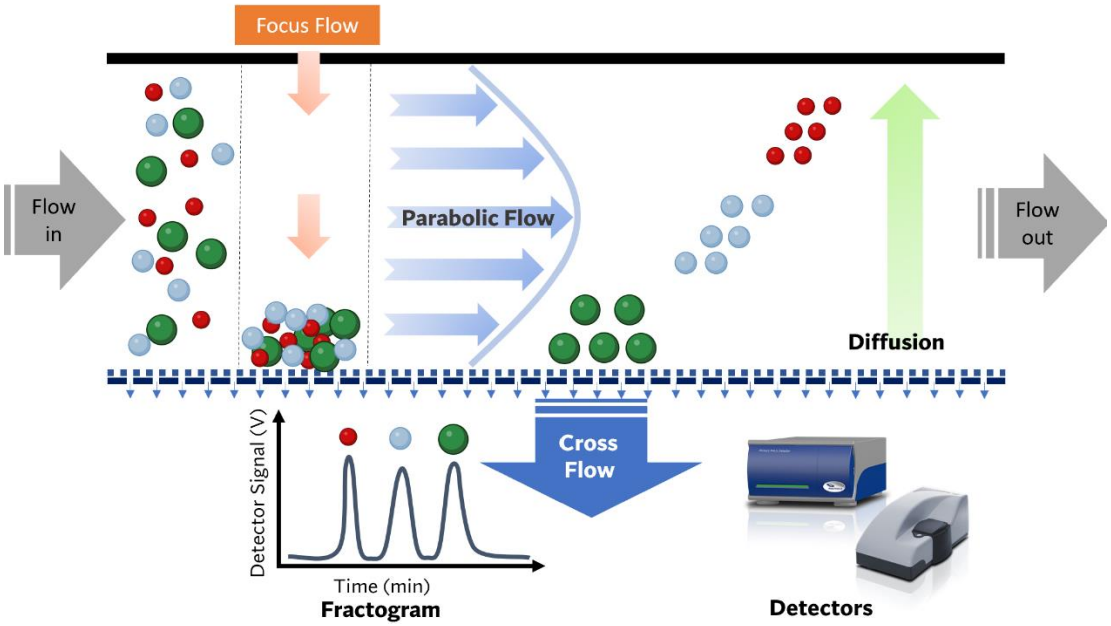


**Figure 1.6** Schematic representing the principle of flow field flow fractionation for the resolution of different species according to size. (Created in Biorender).

## 1.6 Techniques used to analyse the nanoparticle-protein corona

Most approaches for the analysis of the nanoparticle-protein corona rely on the separation of nanoparticle-protein complexes from bulk biological incubation media, which for compositional analysis of the protein corona is followed by desorption of the protein content from the nanoparticle. Previous work has shown that some protein corona constituents with a high affinity for nanoparticles are not desorbed adequately and are consequently not identified during analysis.[72]

Taking into consideration the challenges in profiling the nanoparticle protein corona, and a lack of harmonisation efforts in the field to introduce consistency, a more detailed knowledge of the approaches used for analysis of the nanoparticle protein corona is required, which I review in this section.

Generally, two broad approaches are applied to the analysis of the nanoparticle protein corona- which may be referred to as direct or indirect in nature.

Direct protein corona characterisation techniques can be further classified into two categories, qualitative techniques that directly identify the identity of the proteins which are adsorbed onto the nanoparticles. Examples of these techniques include sodium dodecyl sulphate polyacrylamide gel electrophoresis (SDS-PAGE) and liquid chromatography-mass spectrometry proteomics-based analysis of the nanoparticle protein corona composition based on identity and abundance of proteins.[73,74] Furthermore, this category includes techniques that identify the conformation of proteins such as circular dichroism (CD).[75] The other category includes quantitative techniques which can be used to determine the total protein concentration adsorbed onto the nanoparticle surface, and includes the use of colorimetric protein quantification assays (Bradford protein assay, Bicinchoninic acid (BCA) assay) and liquid chromatography-mass spectrometry.[76]

These approaches are summarised and depicted as follows;

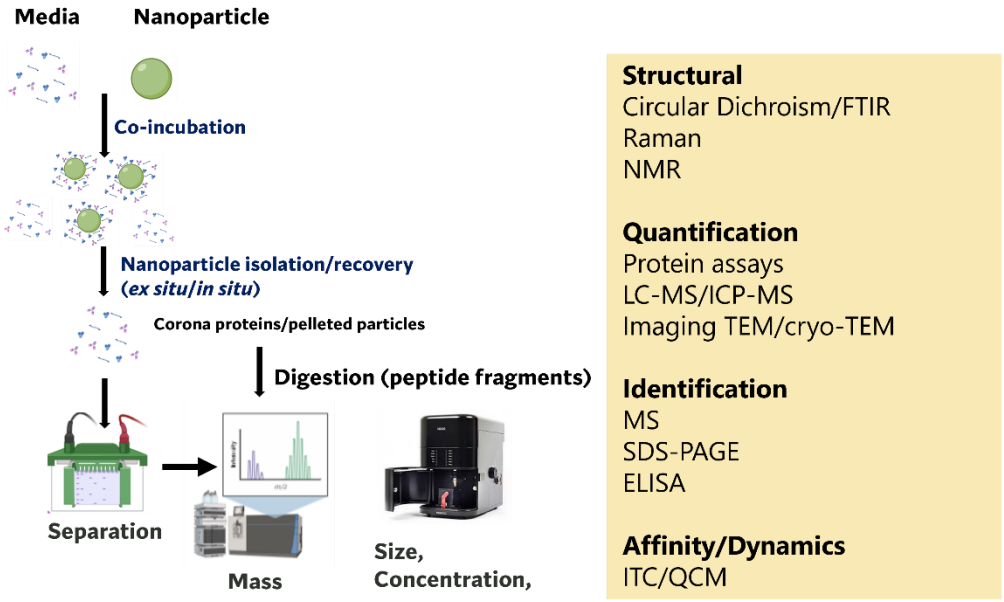


**Figure 1.7** Summary of the range of techniques used to profile the nanoparticle protein corona. Adapted from (Carrillo-Carrion, Carril and Parak, 2017). Created in Biorender.[76] *FTIR: Fourier transform infrared spectroscopy, LC-MS: Liquid chromatography-mass spectrometry, ICP-MS: Inductively-coupled plasma mass spectrometry, TEM: Transmission electron microscopy, MS: Mass spectrometry, SDS-PAGE: Sodium dodecyl sulfate-polyacrylamide gel electrophoresis, ELISA: enzyme-linked immunosorbent assay, ITC: Isothermal titration calorimetry, QCM: Quartz crystal microbalance*.

The Bradford and BCA assays are simple colorimetric protein quantification assays, which can be used to calculate the total protein concentration in a sample. Prior to performing an experiment, it is crucial to perform preliminary studies to determine the compatibility of the formulation buffer and nanoparticles with the assay to ensure accurate results, since some nanoparticle materials can interfere with these assays through background colorimetric contributions to the sample. Protein quantification assays are often performed prior to SDS-PAGE fingerprinting of the protein corona to ensure that the same concentration of protein is loaded into each well to allow for semi-quantitative comparison (i.e., normalisation of the total protein content loaded onto each gel lane).[77]

SDS-PAGE is a technique which separates proteins in each sample based on their molecular weight and electrophoretic mobility under an applied electrical charge, which can then be compared to a known reference on the ladder to determine the protein's estimated molecular weight. This technique can also be used to investigate the affinity of certain proteins for specific nanoparticles by identifying the difference in protein composition fingerprint following protein corona formation in different nanoparticles. As SDS-PAGE can only provide qualitative information on the composition of the protein corona it is often followed up with mass spectrometry for quantitative fingerprinting of the protein corona composition.[78] Using techniques such as liquid chromatography in tandem with mass spectrometry, and inductively coupled plasma-mass spectrometry (inorganic nanoparticles) it is possible to perform highly robust identification and quantification of proteins.[79]

The main limitation direct protein corona characterisation techniques face is that protein-nanoparticles need to be isolated from the incubation media (e.g. serum) to ensure that unbound proteins from the bulk incubation media do not interfere with measurements. As previously discussed, the soft protein corona is composed of low affinity proteins and during current isolation techniques often result in the desorption of these proteins, such that only the hard protein corona is analysed.[80]

Indirect techniques such as dynamic light scattering (DLS) and nanoparticle tracking analysis (NTA) are optical particle metrology tools used to measure changes occurring in nanoparticle size distributions and polydispersity following protein corona formation.

### 1.7 How nanoparticle characteristics affect protein corona formation and composition

The physical and chemical properties of nanoparticles determine the biological fate of nanoparticles. Protein corona formation alters these properties which subsequently impacts the biological fate of nanoparticles. In this section we will focus on how these different properties impact protein corona formation and the subsequent impact on biological interactions.

A general trend can be observed on the effect of nanoparticle size on the protein corona, with smaller nanoparticles adsorbing a larger quantity of proteins due to a larger surface area. However, a study performed by (Partikel, K. *et al. 2019)* [81] compared the changes in protein corona formation between PLGA nanoparticles of varying sizes (i.e., 100 and 200 nm) following incubation with foetal bovine serum (FBS) to induce protein corona formation, concluding that the difference in protein adsorption was independent of nanoparticle size.

The surface functionality of nanoparticles is an important factor for protein corona formation and many different surface functionalisation have been explored in the design of nanoparticles to enhance their circulation time. This strategy is referred to as 'stealthing' and reduces the clearance of nanoparticles by the MPS, prolonging their circulation time and reducing accumulation in the liver and spleen.[82] The PEGylation of nanoparticles is one of the most common surface modification strategies employed to mitigate for MPS clearance. In one study, PLGA nanoparticles were PEGylated, and protein corona formation was compared between non-PEGylated and PEGylated nanoparticles. The results from this study showed a significant reduction in the quantity of proteins adsorbed onto PEGylated nanoparticles with a significant reduction in proteins involved in the immune response such as complement proteins.[81] The PEGylation of nanoparticles reduces the quantity of opsonin proteins bound onto nanoparticles surface, which reduces their interactions with the complement system and thereby increasing their circulation time. PEGylation stealthing can also render nanoparticles more hydrophilic, offering formulation advantages.[83]

The shape of nanoparticles plays an important role in protein corona formation with a study comparing two nanoparticles with identical physicochemical properties and different morphologies (rods and spheres). These nanoparticles were incubated in human serum and the results showed that rod like nanoparticles adsorbed a significantly larger number of proteins when compared to spherical nanoparticles. The impact of shape on the protein corona was further highlighted in this study which showed that the composition of the protein corona in rod-like nanoparticles contains 57% immunoglobulins

while spherical nanoparticles only had 42% immunoglobulins and this difference will have a significant impact on the biological fate.[84]

Another study investigating the role of hydrophobicity reported that hydrophobic gold nanoparticles adsorbed 2.1-fold more proteins when compared to hydrophilic nanoparticles, caused by an increase in hydrophobic interactions. This study identified that the composition of the PC was mainly smaller nanoparticles (< 50 kDa) negatively charged nanoparticles showing a higher affinity for hydrophobic nanoparticles. Furthermore, it was identified that the protein composition of nanoparticles was also impacted by hydrophobicity, with certain proteins preferring hydrophobic nanoparticles (albumin), others prefer hydrophilic nanoparticles (vitronectin) while some proteins (apolipoproteins) showed no preference.[83] The general trend is that negatively-charged nanoparticles will typically adsorb a larger amount of proteins, however a study performed by [85] showed that PEGylation of nanoparticles will also overall decrease the amount of adsorbed proteins and may be a method to mitigate for the impact of surface charge.

### 1.8 The impact of protein corona formation on nanoparticle biological fate

The lack of understanding of the biological interactions governing nanoparticle-protein interactions and their downstream effects is one of the key obstacles faced in the translation of nanoparticles. Therefore, it is important to develop knowledge of how the protein corona leads to changes in nanoparticle biological fate, in order to inform the rational design of next-generation nanomedicines.[86]

Protein corona formation is one of the main obstacles, which actively targeted nanoparticles face as the adsorption of proteins reduce the targeting ability of nanoparticles and their organ biodistribution. A study with silica nanoparticles showed that protein corona formation led to the loss of targeting ability for these nanoparticles.[87] The targeting ability of nanoparticles following protein corona formation is dependent on the method of targeting ligand conjugation and the affinity of the targeting ligand. Studies have shown that protein corona formation leads can reduce the interaction of targeting with the target receptor.[88,89] Conversely, another study showed that nanoparticles incubated

with human serum albumin demonstrated enhanced targeting ability. Albumin was shown to reduce the clearance of nanoparticle by the MPS, which increased the probability of nanoparticles reaching their target site.[90]

The formation of the protein corona can impact the cellular uptake of nanoparticles, with reports of the mechanism of uptake changing from micropinocytosis to CDE for lipid nanoparticles following protein corona formation. These findings were also observed in another study in which protein corona formation changed the uptake pathway from CDE to CME in lipoplexes due to aggregates forming and increasing nanoparticle size.[88]

We have discussed the mechanisms by which nanoparticle protein corona formation can increase the toxicity of nanoparticles; however, the reverse trend is also true in some instances. For example, Zinc oxide and silver nanoparticles have a surface chemistry which leads to the formation of reactive oxidative species (ROS), which can cause toxicity and cell death. However, studies have shown that the formation of the protein corona can alter their surface chemistry and reduce the formation of ROS therefore making these nanoparticles more biocompatible.[91]

The formation of the protein corona has also been demonstrated to impact the release profile of payload drug from nanoparticles. For example, this has been demonstrated with Abraxane, where following protein corona formation nanoparticles showed a significant reduction in the burst effect, furthermore porous silica nanoparticles loaded with camptothecin showed a complete loss of drug release following protein corona formation.[90]

Overall, in this section we highlight the need for the case-by-case analysis of novel nanomaterials for downstream biological effects of the protein corona on biological fate in the context of nanomedicine safety and efficacy profiles.

## 1.9 Analytical techniques used to measure protein corona impact on nanoparticle physicochemical properties

Currently, the most used measurement techniques for the analysis of changes occurring in nanoparticle size, include DLS and NTA for the characterisation of nanoparticle suspensions and it is important to understand the advantages and limitations of each technique to ensure accuracy and reproducibility.

*Dynamic Light Scattering (DLS)*[92] measures nanoparticle size through tracking fluctuations in the scattered light intensity resulting from the Brownian movement of nanoparticles. It is a quick and relatively accurate technique for determining the size of nanoparticles. When an incident beam of laser light encounters nanoparticles and biomacromolecules undergoing Brownian motion, the light will be scattered in all directions, which can be attributed to the particle size and morphology. By solving the intensity fluctuations over time, a diffusion coefficient can be determined that is related to the hydrodynamic size of the particle, viscosity of the solvent in which the sample is dispersed and the temperature.[93]

$$R_h = \frac{\kappa T}{6\pi\eta D}$$ **Equation 1.1.2**

Where $R_h$ represents the hydrodynamic radius, $k$ the Boltzmann constant, $T$ the temperature, $\eta$ the viscosity of the dispersant, and $D$ the measured diffusion coefficient.

However, the main limitation of this approach is that it is very sensitive to the presence of aggregates and the size measurement in highly polydisperse systems may not truly reflect the sample as due to angle dependency of light scattering intensity, measurements are often biased to larger particles (due to the scattering intensity depending on the $6^{th}$ power of the size of the molecule) will cause more light scattering when compared to smaller ones. The signal obtained from DLS is also very dependent on the sample optical properties, including the size and concentration of molecules, requiring optimisation of analyte concentration ranges.

*Nanoparticle Tracking Analysis (NTA)* is similar to DLS in that it also uses Brownian movement of nanoparticles and light scattering to measure

nanoparticle size distributions contained within a sample. However, this method tracks single particles with a high resolution and can provide accurate size distribution information in highly polydisperse samples allowing the detection of multiple peaks. The main advantage of NTA over DLS is that this method does not show any bias in terms of aggregates although this method has a few drawbacks including the need to optimise many parameters such as camera levels, and particle concentration. Furthermore, NTA is a complicated and time-consuming method which can take up to 5-60 mins per measurement.[94]

**Table 1.2** summarises and compares different nanoparticle characterisation techniques currently available for the analysis of the nanoparticle protein corona.

**Table 1.2** Comparison of techniques that can be used for the analysis of nanoparticle suspensions. Adapted from (Modena et al., 2019) [95]

| Technique | Measured Parameters | Advantages | Limitations |
|---|---|---|---|
| **DLS** | Size (5 nm- 10 µm)<br><br>Size distribution (Intensity) | Rapid<br><br>Provides data on colloidal stability in solution. | Biased towards aggregates.<br><br>Provides no information on shape. |
| **NTA** | Size (30 nm- 1 µm) | Can analyse one nanoparticle at a time so can be used to analyse samples with high polydispersity | Difficult to use and time-consuming |
| | Size distribution (number-based) | | Not suitable for all materials the nanoparticles must be highly scattering |
| | Particle concentration | | |
| **Electrophoretic light scattering** | Zeta Potential | Rapid and same system as DLS (zetasizer) | Indirect estimation from electrophoretic mobility |
| **AF4** | Size (1-10,000 nm), zeta potential in EAF4 mode | High resolution separation of polydisperse samples, with simultaneous inline analysis of particle size and geometry | Poor recovery, limitations in resolution, limit of detection |
| **SEC** | Size (1-200 nm)<br><br>Size Distribution (population based) | Can separate samples with high polydispersity into highly monodisperse fragments. | Dilution effects, adsorption to column matrix materials |

The main advantages of using NTA is that it can measure the changes occurring in nanoparticle size following incubation with protein-containing media without the need for prior nanoparticle isolation from incubation media. This is advantageous because during isolation of nanoparticles from media, the protein corona can be altered by the recovery method. However, the limitations of these techniques need to be taken into consideration as the background signal from sample buffer may interfere with the ability of NTA to accurately measure nanoparticle size and particle concentration.

A study was performed using silica nanoparticles to compare measurement techniques (DLS, NTA, X-ray scattering and centrifugal liquid sedimentation) for these nanoparticles when in cell culture and the study found that DLS data was no longer usable and that the size of nanoparticles in NTA were significantly higher. Centrifugation was able to differentiate between agglomerates of different sizes however the limitations of this method must also be considered as false positives are common due to high centrifugation times and gravitational forces.[96]

AF4 has previously been used in combination with DLS to provide the size of nanoparticles without prior isolation which overcomes the technical limitations of DLS to provide accurate size distribution of nanoparticles. The development and optimisation of AF4 coupled with techniques such as DLS and NTA may be a viable pipeline for the characterisation of nanoparticles *in situ* in their incubation media without damaging the protein corona.[97]

### 1.10 The model nanoparticles used in this thesis

Polystyrene latex nanoparticles dispersed in ultrapure water as stable individual particles, and due to the properties of particles on the nanoscale these systems have attracted interest for many different uses including use as a model for nanocarriers.[98] For the purpose of this thesis, we will be latex polystyrene (100 nm) nanoparticles with amine-modified and carboxylate surface modifications, representing different surface charge properties.

Polystyrene is an aromatic polymer which is synthesised via the polymerisation of styrene monomers which results in the spontaneous

formation of spherical nanoparticles. The polymerisation reaction is initiated using an initiator for example potassium persulfate.[99]

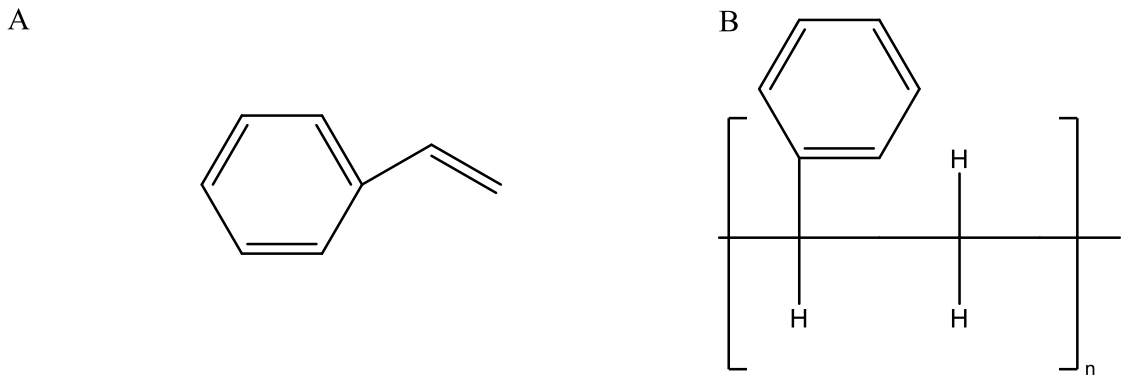


**Figure 1.8** Graphical representation for the polymerisation of Styrene to form latex polystyrene beads. (A) showing the chemical structure for the monomer styrene and (B) showing the chemical structure for the polymer polystyrene.

The polymer chains formed will coil and entangle due to the aromatic benzene ring and the polymerisation step ends when two chains react to form a sulphate-terminated polymer chain. The polymerisation phase ends when two polymer chains react to form a sulphate-terminated polymer chain. Sulphate is a negatively charged ion which can be found on the latex polystyrene nanoparticle surface, which is why polystyrene latex nanoparticles carry a negative surface charge.[100] Furthermore, the latex nanoparticle surface is also hydrophobic due to the presence of the benzene rings, mimicking hydrophobic nanocarrier based systems.

There is a high interest for the use of polystyrene nanoparticles as models to study protein corona formation and composition because of their availability in many different sizes (0.1- 3.0 μm) and high colloidal stability. Furthermore, these nanoparticles can be labelled with a range of fluorescent dyes and surface modification can be performed (PEGylation and amine modification) to mimic different surface chemistries. There are currently > 60 different studies, which mention the use of polystyrene nanoparticles for studying nanoparticle protein corona formation.[50]

The surface modification of nanoparticles is a technique used to alter the physiochemical properties of nanoparticles, which subsequently impact their interactions with biomolecules.

The amine modification of nanoparticles leads to a change in the surface charge with the zeta potential becoming more positive, which in turn will impact the identity of surface-adsorbed proteins and may affect the colloidal stability of the nanoparticles making them less stable and more prone to agglomeration.[101]

Polystyrene latex nanoparticles will be characterised in this thesis using orthogonal sizing techniques, including dynamic light scattering (DLS) and nanoparticle tracking analysis (NTA) to measure nanoparticle size. Electrophoretic light scattering (ELS) and electric asymmetric flow field flow fractionation will be used to measure electrophoretic mobility and zeta potential under formulation conditions (baseline control) and following exposure to media containing serum.

### 1.11 Hypothesis, aims and objectives.

The hypothesis of this thesis is that existing pipelines for the isolation of nanoparticles from biological media during screening of the nanoparticle protein corona can be improved. An improvement in existing pipelines is underpinned by developing our knowledge of the fundamental role of different nanoparticle isolation protocols and analytical approaches.

Nanoparticle physicochemical properties for drug delivery include a narrow particle size distribution between 100-200 nm (PDI<0.2), targeting capability, long shelf lives, high drug loading capacity (> 10%) and responsive drug release in the target tissue. However, all these factors can be altered following the introduction of nanoparticles to biological media and cellular environments during administration *in vivo*.

The overall aim of this thesis is to characterize the impact of nanoparticle isolation parameters, which can overall control the nanoparticle physical and chemical identity, with a direct focus on how these approaches alter the size properties of different nanoparticle surface charges.

For this purpose, I used polystyrene latex nanoparticles with different surface modifications, representing positively- and negatively-charged nanoparticles. The rationale for selecting these nanoparticles as a model system is that they are not biodegradable, eliminating an additional variable during biorelevant assay development for studying nanoparticle-protein interactions.

The main aim of this can be divided into three experimental chapters which are structured as follows:

Chapter 1 provides a broad introduction to nanomedicines, the nanoparticle protein corona, and the current state of the art for the analysis of the nanoparticle protein corona.

Chapter 2 describes an evaluation of the impact of incubation duration and nanoparticle isolation approaches on nanoparticle physicochemical properties, considering centrifugation-resuspension and *in situ* nanoparticle tracking analysis. The impact of physiologically relevant flow conditions on the relative composition of the protein corona and nanoparticle size and charge parameters was analysed.

Chapter 3 details the optimisation and application of AF4 for the high-resolution separation of nanoparticles from bulk protein containing media and the range of parameters that can be inferred and monitored using this approach. I investigate the impact of linear and decay profiles on the quality of separation (resolution) and recovery of nanoparticles for downstream multidetector analysis. These findings are compared with orthogonal analytical approaches such as NTA in fluorescence and scattering modes. Using this approach, the utility of AF4-MD in profiling the nanoparticle protein corona physical parameters is explored. Findings from chapter 3 are compared with the centrifugation-resuspension approach detailed in chapter 2.

Chapter 4 outlines the application of electric flow field flow fractionation (EAF4), using electric fields as a means for resolving different species based on electrostatic charge. In this chapter the use of EAF4 hyphenated with multidetector approaches is explored for the charge-based separation and analysis of nanomaterials and their interactions with protein-containing media in response to protein corona formation.

In this chapter, I also compare the EAF4 approach to resolution of nanoparticles from protein-containing media with the latest mode of nanoparticle tracking analysis in fluorescence and scatter mode, comparing my observations with findings in Chapters 2-3. Overall, EAF4 was found to be useful as a technique for studying both the morphology and the impact of surface electrostatic effects resulting from protein surface adsorption onto nanoparticles.

Chapter 5 discusses the overall outcomes of this thesis and future work directions.

# Chapter 2 Nanoparticle isolation from biological media for protein corona analysis: The impact of incubation and recovery protocols on nanoparticle properties

This chapter contains the results from the published article in the Journal of Pharmaceutical Sciences (Daramy, K; Punnabhum, P, Hussain, M; Pei, Y; Minelli, C; Rattray NJW; Perrie, Y.; Rattray, Z. Nanoparticle isolation from biological media for protein corona analysis: The impact of incubation and recovery protocols on nanoparticle properties, J Pharm Sci 2023, https://doi.org/10.1016/j.xphs.2023.12.021). For this work, I designed, analyzed, and carried out all the experimental work presented in this manuscript and chapter. I also prepared the manuscript draft for submission. Muattaz Hussain trained me on the use of the Bio-Rad gel imaging system.

## 2.1 Abstract

Nanoparticles are increasingly implemented in biomedical applications, including the diagnosis and treatment of disease. When exposed to complex biological media, nanoparticles spontaneously interact with their surrounding environment, leading to the surface-adsorption of small and bio-macromolecules- termed the “corona”. Corona composition is governed by nanoparticle properties and incubation parameters. While the focus of most studies is on the protein signature of the nanoparticle corona, the impact of experimental protocols on nanoparticle size in the presence of complex biological media, and the impact of nanoparticle recovery from biological media has not yet been reported. Here using a non-degradable robust model, I show how centrifugation-resuspension protocols used for the isolation of nanoparticles from incubation media, incubation duration and shear flow conditions alter nanoparticle parameters including particle size, zeta potential and total protein content.

Results show significant changes in nanoparticle size following exposure to media containing protein under different flow conditions, which also altered the composition of surface-adsorbed proteins profiled by SDS-PAGE. In-situ analysis of nanoparticle size in media containing protein using particle tracking analysis highlights that centrifugation-resuspension is disruptive to agglomerates that are spontaneously formed in protein containing media, highlighting the need for in situ analytical methods that do not alter the intermediates formed following nanoparticle exposure to biological media.

Nanomedicines are mostly intended for parenteral administration, and our findings show that parameters such as shear flow can significantly alter nanoparticle physicochemical parameters. Overall, I show that the centrifugation-resuspension isolation of nanoparticles from media significantly alters particle parameters in addition to the overall protein composition of surface-adsorbed proteins. From these results, it is recommended that nanoparticle characterization pipelines studying bio-nano interactions during early nanomedicine development consider biologically-relevant shear flow conditions and media composition that can significantly alter particle physical parameters and subsequent conclusions from these studies.

## 2.2 Introduction

Nanoparticle-based delivery systems have emerged as an attractive approach for the safe and effective delivery of a diverse range of drugs through altered organ biodistribution and controlled drug release.[102] Upon administration to a biological system, colloidal nanoparticles will encounter and interact with biomacromolecules and cells in their immediate environment over time, following which spontaneous surface-adsorption of biomolecules including proteins occurs. The protein corona- has a fundamental impact on the chemical and biological identity of nanoparticles, and their subsequent biological fate.[73,103]

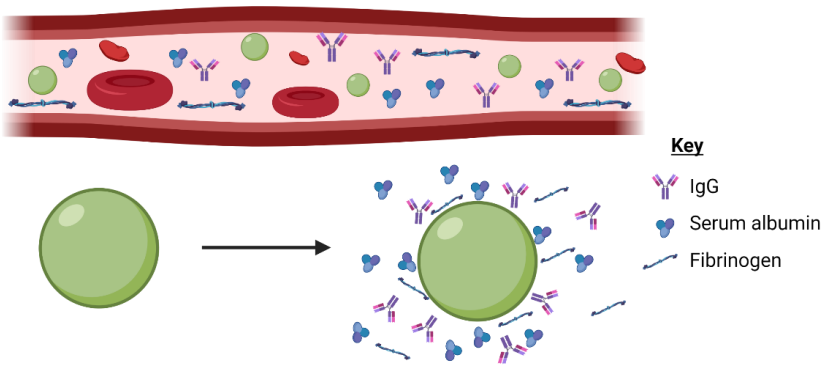


**Figure 2.1.** Graphical representation of nanoparticle protein corona formation following introduction to protein-containing media, and interaction with abundant proteins.

Formation of the protein corona is a process governed by nanoparticle physical and chemical properties, and the composition of biological fluids to which nanoparticles are introduced. A variety of nanoparticle,[103] and biological fluid composition parameters are known to influence this process.[104] Knowledge of the protein corona composition and its impact on nanoparticle physical and chemical characteristics is crucial for understanding protein corona effects on the biological fate of nanomedicines, which can inform the design of novel nanoparticle prototypes with pre-defined target organs, release rates, immune responses, and circulation times.[104,105] These observations have been attributed to the formation of the surface-adsorbed nanoparticle protein corona. More recently, the non-specific adsorption of other biomolecules (e.g., DNA and sugars) has been considered to impact the composition of the protein corona and lead to observed effects on nanoparticle biological fate.[103,106] Though associations between nanoparticle surface charge, morphology and the composition of the protein corona have been reported in numerous studies, a direct comprehensive link between nanoparticle physicochemical properties, composition of the protein corona and biological fate are yet to be established.

The composition of the nanoparticle protein corona is dynamic, complex, and directly dependent on the makeup of the biological media to which the nanoparticle is introduced. The adsorption and desorption rate for each protein on the nanoparticle surface will dictate whether the protein remains as a component of the irreversible corona layer (hard corona) or adsorbs and desorbs (soft corona) in equilibrium with its surrounding environment.[107] Many

nanomedicines are intended for intravenous administration,[108] which will subject them to the forces associated with blood flow rates within the circulatory system, as well as biomolecules and cells contained within blood.[109] Therefore, understanding the role of hemodynamic parameters as a function of nanoparticle circulation time and techniques used to recover nanoparticles for downstream analysis of protein composition, and their implications for nanoparticle-protein interactions and subsequent cellular effects is an important aspect requiring consideration in the early assessment of nanoparticle biological performance.

To develop a deeper understanding of the correlation between nanoparticle attributes and their biological fate, sample handling and preparation protocols, including composition of the biological media, incubation conditions (i.e., temperature, agitation) as well as the recovery and analysis methods of nanoparticles should be carefully considered and selected.[104,105]

Recent studies using liposome nanoparticles functionalised with an outer polyethylene glycol (PEG) molecular layer have shown that protein corona formation is governed by additional parameters beyond nanoparticle surface charge.[110] In addition, the conditions used for nanoparticle incubation with protein containing media, their recovery procedure and the analytical method need to be considered for the comprehensive assessment of novel nanoparticle prototypes for biomedical applications and to enable comparability across multiple studies.

The development process for nanoparticle-based drug formulations includes the in vitro screening of cellular cytotoxicity,[111] cellular interactions and uptake,[112] and intracellular trafficking.[113] Routine *in vitro* experiments typically rely on either serum-free conditions or medium supplemented with foetal bovine serum (FBS) to evaluate the rate and extent of nanoparticle cellular uptake. Limitations associated with these experiments are the non-competitive particle uptake when treating cellular systems with serum-free media, and the lack of biologically-relevant cell culture conditions (i.e., flow, 3D structure).[7]

The goal of the study reported in this chapter was to investigate the impact of nanoparticle surface chemistry on interactions with media containing foetal bovine serum concentrations used in routine cell culture conditions and the resulting physical and chemical properties of the nanoparticle.

Previous work has shown the *in-situ* agglomeration of polymeric nano- and micro-particles following administration to pre-clinical species, an aspect that has not been investigated during *in vitro* assessment of nanoparticle interactions with biological media.[114,115] Specifically, polystyrene latex nanoparticles were used as a model nanoparticle system (due to minimal polymer hydrolysis effects) and employ sample media with the same protein content and composition as those studied for *in vitro* cellular experiments of nanoparticle cellular uptake and biocompatibility evaluation. The centrifugation-resuspension approach was investigated for recovering nanoparticles from biological media, since this is the most routinely-used method in the literature.[50]

In this chapter I demonstrate the differences in nanoparticle protein corona impact on the physicochemical characteristics of nanoparticles in response to different experimental protocols used for the isolation of nanoparticles prior to analysis. With most nanoparticles intended for parenteral administration it becomes crucial to understand the impact of physiological shear flow conditions on nanoparticle-protein interactions and subsequent protein corona formation. Here, the impact of existing nanoparticle recovery approaches and shear flow conditions on nanoparticle parameters following exposure to protein containing media were investigated.

While extensive evaluation of the protein corona composition has been performed in nanoparticles to-date, the impact of co-incubation with protein has been investigated to a lesser extent. Therefore, this study provided new insights into how sample handling procedures during nanoparticle protein corona recovery can have such profound impacts on sample characteristics and the nanoparticle corona composition.

## 2.3 Materials and Methodology

## 2.4 Materials

Unmodified (Cat #LB1, Merck, Glasgow, UK), carboxylate- (Cat #F-8803, ThermoFisher, Renfrew, Renfrewshire, UK) and amine-modified (Cat #L9904, Merck, Glasgow, UK) polystyrene latex nanoparticles were used for all the measurements reported in this study. FBS was purchased from Fisher Scientific (Invitrogen, Renfrew, Renfrewshire, UK) and centrifuged to remove any large agglomerates prior to use. Phosphate-Buffered Saline (PBS) was purchased from Fisher Scientific (Invitrogen, Renfrew, Renfrewshire, UK). Mini-PROTEAN TGX precast Gels (Cat#4561094) and 4X Laemmeli sample buffer (Cat#1610747) were purchased from Bio-Rad (Bio-Rad Laboratories, Watford, Hertfordshire, WD17 1ET) used for SDS-PAGE analysis. The QC Colloidal Coomassie Stain (Bio-rad, Hertfordshire, UK, #1610803) was used for gel staining.

## 2.5 Methods

### 2.5.1 Sample Preparation

Polystyrene latex nanoparticles (100 nm particle diameter for all surface chemistries) with different surface chemistries (unmodified, amine-modified, and carboxylate-modified) stock were prepared to maintain the same polymer equivalent concentration of 1 mg/mL (corresponding to a total polystyrene latex nanoparticle number of ~ 1.83 x$10^{12}$ particles/mL) across all samples studied. The following equation was used to determine the total particle concentration used in every experiment for consistent normalization of sample concentration relative to protein across all three sample chemistries studied.

$$N = \frac{(6 \times 10^{10}) \times S \times P_L}{\pi \times P_S \times d^3} \qquad \textbf{(Equation 2.1)}$$

Where $S$ is the concentration of solids expressed in *% w/w*, d the diameter in µm, $P_L$ the density of latex in g/mL, and $P_S$ the density of the bulk polymer in g/mL. The concentration of foetal bovine serum (FBS) selected (10% *v/v*, corresponding to 3.9 mg/mL total protein concentration), was used to

represent the composition and concentration of protein used in cell culture-based experiments.

Incubations in the absence of shear flow for protein corona incubation experiments, polystyrene latex nanoparticles were dispersed in either PBS (control), or PBS containing 10 %vol FBS and incubated for 2 hour and 24-hour periods in a low protein-binding microcentrifuge tube in a temperature-controlled room (37 °C).

Incubation of samples under flow for samples subjected to biologically relevant flow conditions, a peristaltic pump (Cole Palmer, Cambridgeshire, UK) was used to control flow and recirculate nanoparticle suspensions dispersed in either PBS or 10% vol FBS were introduced to tubing (Cole Palmer, #WZ-06411-62, 1.6 mm. inner diameter and 3.2 mm outer diameter) at 37 °C for 2 hours at (0.85 cm/s) and (8.5 cm/s) to mimic median cubital vein and arterial blood flow conditions, respectively.[56,116]

Nanoparticle recovery following incubation in either PBS or 10 %vol FBS in the absence and presence of flow, was performed by three centrifugation-resuspension cycles to remove unbound proteins from bulk incubation media. Nanoparticle samples were subjected to three centrifugation-resuspension cycles in a pre-chilled centrifuge (4 °C) to reduce any further nanoparticle-protein, and protein-protein interactions.

### 2.5.2 Sample Analysis

#### Dynamic Light Scattering (DLS) and Electrophoretic Light Scattering

A Zetasizer Nano ZS (Malvern Panalytical, Malvern, UK) equipped with a 633 nm Helium-Neon laser was used for all DLS measurements. Nanoparticle size and polydispersity index (PDI) were measured prior to and following recovery from incubation media (PBS control or 10 %vol FBS, following 2- and 24-hour incubation) in non-invasive backscatter mode (173°). All measurements were performed using three independent biological replicates, with five technical replicates for each biological replicate.

**Electrophoretic Light Scattering** was performed to measure changes in the zeta potential of the nanoparticles following recovery from incubation media,

and the Smoluchowski approximation was used for data processing. All size and zeta potential measurements were performed at 25 °C with 120 second equilibration time. The mean (±standard error) for each sample was determined from five independent technical replicates.

**Particle Tracking Analysis (PTA)**

PTA measurements were performed to measure the number-based distribution of the spherical-equivalent hydrodynamic diameter of particles suspended in PBS (control particles and particles recovered following incubation in protein-containing medium) and treatment medium (*in situ* analysis). These measurements were performed using the NanoSight NS300 system (Malvern Panalytical, Malvern, UK) equipped with a 488 nm laser module and a high-sensitivity CMOS camera. Five, 60-second videos were acquired for all measurement and averaged. All samples were analysed under constant flow conditions (flow setting 100) and at ambient temperature (~25 °C). The video capture parameters were set at a camera level of 6, with post-processing analyses being performed at a detection threshold of 4. Data were analysed using the NTA software (v3.4.0.0.3). Three biological replicates and five technical replicates were performed for each sample.

### 2.5.3 Protein Quantification

Analysis of protein content was performed following a centrifugation-resuspension protocol for the isolation of incubated nanoparticles from incubation media. Isolated samples were treated with Laemmli buffer and detergent overnight at ambient temperature (25 °C) under gentle agitation to elute proteins, followed by centrifugation to recover the proteins. The total protein content was quantified using the 660-nm protein assay (ThermoFisher, Rockford, USA) as per the manufacturer's instruction, and absorbance measurements were performed at 660 nm using a FlexStation III Microplate Reader (Molecular Devices, UK).

### 2.5.4 SDS-PAGE

The composition and relative abundance of proteins eluted from the polystyrene latex nanoparticles was analysed with SDS-PAGE. In brief, following quantification of the total protein content eluted from isolated polystyrene nanoparticles, a sample containing 20 µg of protein was loaded onto each lane of a Mini-Protean 4-20 % Pre-cast gel. The Coomassie Stain was used to stain all gels as per manufacturer instructions. All gels were imaged using the Bio-RAD Gel Doc EZ imaging system.

### 2.5.5 Statistical Analysis

Unless otherwise stated, all experimental conditions were performed using a minimum of three biological replicates, and a one-way analysis of variation (ANOVA) was performed to compare the impact of incubation parameters on nanoparticle properties. A Shapiro-Wilks normality test was performed on all datasets, and for non-normal data the Kruskal-Wallis test was used to compare nanoparticle samples subjected to flow conditions versus non-incubated baseline conditions (Control). All statistical analyses were performed in Prism (v. 8.0.1).

## 2.6 Results

Nanoparticle analysis following treatment with protein containing media and a comparison of centrifugation-resuspension effects versus *in situ* measurements with PTA Multiparametric measurement of changes occurring in polystyrene latex nanoparticles following treatment in protein-containing media (10% vol, corresponding to 3.9 mg/mL total protein concentration) was carried out following incubations up to 24 hours at 37 ℃. Global patterns of nanoparticle parameter changes were tracked to map changes as a function of incubation time and nanoparticle surface chemistry.

**Analysis of polystyrene latex nanoparticle physical stability in PBS**

Prior to performing studies of polystyrene latex nanoparticle interactions with FBS containing media, their stability was studied under refrigerated and at physiologically relevant temperature in PBS for up to 24 hours. DLS was used to measure any changes occurring in nanoparticle size and zeta potential.

A summary of the parameters obtained from this analysis across the three different nanoparticle surface chemistries is represented in **Table 2.1**.

**Table 2.1** Measurements of particle size (mean ± standard deviation), polydispersity index (PDI, mean ± standard deviation), and zeta potential for latex polystyrene and amine-modified latex nanoparticles dispersed in PBS and water as measured using the Zetasizer Nano ZS at (4 and 37 ℃).

| Samples | Temperature (°C) | Size (nm) | PDI | Zeta potential (mV) |
|---|---|---|---|---|
| **Unmodified** | 4 | 127±1.2 | 0.04±0.02 | -38.8±1.0 |
| **Unmodified** | 37 | 128±2.3 | 0.03±0.01 | -38.8±1.0 |
| **Amine-modified** | 4 | 94±4.0 | 0.08±0.01 | 62.5±1.2 |
| **Amine-modified** | 37 | 94±1.8 | 0.07±0.02 | 62.5±1.2 |
| **Carboxylate-modified** | 4 | 113±0.6 | 0.01±0.0.01 | -36.9±1.0 |
| **Carboxylate-modified** | 37 | 112±0.4 | 0.01±0.01 | -36.4±1.1 |

Following the establishment of stability in the buffer in the absence of protein, polystyrene latex nanoparticles were incubated for 2- and 24-hour durations at 37 °C. Corresponding trends for each particle type in response to incubation are represented in Figure 2.2:

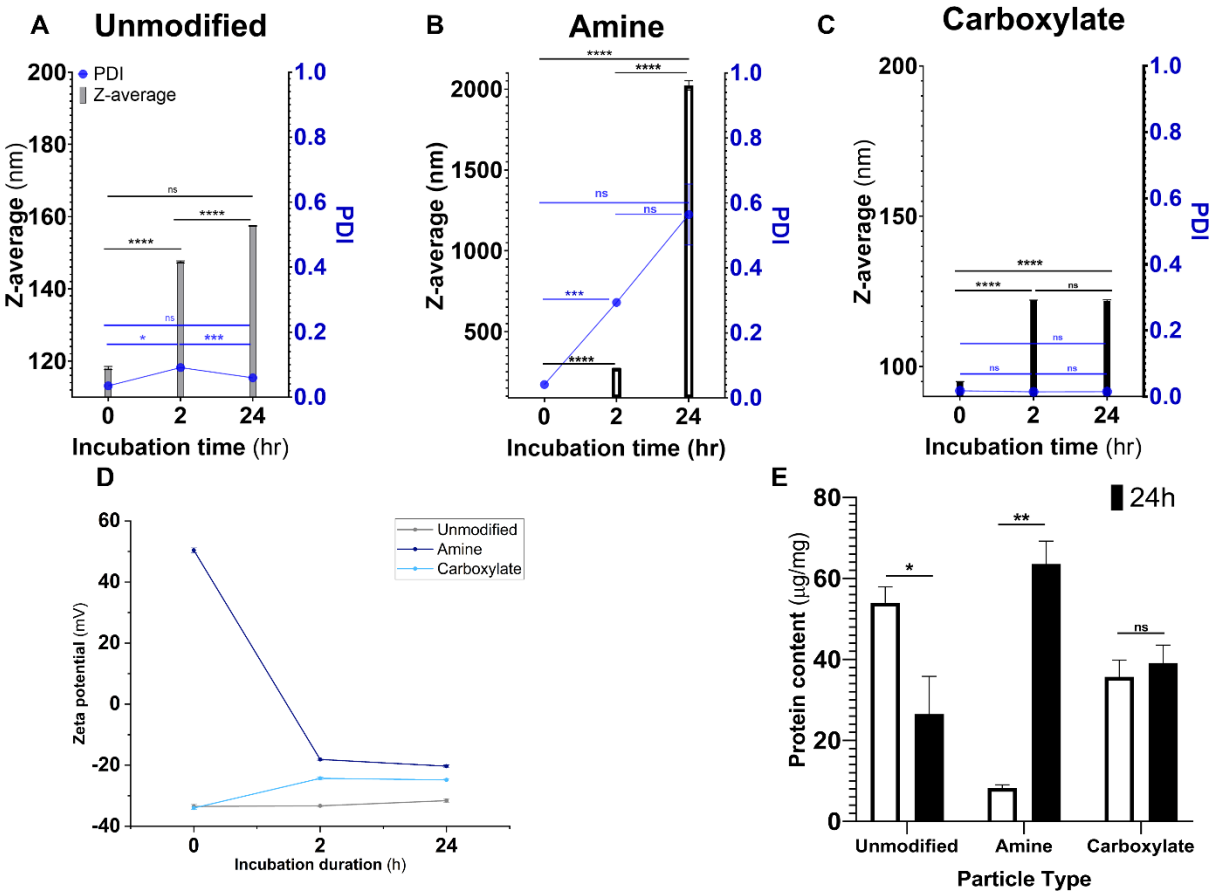


**Figure 2.2** Differential trends in nanoparticle physicochemical parameters following incubation with protein containing media and isolation using centrifugation-wash. Mean (± standard error) z-average and polydispersity index (PDI) measured by DLS (A-C), and corresponding mean (±standard error) zeta potential for polystyrene latex nanoparticles (unmodified, amine, and carboxylate) nanoparticles (D) and changes in mean (±standard error) measured protein concentration at 2- and 24-hour incubations (E) for nanoparticles recovered from media containing 10% vol FBS (3.9 mg/mL total protein concentration) following a 2- and 24-hour incubation using the centrifugation-resuspension approach (n=3). All nanoparticles were recovered using the centrifugation-resuspension approach (n=3). * P<0.05, ** P<0.01, *** P<0.001, **** P<0.0001, ns: non-significant, following a Kruskal-Wallis for (A-C) and a single factor ANOVA for E.

Measured baseline characteristics for each nanoparticle were in the manufacturer specified size range (100 nm diameter, PDI ≤0.1). The z-average significantly increased from baseline (0 hr) to 24 hr treatment for amine-, carboxylate- modified and untreated polystyrene latex nanoparticles with 126%, 36.2% and 28.7% increases in nanoparticle diameters measured by DLS (Figure 2.2 A-C), respectively. The extent of measured nanoparticle diameter increase observed was most significant between 0 hour and 2-hour incubation measurements. This observed increase in mean particle diameter (69.8%) was accompanied by an increase in PDI for amine-modified nanoparticles, while the extent of diameter increase was to a lesser extent in the case of carboxylate- and unmodified nanoparticles. An increase in particle mean size was also observed in PTA-measured diameters, with a corresponding 36.3% (carboxylate), and 28.8% (unmodified) increase in particle size relative to control following incubation. PTA was used as an orthogonal higher resolution particle sizing technique for measuring changes in particle size following exposure to protein-containing media.

Nanoparticle surface charge plays an important role in nanoparticle-protein interactions, with zeta potential changes observed following incubation with protein-containing media for all samples. The most significant change in zeta potential was observed in the amine-modified nanoparticles (+50.4 at baseline to -18.1 mV at 2 hours, and -20.3 mV at 24 hours). A small change in zeta potential was observed for unmodified nanoparticles from -33.5 mV to -31.6 mV following 24-hours. The zeta potential of negatively charged carboxylate-modified nanoparticles changed from -34.0 mV at baseline, to -24.3 mV at 2 hours with no further change in zeta potential at 24 hours (-24.8 mV) (Figure 2.2D). These results overall indicate that nanoparticle-protein interactions occur to a lesser extent with the negatively-charged polystyrene latex nanoparticles.

Total protein content measured was observed to be the highest following 24 hours incubation for amine-modified, carboxylate-modified and unmodified nanoparticles in descending order of detected protein content. There was no

statistically significant difference in protein content measured for 2 hour and 24 hour incubations for carboxylate-modified nanoparticles with only unmodified (half protein content at 24 hours versus 2 hours) and amine-modified (8-fold increase in protein content at 24 hours versus 2 hours) nanoparticles showing a significant change in protein content following 24-hr incubation (**Figure 2.2E**).

## 2.7 Measurement of nanoparticle properties following incubation under shear flow.

Unmodified, amine-modified, and carboxylate-modified polystyrene latex nanoparticles were incubated for 2 hours and subjected to shear flow conditions of 0.85 cm/s (mimicking median cubital vein blood flow) and 8.5 cm/s (mimicking arterial blood flow) and recirculated using a previously described method.[59]

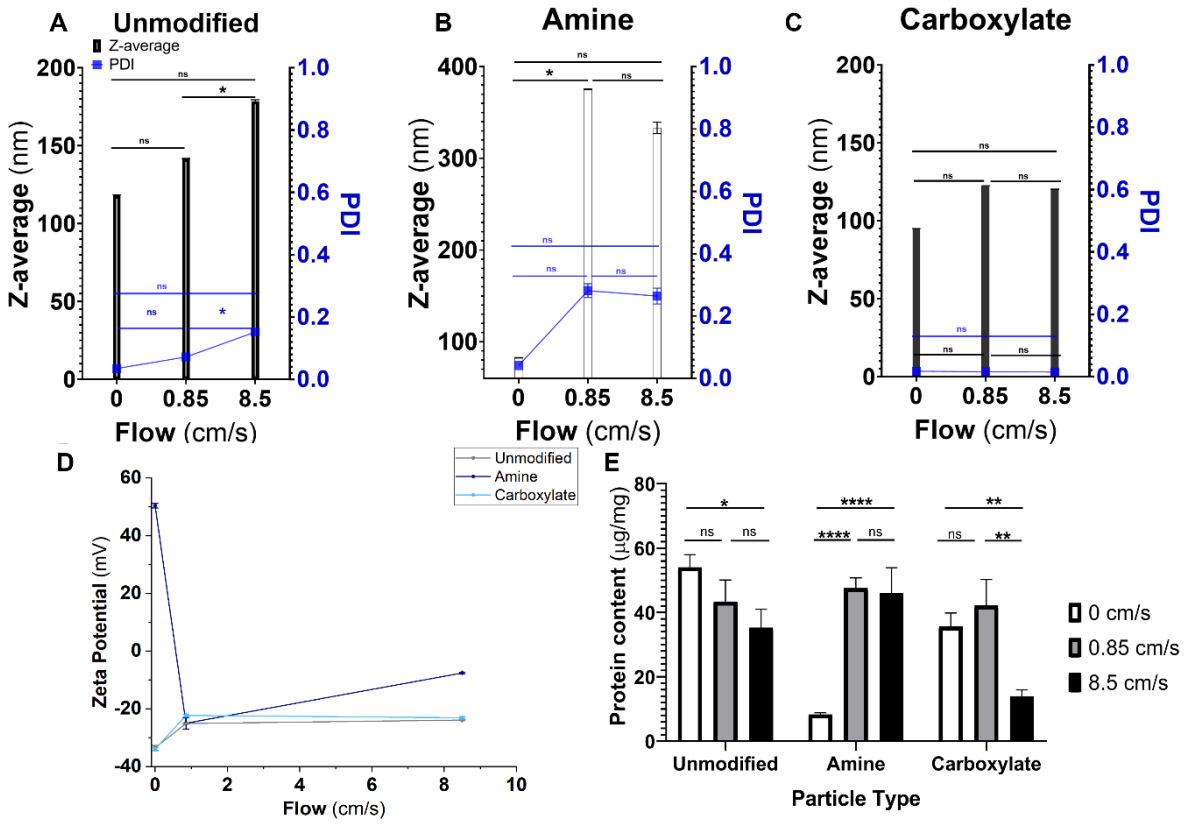


**Figure 2.3** Trends in nanoparticle physicochemical parameters after incubation with protein containing media under different flow conditions and centrifugation-wash recovery. Trends in nanoparticle Z-average and PDI as measured by DLS (A-C), and changes in zeta potential change occurring for polystyrene latex nanoparticles (unmodified, amine, and carboxylate) nanoparticles (D) and changes in protein concentration as a function of incubation time (E) for nanoparticles recovered from media containing 10% vol FBS (3.9 mg/mL total protein concentration) following a 2 hour incubation under 0 (static), 0.85 and 8.5 cm/sec shear flow. All nanoparticles were recovered using the centrifugation-resuspension approach (n=3). * P<0.05, ** P<0.01, *** P<0.001, **** P<0.0001, ns: not significant following a Kruskal-Wallis for (A-C) and a single factor ANOVA for E.

A significant increase in nanoparticle size was observed for all particles studied following incubation within protein media under physiological shear flow conditions (median cubital vein) with a 31% increase in mean diameter observed for unmodified particles (versus baseline), and a 24% increase for carboxylate-modified nanoparticles. The most significant increase in mean diameter was observed for amine-modified particles with a 118 % increase. A further increase in mean particle diameter (49%) was observed for unmodified particles when incubated under higher shear flow conditions (8.5 cm/s) (**Figure 2.3A-C**).

The results suggest a change in particle-protein interactions when incubated under shear flow conditions with overall trends in size analysis showing significant changes occurring in particle size across nanoparticle surface chemistries in response to different shear flow rates. This is further supported by the shift in zeta potential from (-25 ± 2 mV) at 0.85 cm/s to (-7.6 ± 0.3 mV) at 8.5 cm/s for amine-modified nanoparticles which indicates a change in the protein corona composition (**Figure 2.3D**). The observed shifts in zeta potential for amine-modified nanoparticles were consistent with changes in measured adsorbed protein content, where the most significant increase in protein concentration was observed between static and 0.85 cm/s flow conditions (8-fold increase), with no significant change in measured protein content observed between 0.85 and 8.5 cm/s flow conditions. In the case of unmodified and carboxylate-modified nanoparticles only small changes were observed between static and 0.85 cm/s flow conditions, with a reduction in protein concentration observed at higher shear flow rate conditions (i.e., 8.5 cm/s).

## 2.8 The impact of the centrifugation-resuspension recovery process on nanoparticle size as measured by particle tracking analysis.

### Time-based incubations

Unmodified, amine-modified, and carboxylate-modified polystyrene latex nanoparticles were incubated at 37 ˚C for 2 and 24 hours in incubation media, and isolated using the centrifugation-resuspension method. In parallel, additional samples were incubated with treatment media for 2 and 24 hours and analysed with PTA without recovering the nanoparticles (*in situ*) from protein incubation medium **(Figure 2.4**).

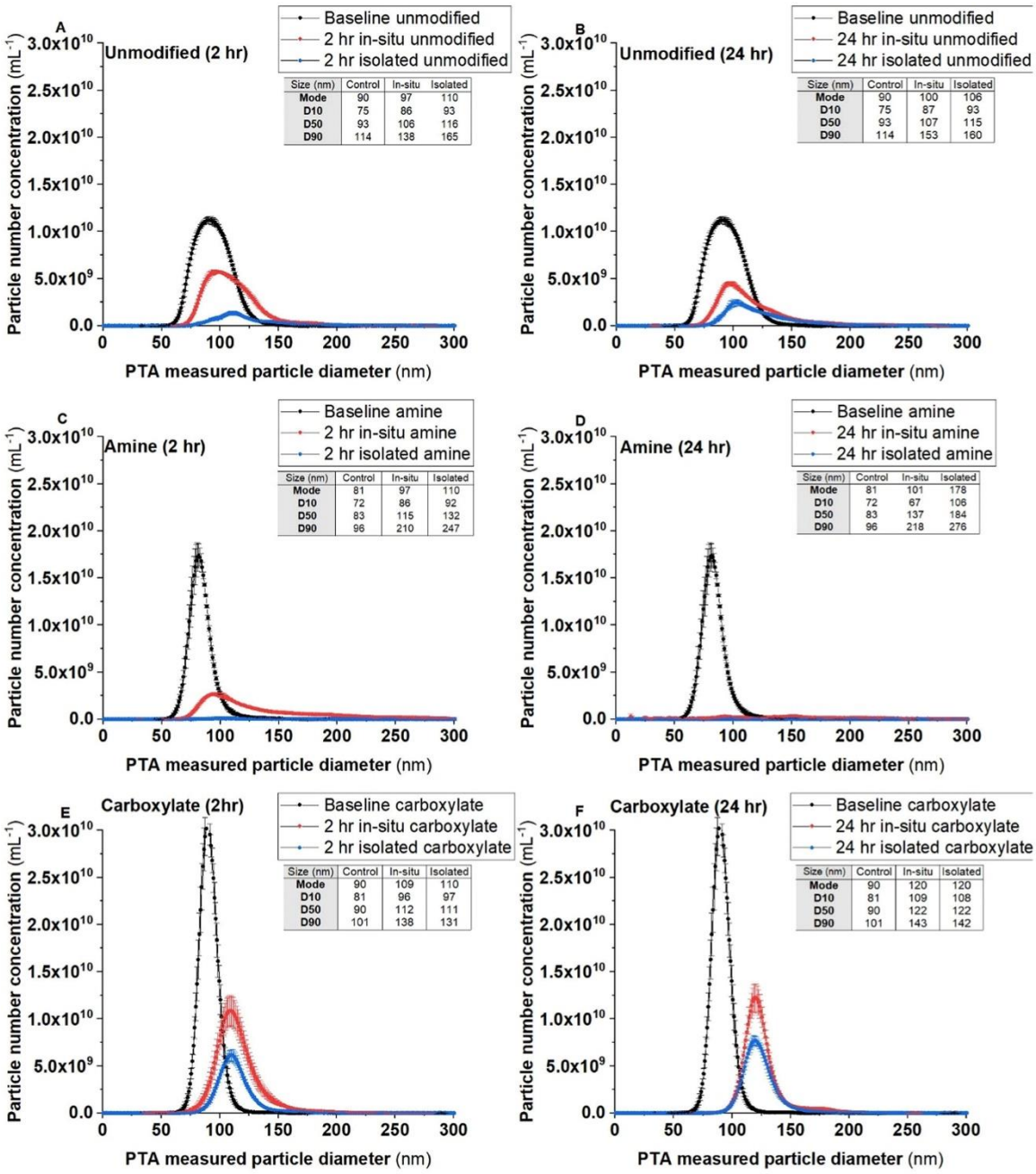


**Figure 2.4**. PTA particle size distributions for A) unmodified (2 hour), B) unmodified (24 hour), C) amine- (2 hour), D) amine- (24 hour), E) carboxylate- (2 hour), and F) carboxylate-modified (24 hour) polystyrene latex nanoparticles measured following incubation with treatment medium (mean ± standard error, n=3). The size distributions represented in each graph are control measurements (black), *in-situ* measurement (red) and nanoparticles isolated using centrifugation-resuspension process (blue).

For all polystyrene latex nanoparticle samples, the *in situ* analysis of particle size distribution showed a reduction in nanoparticle concentration across all sample types following 2 hour and 24 hour incubation in protein media at 37 ℃. Consistent with this observation, peak broadening of the size distribution to higher sizes was observed across all nanoparticle types examined. This observation is consistent with particle agglomeration, which resulted in lower

particle concentration and the emergence of nanoparticles at higher size distributions. It is also likely that protein-particle agglomerates were formed and precipitated prior to measurement.

This observed effect was absent for all polystyrene latex nanoparticle samples incubated in PBS without protein. Corresponding PTA measurement data obtained for *in situ* analysis and centrifugation resuspension protocols are presented below in **Figure 2.5** and **Figure 2.6**, respectively.

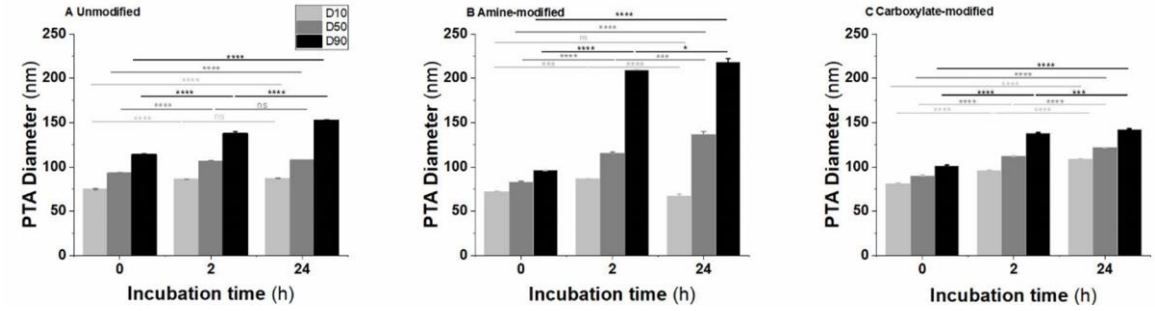


**Figure 2.5** Incubation time differentially impacts polystyrene nanoparticles with different surface chemistries under *in situ* analytical conditions. Corresponding measured mean (± standard error) PTA particle diameters (D10, D50, D90) values for (A) unmodified (B) amine-modified, and (C) carboxylate-modified polystyrene latex nanoparticles incubated in 10% vol FBS, followed by direct analysis with PTA (*in situ*, n=3). ns: not significant, * P<0.05, ** P<0.01, *** P<0.001, **** P<0.0001, following a Kruskal-Wallis for (A-C) and a single factor ANOVA.

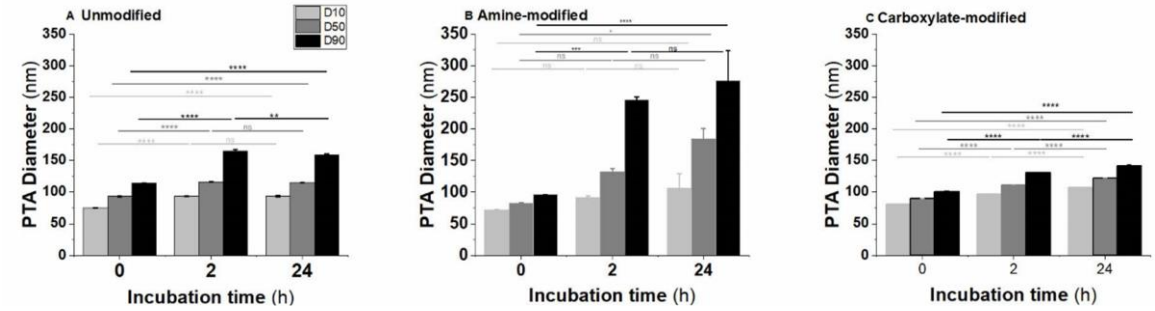


**Figure 2.6** Incubation time differentially impacts polystyrene nanoparticles with different surface chemistries. Corresponding measured mean (± standard error) PTA particle diameters (D10, D50, D90) values for (A) unmodified (B) amine-modified, and (C) carboxylate-modified polystyrene latex nanoparticles incubated in 10% vol FBS, followed by centrifugation-resuspension isolation, and subsequent PTA analysis (n=3). ns: not significant, * P<0.05, ** P<0.01, *** P<0.001, **** P<0.0001, following a Kruskal-Wallis for (A-C) and a single factor ANOVA.

When comparing the particle concentration detected by PTA between *in situ* measurements and nanoparticles recovered using the centrifugation-resuspension

protocol, a notable reduction in particle concentration was observed across all samples for particles isolated from protein-containing treatment media. Amine-modified polystyrene nanoparticle size was the most susceptible to effects of the particle recovery protocol (**Figure 2.4**). This is likely caused by agglomerates formed from nanoparticle-protein and protein-protein interactions which cannot be measured using PTA or may have precipitated. A summary of the measured nanoparticle attributes at the different incubation timepoints is included in **Table 2.2** as follows:

**Table 2.2** PTA-measured diameter, Z-average (DLS), polydispersity index (PDI), zeta (ζ) potential and measured protein content of polystyrene latex nanoparticles (microgram per milligram of nanoparticle, expressed as μg/mg). The protein-treated samples were measured before and following 2 hour and 24-hour incubation in protein media (10% vol FBS in PBS, 3.9 mg/mL total protein content) and isolation using a centrifugation-resuspension process (mean ± standard error, n=3). ND: Not detected.

| Incubation time | PTA-measured Diameter (nm) | Z-average (nm) | PDI | ζ-Potential (mV) | Protein content (μg/mg) |
|---|---|---|---|---|---|
| **Unmodified** | | | | | |
| 0 h | 94.3 ± 0.6 | 118.1 ± 0.5 | 0.035 ± 0.003 | -33.5 ± 0.8 | ND |
| 2 h | 124.3 ± 0.9 | 147.4 ± 0.3 | 0.091 ± 0.009 | -33.3 ± 0.4 | 54 ± 2 |
| 24 h | 121.5 ± 0.5 | 157.4 ± 0.2 | 0.059 ± 0.006 | -31.6 ± 0.6 | 27 ± 5 |
| **Amine** | | | | | |
| 0 h | 84.0 ± 0.5 | 82.4 ± 0.2 | 0.041 ± 0.007 | +50.4 ± 0.8 | ND |
| 2 h | 151 ± 1 | 273.1 ± 0.8 | 0.294 ± 0.009 | -18.1 ± 0.3 | 8 ± 1 |
| 24 h | 190 ± 20 | 2020 ± 30 | 0.56 ± 0.09 | -20.3 ± 0.4 | 64 ± 3 |
| **Carboxylate** | | | | | |
| 0 h | 91.1 ± 0.6 | 94.9 ± 0.2 | 0.017 ± 0.002 | -34.0 ± 0.5 | ND |
| 2 h | 113.7 ± 0.0 | 121.9 ± 0.2 | 0.015 ± 0.001 | -24.3 ± 0.4 | 36 ± 2 |
| 24 h | 124.2 ± 0.1 | 121.8 ± 0.3 | 0.015 ± 0.002 | -24.8 ± 0.4 | 39 ± 3 |

### Incubation under shear flow

Polystyrene latex nanoparticles were incubated for 2 hours under shear flow mimicking the median cubital venous (0.85 cm/s) and arterial (8.5 cm/s) blood flow rates, and nanoparticles isolated by centrifugation-resuspension. In parallel, samples were treated under the same conditions and directly analyzed with PTA in the protein medium (*in situ* analysis).

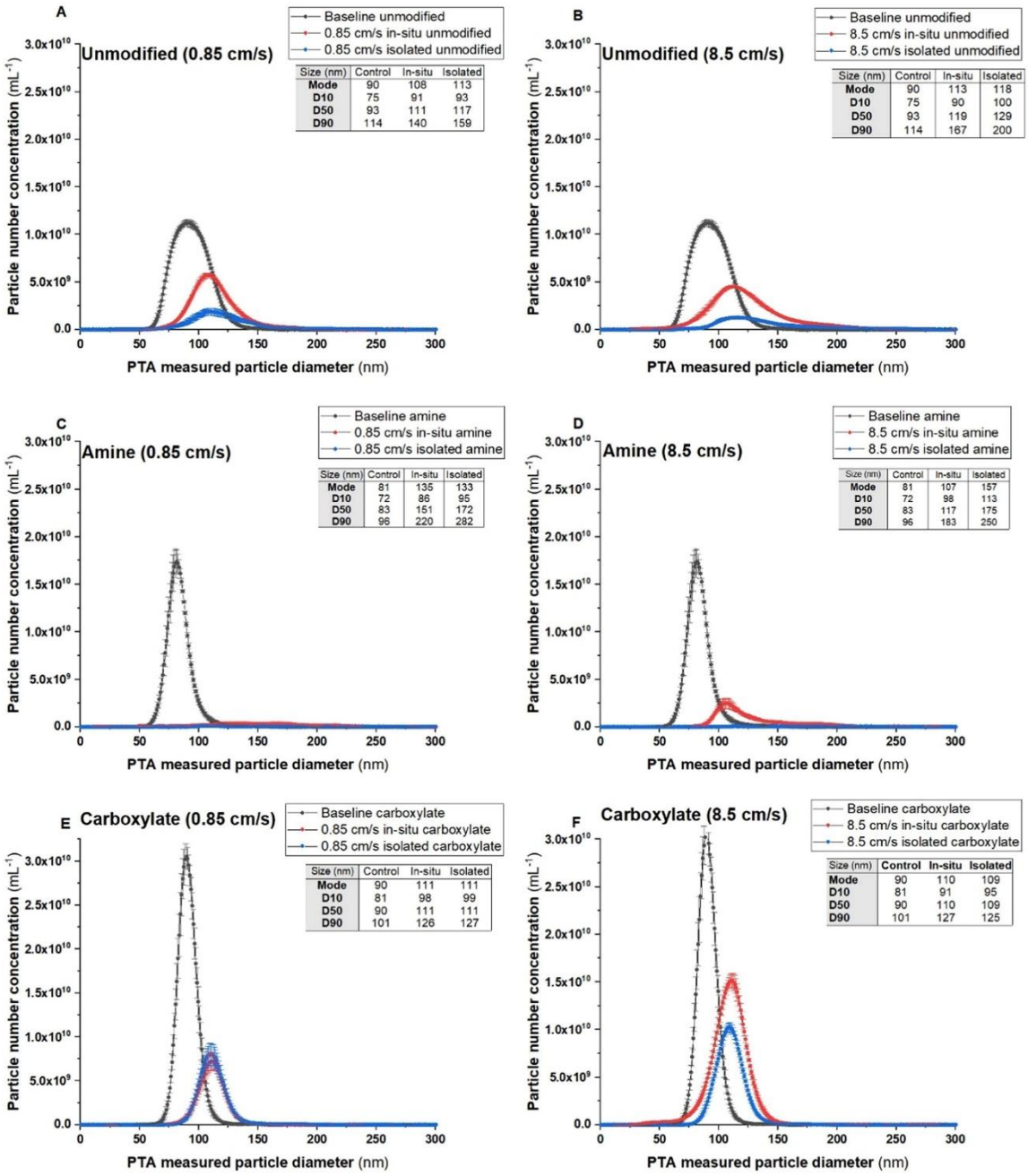


**Figure 2.7**. The centrifugation-resuspension isolation protocols alters the nanoparticle concentration and particle size distribution. With A) unmodified (0.85 cm/s), B) unmodified (8.5 cm/s), C) amine- (0.85 cm/s), D) amine- (8.5 cm/s), E) carboxylate- (0.85 cm/s), and F) carboxylate-modified (8.5 cm/s) polystyrene latex nanoparticles measured after 2 hour incubation with 10% vol FBS at 0.85 cm/s and 8.5 cm/s, (mean and standard error, n=3). One-way ANOVA with Tukey's comparison test was performed to determine significant difference. Corresponding traces represented are control measurements (black), in-situ measurement (red) and nanoparticles isolated by centrifugation-resuspension (blue).

*In situ* analysis of particle size following incubation at 37℃ for 2 hours under shear flow (0.85 cm/s and 8.5 cm/s) showed an overall reduction in particle concentration across all surface modifications, with amine-modified particles showing the most significant decrease in the number of particles detected. As shown with previous measurements, this trend is accompanied by an increase

in mean particle diameter and peak broadening across all particles examined. Particles incubated in PBS in the absence of protein did not show this effect. There was a further decrease in particle concentration detected by PTA measurements across all polystyrene latex nanoparticles following recovery by centrifugation-resuspension.

PTA analysis for samples at (8.5 cm/s) (**Figure 2.7**) showed a shift to larger sizes in comparison to samples incubated at 0.85 cm/s and 2-hour static (**Figure 2.4**) conditions across all particle types. Further PTA analysis showed a widening of the particle size distribution span for unmodified nanoparticles with a baseline span of 0.42, which increased to 0.62 (isolated), and 0.49 (*in situ*) following 2-hour incubation (**Table 2.4**). Under shear flow conditions an increase in particle size distribution span to 0.45 (*in situ*), and 0.56 (isolated) was observed following incubation at (0.85 cm/s). A similar increase was seen for particles incubated at (8.5 cm/s) with a particle size distribution span increase to 0.65 (*in situ*) and 0.78 (isolated) (**Table 2.4**).

Amine- and carboxylate-modified nanoparticles showed a decrease in particle size span in comparison to static incubation (2 hours) following incubation under shear flow conditions (0.85 cm/s, 8.5 cm/s).

Corresponding PTA measured diameter data obtained for these measurements are presented as follows:

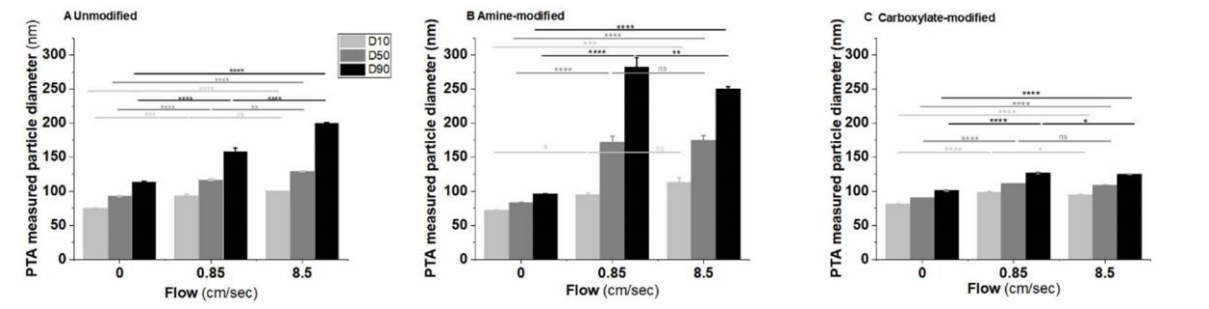


**Figure 2.8** Shear flow conditions differentially impact polystyrene nanoparticles with different surface chemistry. Corresponding mean (± standard error) PTA-measured particle diameters (D10, D50, D90) for (A) unmodified (B) amine-modified, and (C) carboxylate-modified polystyrene latex nanoparticles incubated for 2 hours with 10% vol FBS under 0.85 cm/s and 8.5 cm/s flow speeds and isolated from media using the centrifugation-resuspension protocol (n=3 biological replicates). ns: not significant, * P<0.05, ** P<0.01, *** P<0.001, **** P<0.0001, following a Kruskal-Wallis for (A-C) and a single factor ANOVA.

This observation is likely a consequence of an increase in particle-protein interactions due to increased contact between particles and protein under shear flow conditions leading to an emergence of particle sub-populations within the sample and the formation of large agglomerates which precipitate and can no longer be measured using PTA.

Key measured attributes and corresponding parameters at different flow rates for 2-hour incubations are summarised as follows:

**Table 2.3** Table summarising measured polystyrene latex nanoparticle attributes in this chapter. PTA-measured mean diameter, DLS measured z-average, and polydispersity (PDI), ζ-potential, and protein content measured for polystyrene latex nanoparticles (μg protein per milligram of polystyrene latex concentration) in protein containing samples under control and shear flow. The samples were measured before and after incubation in protein media (10% vol FBS in PBS) under a 0, 0.85 and 8.5 cm/s incubation flow rate, and following isolation using a centrifugation-resuspension process (mean ± standard error, n=3 biological replicates). ND: Not detected

| Flow rate | PTA-measured Diameter (nm) | Z-average (nm) | PDI | ζ-Potential (mV) | Protein content (μg/mg) |
|---|---|---|---|---|---|
| Unmodified | | | | | |
| 0 hr | 94.3 ± 0.6 | 118.1± 0.5 | 0.035 ± 0.003 | -33.5 ± 0.8 | ND |
| 0 cm/s | 124.3 ± 0.9 | 147.4 ± 0.3 | 0.091 ± 0.009 | -33.3 ± 0.4 | 54 ± 2 |
| 0.85 cm/s | 123 ± 2 | 141.4 ± 0.4 | 0.072 ± 0.005 | -25.1 ± 0.2 | 43 ± 6 |
| 8.5 cm/s | 140.0 ± 0.3 | 179 ± 1 | 0.152 ± 0.007 | -23.9 ± 0.2 | 35 ± 5 |
| Amine | | | | | |
| 0 hr | 84.0±0.5 | 82.4±0.2 | 0.041 ± 0.007 | +50.4 ± 0.8 | ND |
| 0 cm/s | 151 ± 1 | 273.1 ± 0.8 | 0.294 ± 0.009 | -18.1 ± 0.3 | 8 ± 1 |
| 0.85 cm/s | 181 ± 4 | 375.4 ± 0.4 | 0.280± 0.020 | -25 ± 2.0 | 48 ± 2 |
| 8.5 cm/s | 178 ± 5 | 333.0 ± 6 .0 | 0.260 ± 0.030 | -7.6 ± 0.3 | 45 ± 4 |
| Carboxylate | | | | | |
| 0 hr | 91.1 ± 0.6 | 94.9 ± 0.2 | 0.017 ± 0.002 | -34.0 ± 0.5 | ND |
| 0 cm/s | 113.7 ± 0.0 | 121.9 ± 0.2 | 0.015 ± 0.001 | -24.3 ± 0.4 | 36 ± 2 |
| 0.85 cm/s | 112.9 ± 0.4 | 122.1 ± 0.5 | 0.015 ± 0.001 | -22.3 ± 0.4 | 42 ± 5 |
| 8.5 cm/s | 110.2 ± 0.5 | 119.9 ± 0.4 | 0.015 ± 0.002 | -23.1 ± 0.4 | 14 ± 1 |

A summary of the PTA- measured particle size distribution span as a function of polystyrene latex nanoparticle type and incubation duration with 10% vol FBS and flow rate conditions is summarised below:

**Table 2.4** Representative polystyrene latex nanoparticle particle size distribution spans measured for the *in situ* and isolated polystyrene latex nanoparticles calculated from PTA size distributions (N=3).

| Sample | *In situ* | Isolated |
|---|---|---|
| **Unmodified** | | |
| **Control (0h)** | N/A | 0.42±0.00 |
| **2 h** | 0.49±0.02 | 0.62±0.02 |
| **24 h** | 0.62±0.01 | 0.58±0.02 |
| **0.85 cm/s** | 0.45±0.01 | 0.56±0.02 |
| **8.5 cm/s** | 0.65±0.02 | 0.78±0.01 |
| **Amine-modified** | | |
| **Control (0h)** | N/A | 0.29±0.09 |
| **2 h** | 1.08±0.02 | 1.17±0.06 |
| **24 h** | 1.11±0.05 | 1.08±0.28 |
| **0.85 cm/s** | 0.92±0.03 | 1.09±0.05 |
| **8.5 cm/s** | 0.73±0.04 | 0.80±0.09 |
| **Carboxylate-modified** | | |
| **Control (0h)** | N/A | 0.23±0.01 |
| **2 h** | 0.38±0.02 | 0.31±0.00 |
| **24 h** | 0.28±0.01 | 0.28±0.01 |
| **0.85 cm/s** | 0.24±0.01 | 0.26±0.02 |
| **8.5 cm/s** | 0.34±0.02 | 0.27±0.00 |

Analysis of compositional changes in surface-adsorbed proteins in response to sample incubation and isolation conditions.

For comparison of the composition of surface-adsorbed proteins across the particle chemistry and incubation parameters, SDS-PAGE analysis was performed following the incubation of nanoparticle samples for pre-defined times (2- and 24-hours) and shear flow conditions (0.85 and 8.5 cm/s). Nanoparticles were recovered from incubation media using the centrifugation-

resuspension process, and the surface-adsorbed proteins eluted from the nanoparticles prior to loading onto SDS-PAGE gels (**Figure 2.9**).

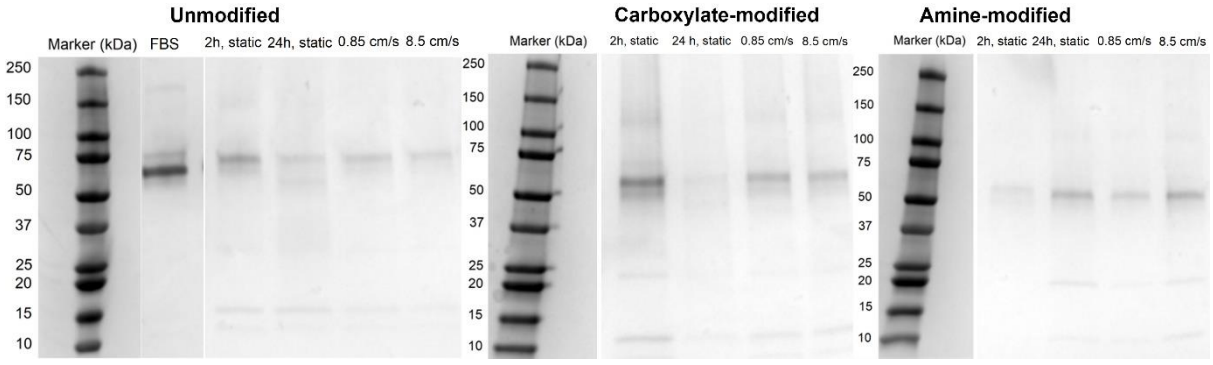


**Figure 2.9.** Protein isolated from polystyrene latex nanoparticles after 2- and 24-hour incubations under static (0 cm/s) and shear flow (0.85 and 8.5 cm/s) conditions. Corresponding SDS-PAGE gel images. 20 µg of protein was loaded per lane and all gels were stained with QC Colloidal Coomassie Stain and imaged. Marker: molecular weight marker (Kaleidoscope ladder); FBS: foetal bovine serum.

Multiple protein bands were detected for each sample type, predominantly occurring at 60 which was likely bovine serum albumin.[117,118] Bands corresponding to lower molecular weight species were also observed at 12 and 25 kDa.

In parallel to analysis of protein corona fingerprint normalized to total eluted protein content, we also performed SDS-PAGE analysis of protein fingerprint for 20 µL of eluted protein sample, in the absence of protein content normalisation to compare differences in protein corona fingerprint based on sample volume.

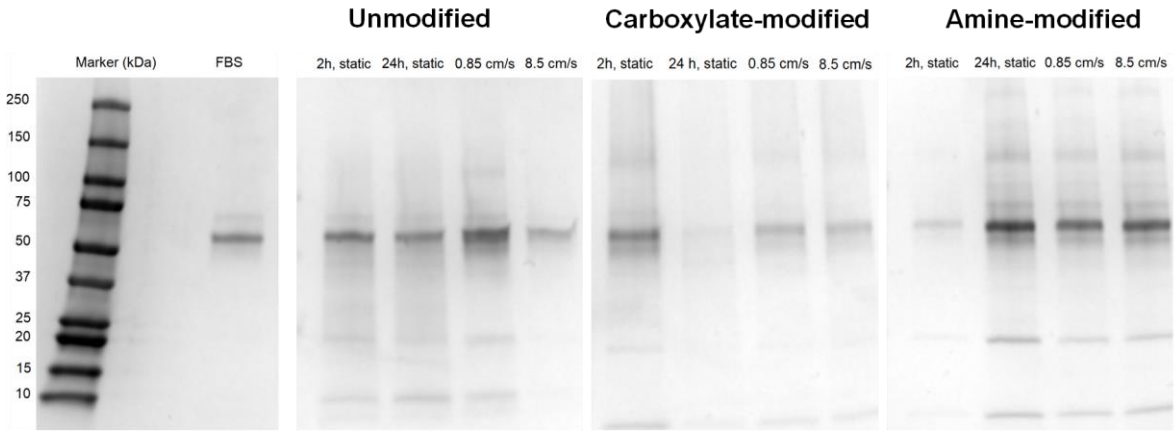


**Figure 2.10** Representative panel of Coomassie stained SDS-PAGE gels for unmodified, carboxylate-modified and amine-modified polystyrene latex nanoparticles as a function of incubation conditions. Corresponding SDS-PAGE gel images. 20 µL of eluted protein collected following the centrifugation-resuspension recovery protocol was loaded per lane and all gels were stained with QC Colloidal

Coomassie Stain and imaged. Marker: molecular weight marker (Kaleidoscope ladder); FBS: foetal bovine serum.

Across all polystyrene nanoparticle types examined, a change in the protein corona composition was observed following incubation under various shear flow conditions. Across all nanoparticle chemistry examined, shear flow conditions at 0.85 cm/s led to an increase in the number of bands and their intensity, suggesting the importance of examining protein corona formation under physiologically relevant flow conditions. We also observed time-dependent changes in the intensity of gel bands and relative composition of protein between 2- and 24-hour incubation timepoints. This observed effect was more pronounced for unmodified and amine-modified nanoparticles.

## 2.9 Discussion

The nanoparticle protein corona plays a key role in the biological fate of nanoparticles following administration to biological systems. Regulatory bodies including the European Medicine Agency (EMA),[119] recommend the characterisation of nanoparticle physicochemical properties and their interaction with biological media across different stages of the nanomedicine drug development life cycle including in vitro and pre-clinical in vivo studies during early development. The adsorption of proteins onto the particle surface leads to changes in the nanoparticle physicochemical parameters including size, zeta potential, shape, surface chemistry, surface charge and colloidal stability. These parameters influence nanoparticle-cellular interactions and changes in these parameters will subsequently alter the nanoparticle biological fate.[6,120]

Our goal in this work was to assess the role of nanoparticle surface chemistry in the physical fate of nanoparticles exposed to protein containing media under conditions mimicking cell culture protein content. Here, we studied the role of nanoparticle physical parameters in the range of nanoparticle-protein interactions using polystyrene latex nanoparticles (unmodified, amine-, and carboxylate-modified) as model nanoparticles. It is well known that proteins adsorb onto nanoparticle surfaces to form a protein corona, however there is a current lack of understanding on how the corona formation impacts nanoparticle size and size distribution, and how this subsequently governs the

physical and compositional role of the nanoparticle protein corona in dictating nanoparticle pharmacological activities.[120,121] Conversely, there is also a lack of understanding of how the protein corona contributes to an altered biological fate in the context of changes occurring in nanoparticle physical parameters (i.e., size and charge) following exposure to protein containing media and subsequent protein corona formation.

While the focus of many studies to-date has been on the quantitative compositional analysis of the protein corona, there has been a limited focus on the quantitative physical changes occurring in nanoparticle systems in response to protein treatment.[78] As such there is a clear need to develop a novel bioanalytical pipeline for the reproducible measurement of nanoparticle parameters in response to exposure to biological media as a crucial step in the development and translation of novel drug delivery systems.[29]

Here, I assessed the impact of nanoparticle surface chemistry on changes in particle size and size distribution in response to treatment with media containing FBS. Polystyrene latex nanoparticles were selected as a model system due to their chemical stability over the duration and range of conditions examined in this study, to exclude effects resulting from polymer degradation. The protein incubation conditions selected for this work were based on the typical protein serum concentrations used in *in vitro* cell culture experiments, which are normally used for the early *in vitro* evaluation of nanoparticle interactions with biological media. I selected PBS as the dispersant as opposed to cell culture media (e.g., DMEM, RPMI), to exclusively study the protein content of serum and its role in nanoparticle physicochemical properties, since cell culture media are known to contain other biomolecules.

In most cases, I saw an increase in mean nanoparticle size following (unmodified, amine-modified) polystyrene latex particle incubation with protein-containing media and a further increase in nanoparticle size during exposure to protein-containing medium for up to 24 hours (**Figure 2.2**). This trend correlates with previous findings where gold nanoparticles showed an increase in particle size following prolonged incubation within protein containing media.[122] Previous work has suggested that the increase in

nanoparticle size is likely due to the displacement of lower affinity proteins with high abundance by higher affinity proteins with lower abundance that form the tightly bound hard corona (Vroman effect), coupled with an increase in protein adsorption (protein concentration) over time.[123]

Here, I show the development of a pipeline for the robust characterization of nanoparticles prior-to and following introduction to protein containing media. I have addressed some of the key challenges facing nanoparticle-protein interactions as shown by our findings. These data suggest that surface chemistry plays a significant role in governing nanoparticle-protein interactions, where we demonstrated that the carboxylate-modified nanoparticles adsorbed the least amount of protein, accompanied with the lowest increase in particle size following incubation across all conditions (2-hour, 24-hour, 0.85 cm/s, and 8.5 cm/s). Furthermore, I show that amine-modified particles are positively charged before incubation (**Table 2.1**) and adsorb more proteins onto the particle surface following incubation when compared to the negatively-charged carboxylate-modified polystyrene latex nanoparticles. This is the result of the incubation medium containing predominantly negatively-charged proteins at physiological pH.[24] The unmodified polystyrene latex nanoparticles, despite having a similar charge to carboxylate-modified nanoparticles showed more protein adsorption when compared to carboxylate-modified nanoparticles and possessed a higher mean particle size. This is due to the exposed carboxyl groups found on the particle surface following functionalisation which impacts nanoparticle-protein interactions.[123] Similar observations were made by Lundqvist et al.,[124] which compared polystyrene latex nanoparticles with similar surface chemistry incubated in human serum.

Centrifugation and resuspension of nanoparticle pellets following nanoparticle treatment with protein-containing media remains the most frequently used approach to isolate nanoparticles for analysis. Here, I examined the role of sample isolation using this approach on measured particle characteristics, since it is well known that the centrifugation-resuspension approach for nanoparticle recovery from bulk media, significantly alters nanoparticle physicochemical properties (particle size and concentration) when compared

to *in situ* sample measurements.[125] My findings show that (**Figure 2.4, Figure 2.7**), there was an increase in mean nanoparticle size for protein-treated nanoparticles following recovery using this method when compared to particles measured within protein-medium. This was most likely due to protein aggregation and particle agglomeration induced by high-speed centrifugation.[126]

Furthermore, there was an observed significant loss in nanoparticle concentration measured by PTA for particles subjected to the centrifugation-wash method and in-situ measurements, which was likely caused by the formation of large agglomerates which precipitate or fall outside the PTA dynamic range in both cases. I also observed an apparent significant increase in the measured total protein concentration between 2- and 24-hour incubation timepoints for amine-modified nanoparticles (see Figure 3E). Such a significant increase in protein content may be attributable to the loss of colloid stability resulting from the presence of protein containing media. Moreover, the process of centrifugation-resuspension for the isolation of nanoparticles may enrich for agglomerated and precipitated particles that contain higher surface-adsorbed protein content. Overall, this process may lead to an overestimation of surface-adsorbed protein content at later timepoints.

When compared with in-situ measurements of nanoparticle concentration (in incubation media), however, there is a clear higher loss for samples subjected to the centrifugation-wash methods which can be explained by the loss of sample during the centrifugation and resuspension steps. The resuspension step could potentially lead to the dissociation of nanoparticle and protein agglomerates, rendering the accurate assessment of nanoparticle size distribution challenging following recovery from incubation media. Therefore, the nature and range of techniques used for nanoparticle isolation from protein-containing media becomes a key step in the pipeline for nanoparticle characterisation and analysis of their interactions with biological systems. These findings have implications for the design of protein corona studies, suggesting the need for more gentle separation techniques such as field-flow fractionation,[127] or *in situ* analytical approaches for measuring changes in nanoparticle parameters to minimize sample disruption through dissociation

of particle agglomerate or particle-protein complexes, and subsequent alteration of the protein corona composition.

A limitation associated with the present analyses of particle size concentration changes is that metrology techniques such as PTA and DLS are unable to differentiate between particle types by composition (i.e., polymeric versus protein). However, techniques such as asymmetric flow field flow fractionation with inline light scattering and other detector modalities (e.g., fluorescence, UV, RI) can resolve different molecular weight species, allowing for specific intermediates (e.g., protein fraction, nanoparticle-protein complexes, agglomerates) to be studied.[128]

Most nanoparticle formulations are intended for parenteral administration and will result in administered nanoparticles experiencing shear flow conditions in the circulatory system.[129,130] Here I examined the role of shear flow conditions in nanoparticle parameters following treatment with protein containing media, mimicking arterial and venous blood flow. These findings showed that under flow conditions, total surface adsorbed protein content under flow was equivalent to the same levels seen following a 24-hour incubation with end over end rotation conditions. The composition of proteins adsorbed onto nanoparticle surfaces were found to significantly vary depending on nanoparticle surface chemistry, but shear flow did not change the number of bands across particle samples (**Figure 2.9**).

A qualitative fingerprint of the protein corona composition was obtained for samples incubated under various biologically-relevant incubation conditions using SDS-PAGE analysis. We demonstrated that there were changes in protein corona composition when incubated under shear flow as opposed to static conditions across all surface chemistry (unmodified, amine-modified, carboxylate-modified). Unmodified polystyrene nanoparticle data strongly correlates with a study conducted by Jayaram et al.[59] in which similar particles were used, particularly with the trend observed at ~65 kDa where an increase in band intensity is observed at 0.85 cm/s followed by a decrease for corona composition at (8.5 cm/s). A similar change was also demonstrated across all surface chemistries for time-based incubations, which correlates with trends

observed for multiple nanoparticle prototypes including copolymers,[131] and spherical nucleic acids.[132] SDS-PAGE analysis suggests the identity of adsorbed proteins is influenced by the surface functionalisation of particles, with our results showing similar trends in composition to studies performed with the same nanoparticles.[124]

Overall, these results suggest that the biorelevant assessment of nanoparticle-protein interactions requires a consideration of multiple factors that include both nanoparticle and environmental parameters, the intended route of administration for nanoparticles, and the incubation medium and conditions.

Current approaches to the analysis of the nanoparticle protein corona are disruptive in nature, where sample handling steps induce either particle dissociation, agglomeration, and alteration of loosely bound surface proteins (the soft corona) as such I recommend the use of gentle isolation techniques such as field-flow fractionation or *in situ* analysis. Furthermore, current sample handling protocols and analytical processes compromise the purpose of surface modification of nanoparticles. As shown from the results, the surface modified (amine-modified, carboxylate-modified) nanoparticles are more monodisperse with a higher number concentration before incubation as measured by PTA. However, upon exposure to protein-containing medium the functionalised particles (particularly amine) show a more significant change in particle size and size distribution. In comparison, unmodified particles appear more stable following protein corona formation in terms of particle size and size distribution.

## 2.10 Conclusions

The nanoparticle protein corona alters the biological fate of nanoparticles. Experimental parameters during analysis such as environmental incubation variables alter the rate and extent of nanoparticle-protein interactions. This change is dependent upon the physical and chemical properties of nanoparticles. Here, I examined the role of incubation conditions and variables in model nanoparticle systems. I show that nanoparticles with different surface modifications are differentially susceptible to experimental parameters such

as shear flow and incubation duration. Furthermore, I show that the method utilised to isolate particles prior to analysis impact the resulting particle agglomeration and protein corona properties. My findings demonstrate that careful consideration is needed in the design of sample handling and analysis of nano-bio studies where there is a need to understand nanoparticle behaviour under physiologically relevant conditions.

# Chapter 3 The development of AF4-MD pipelines for the *in-situ* separation and analysis of nanoparticle-protein interactions

## 3.1 Abstract

Formation of the protein corona in complex biological matrices alters nanoparticle physicochemical and biological identity, ultimately dictating particle biological fate in the context of safety and efficacy. A diverse range of nanomaterials have been studied for their implementation as delivery systems for drugs with narrow therapeutic index or undesirable physicochemical properties. Therefore, it is important to determine the range of interactions occurring between nanoparticle-based therapeutics and complex biological media. In the area of nano-bio interactions, most research efforts to-date have focused on the implementation of proteomics-based approaches to study alterations in the composition of the protein corona, with little emphasis placed on the recovery of nanoparticles from biological media during these experimental pipelines and the impact of nanoparticle isolation techniques on the protein corona. In chapter 2, I investigated the use of centrifugation-wash based isolation on nanoparticle size and the protein corona composition. I found that significant alterations in signatures associated with both nanoparticle size and the composition of surface-adsorbed proteins.

In this chapter, I investigated the impact of different asymmetric flow field flow fractionation run parameters on the elution profile of model polystyrene latex nanoparticles with different surface charges in the presence and absence of serum containing media. The impact of flow field flow fractionation methodology flow settings on the resolution of separation and nanoparticle-protein complex isolation from bulk protein media was studied. By coupling flow field flow fractionation with multiple orthogonal inline detectors, information on particle size and morphology can be obtained.

I show that at higher cross flow rates peak tailing and a lower signal intensity was observed using the UV and MALS (multiangle light scattering) detectors. Also, the impact of various cross flow profiles on nanoparticle-protein sample resolution is shown, with optimal sample resolution being observed when applying a decay cross flow profile. Furthermore, I show that FI-AF4-MD as robust pipeline for the reproducible characterization of nanoparticles at baseline and following protein corona formation with >80% sample recovery observed for most measured samples. The emergence of multiple sub-populations following nanoparticle incubation within protein-containing medium was studied using MALS, and DLS detectors. These sub-populations show differences in size and shape, which has wider implications for the biological fate of nanoparticles and supports a multi-modal approach for nanoparticle characterization when following protein corona formation.

Overall, the findings in this chapter indicate a strong need to develop individualised methods for the flow field flow-based separation of nanoparticles based on nanoparticle prototype physicochemical properties. Such efforts should consider nanoparticle surface charge, and physicochemical stability in carrier liquid media as the use of more biologically relevant media mimicking the environment experienced by nanomaterials *in vivo*.

## 3.2 Introduction

Polymeric nanoparticles have emerged as a promising platform for the development of novel drug delivery systems. With ~29% of nanomedicines to receive FDA approval since 2016 being polymer-based in composition.[133,134] Polymeric nanoparticle formulations typically offer multiple advantages over conventional medicines including controlled drug release,[135] higher bioavailability,[136] and an improved therapeutic index.[137] Despite these advantages there has been a high attrition rate for nanoparticle translation from bench-to-clinic, with less than 10% of nanoparticle-based therapies progressing to approval for clinical use.[138]

One of the primary challenges faced by nanomedicine clinical translation is a lack of efficacy, particularly during phase II of clinical trials, with an estimated success rate of approximately 48%, which further declines to 14% during phase III clinical trials.[139]

This leaky pipeline is a result of multiple gaps in the knowledge surrounding the target disease biology, the delivery system, and the interface between nanomedicines and biological systems. A knowledge gap in the field of nanomedicine remains a lack of understanding of processes governing nanoparticle interactions with biological systems upon administration into biological media, in particular the formation of the protein corona and the impact of protein corona composition on the biological fate of nanomedicines (i.e., biodistribution, circulation time). Previous work has shown that following exposure to protein-containing medium, nanoparticles spontaneously interact with circulating proteins, which competitively adsorb onto the nanoparticle surface to form the biomolecular protein ‘’corona’’.[49] The nanoparticle-protein corona causes changes in the physical and chemical properties of nanoparticles and significantly defines the nanoparticle biological identity and subsequent downstream interactions that include cellular uptake, cytotoxicity, and organ biodistribution.[140,141] Therefore, it is crucial to understand the drivers of nanoparticle protein corona formation and characterize nanoparticle-protein interactions under physiologically relevant conditions.

The typical pipeline for nanoparticle-protein interactions following incubation with protein containing media involves the isolation of nanoparticle-protein complexes from protein-containing medium using the centrifugation-wash method, which relies on the different densities of nanoparticles, bulk protein from the incubation media, and nanoparticle-protein complexes of interest for downstream analysis.[69] In chapter 2, I showed that the centrifugation-wash isolation of nanoparticles is disruptive to the protein corona composition and colloid stability of the nanoparticle-protein complexes, which may lead to perturbations in

nanoparticle-protein and protein-protein interactions arising from sample sedimentation and the application of centrifugal forces during nanoparticle-protein isolation protocols.[1,50] Furthermore, multiple centrifugation and pellet resuspension steps are required to ensure the removal of high abundance bulk medium proteins (e.g., serum albumins) from nanoparticle-protein complexes, which leads to sample loss during multiple centrifugation and resuspension steps.[142] Another routine method used for the isolation of nanoparticles from bulk biological media is magnetic force separation, which can only be used for nanoparticles with magnetic properties, such as iron nanoparticles.[143] This is typically performed using magnetic columns that while gentler than centrifugation-wash can cause changes in the protein corona composition. Furthermore, this technique is optimal for nanoparticles ≤10 nm in size due to an increased risk of agglomeration for larger particles.[68] The least used technique for nanoparticle-protein sample isolation is size exclusion chromatography (SEC), which is primarily due to changes in the protein corona composition caused by nanoparticle-protein interactions with the stationary phase, which may cause protein desorption from the nanoparticle surface. Samples are also subjected to shear forces within the column which may decrease the interactions between nanoparticle-protein samples and cause sample loss.[49,50]

Following isolation, nanoparticle-protein complexes are usually analysed using a wide range of analytical techniques including physical characterization techniques such as dynamic light scattering (DLS)- the most widely used technique for nanoparticle size characterization due to its low cost and rapid acquisition of size measurements. However, it is well known that size distributions obtained using DLS non-invasive backscattering (NIBS) measurement are often skewed to larger aggregate sizes in the sample, arising from larger-sized particles scattering light at a much higher intensity.[144] Other routine techniques for the physical characterization of nanoparticle parameters include electrophoretic light scattering (zeta potential), particle tracking analysis

(size distribution and particle concentration), and microscopy techniques such as electron microscopy (size distribution and morphology).[145] The composition of the nanoparticle-protein corona can be further analysed using protein quantification techniques exemplified by the 660 nm protein quantification assay to calculate the total quantity of protein bound to the nanoparticle surface.[146] A fingerprint of the nanoparticle protein corona composition can be obtained using SDS-PAGE, [147] following which the identification of protein band identities can be performed using liquid chromatography-mass spectrometry (LC-MS).[148-150]

Nanoparticle protein corona formation is a dynamic process leading to the formation of a ‘’hard corona’’, which is a layer of high affinity, lower abundance proteins that are tightly bound to the nanoparticle surface.[53] The hard corona is surrounded by a loose ‘’soft corona’’ which consists of lower affinity proteins occurring at a higher abundance.[127] The soft corona phenomenon is well known; however, it has often been uncharacterized as studies of the nanoparticle protein corona typically isolate nanoparticle from protein-containing medium using the centrifugation-wash method. This method has been shown to completely remove the soft protein corona during isolation and may alter the composition of the hard surface-bound protein corona.[151] Therefore, to further probe the biological significance of the nanoparticle soft protein corona, it is crucial to develop gentler in-situ separation techniques for the high-resolution separation and in-line analysis of the soft corona complexes resolved from bulk biological media.[152]

Initially invented in 1966, asymmetric flow field-flow fractionation (AF4) with in-line detection has only recently gained popularity as a technique for the in-situ separation and analysis of complex polydisperse samples including colloidal nanoparticles. The use of frit-inlet AF4 as a gentle in situ separation approach has become one of the most widely-used FFF techniques for the high-resolution separation and in-line analysis of nanomedicines.[153] AF4 is a robust fractionation technique, which uses a trapezoidal channel with a spacer separating a non-permeable top plate

and a porous bottom plate, which is layered with an ultrafiltration membrane which retains the sample. The cross flow is perpendicular to the laminar flow of the running buffer and allows for the mobile phase to pass through the filter while retaining analytes, which allows for an equilibrium to form leading to the diffusion of smaller particles towards the centre of the channel where the velocity of the laminar flow is faster, while larger particles remain near the membrane. This leads to smaller particles eluting at earlier timepoints and the separation of analytes according to their hydrodynamic size.[154-156]

After sample injection a key step is the focusing step, or relaxation of samples. In conventional AF4 channels this is performed using the focusing step which may cause sample aggregation, and sample loss due to adsorption onto the membrane. Frit-inlet (FI) achieves sample relaxation due to the slower sample flow interacting with higher frit flow which pushes the samples towards the membrane. Following the sample focus or relaxation step the mechanism of separation in both conventional and FI-AF4 channels is the same as previously describe.[157,158] This is summarized in (**Figure 3.1**) below.

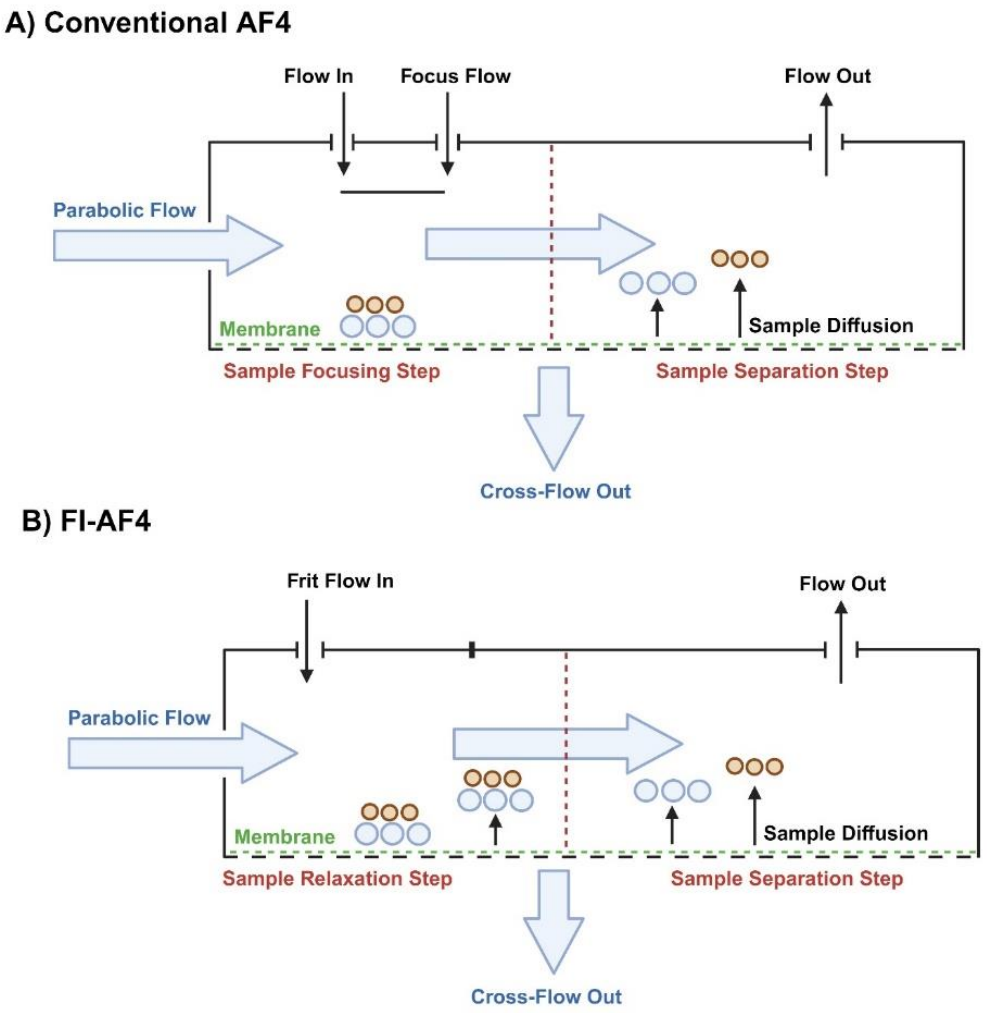


**Figure 3.1**. A schematic representation showing the differences between conventional AF4 channel (A), and FI-AF4 (B) channels. Conventional AF4 relies on the focus flow to push samples towards the membrane (accumulation wall) and force the samples to arrange within different mean layer thickness. FI-AF4 allows for sample relaxation through frit-inlet flow.

One of the main advantages of AF4 compared to chromatographic separation techniques such as SEC is the absence of a stationary phase, and the presence of a wide channel for nanoparticle separation. This allows for the analysis of complex multispecies samples with minimal exposure to shear forces, and the absence of sample interaction with stationary phase, which reduce sample loss and degradation.[159] An additional advantage of using AF4 for nanoparticle isolation from biological media, is that a diverse range of buffers can be used to meet

specific experimental requirements. However, the choice of carrier liquid needs to be optimized to ensure ideal sample separation, while reducing unwanted particle-membrane interactions, carrier incompatibilities with test nanomaterials, and achieving sufficient sample recovery.[160] AF4 is typically coupled with multiple in-line detectors including light scattering multi-angle light scattering (MALS) and DLS (flow mode), which are used for the analysis of particle size and morphological analysis of the molecular shape factor (ratio of the radius of gyration and hydrodynamic radius). Standard optical detectors such as ultraviolet (UV), fluorescence (FL), and refractive index (RI) can also be coupled in-line with AF4, which allow for the accurate quantification of multiple parameters exemplified by molar mass, and aggregation status.[153,161-164] Sample analysis through in-line detection also prevents any sample agglomeration, or aggregation induced due to manipulation arising from experimental handling conditions (i.e., centrifugation-resuspension). Moreover, sample fractions generated during AF4 based fractionation can also be collected for downstream analysis using other analytical methods (i.e., mass spectrometry-based analysis of the corona protein composition).

Despite these advantages, AF4 is primarily used as a technique to measure nanoparticle and protein particle size at a higher resolution [165]- and to a lesser extent- the colloidal stability,[166] polydispersity,[167] and in vitro dissolution profiles of nanoscale-based drug delivery systems.[160,161] A challenge in the application of AF4-based approaches to the separation of nanoparticle-protein complexes from incubation media, in some cases is the lack of separation resolution between the void peak, bulk protein and polymeric nanoparticle, and nanoparticle-protein complexes contained within the incubation media. However, the main goal of such studies is to not necessarily isolate the bulk unbound protein fractions for downstream analysis; therefore, the need to separate bulk proteins contained in the media from the void peak is not a pre-requisite in AF4 method development.

The overarching goal of chapter 3 is to develop AF4-multidetector protocols for the high-resolution separation and in line analysis of polymeric nanoparticle-protein complexes formed following incubation with media containing serum (mimicking protein concentrations and compositions used in cell culture experimental pipelines). Here, polystyrene latex nanoparticles were used as a model, with various surface chemistry modifications (unmodified, and carboxylate-modified) to study the impact of nanoparticle surface charge on differential AF4 separation profiles.

Moreover, polystyrene latex nanoparticles as a model are resistant to hydrolytic degradation at physiologically relevant temperature, which is typically observed with biodegradable polymeric delivery systems. In this chapter polystyrene latex nanoparticles were incubated with 10% vol FBS to mimic the serum composition encountered during cell culture experiments. Using AF4, in-line physicochemical analysis of nanoparticle-protein complexes was performed and changes in size distribution tracked over sample elution time and isolate these complexes from protein-containing media for downstream compositional analyses by techniques such as SDS-PAGE.

## 3.3 Methodology

## 3.4 Materials

Unmodified (Cat #LB1, Merck, Glasgow, UK), and carboxylate- (Cat #F-8803, ThermoFisher, Renfrew, Renfrewshire, UK) polystyrene latex nanoparticles were used for all the measurements reported in this study. Human serum (A/B blood group) was purchased from Merck. The same polystyrene latex nanoparticle concentration was used across all experiments to maintain a constant polymer: protein surface area ratio. Foetal Bovine Serum (FBS) and Phosphate-Buffered Saline (PBS) (Cat#BR0014G) were purchased from Fisher Scientific (Invitrogen, Renfrew, Renfrewshire, UK), and the same batch of serum was used to perform the experiments described in this chapter, to mitigate for any

potential variations in total protein content and protein composition. Novachem was purchased from PostNova Analytics (PostNova Analytics, Landsberg, Germany). Novachem is a surfactant mixture (cationic and anionic) with the following composition by % weight: water 88.8, 138 triethanolamine oleate 3.8, sodium carbonate 2.7, alcohols + C12-14-secondary ethoxylate 139 1.8, tetrasodium ethylenediaminetetraacetate 1.4, polyethylene glycol 0.9, sodium oleate 140 0.5, sodium bicarbonate 0.1. Novachem carrier liquid was prepared at a 0.2 %v/v concentration, pH adjusted to pH 7.4 and made to a final volume of 1000 mL. The 10 mM phosphate buffer was prepared by dissolving 8 g of NaCl,141 200 mg KCl, 240 mg $KH_2PO_4$, and 1.44 g $Na_2HPO_4$. All carrier liquids prepared for AF4 runs were filtered using a 0.2 µm pore-sized polyethersulfone (PES) membrane filter to remove any large particulates from running buffers.

## 3.5 Methodology

### 3.5.1 Nanoparticle protein corona sample preparation

Unmodified, and carboxylate-modified polystyrene latex nanoparticles with a mean baseline diameter of (100 nm) were incubated in PBS containing 10% vol FBS at (1 mg/mL, estimated at 1.8 x $10^{12}$ particles/mL) for all samples at various time-points including 2 hours and 24 hours at physiologically relevant temperature (i.e., 37˚C), and under gentle agitation to minimise potential particle sedimentation effects. The different nanoparticle surface chemistries were selected as a model to represent negatively- and positively- charged nanoparticles.

The total nanoparticle concentration for every experiment, was determined using the same approach described in Chapter 2 of this thesis.

### 3.5.2 Analysis of polystyrene latex nanoparticle properties

**Dynamic light scattering (DLS).** All DLS experiments were performed using a Malvern Panalytical Zetasizer Nano ZS (Malvern Panalytical, Malvern, Worcestershire, UK), using the non-invasive backscatter (173°) setting. Briefly, particle size at baseline was analysed at 25 ℃, with a two-minute equilibration time and three independent replicate measurements for each sample. A refractive index of 1.59 and absorption of 0.010 were used for all DLS measurements, corresponding to the characteristics of polystyrene latex.

**Electrophoretic Light Scattering (ELS).** The corresponding zeta potential for each sample was determined using a Malvern Zetasizer Nano ZS (Malvern Panalytical, Malvern, Worcestershire, UK). ELS was used to measure the zeta potential of nanoparticles at baseline at ambient temperature, with all samples equilibrated for two minutes. The Smoluchowski approximation was used for data processing and zeta potential determination.

**Particle tracking analysis.** The number-based distributions of the polystyrene latex nanoparticles suspended in PBS (at baseline and following exposure to protein-containing incubation media) were analysed by PTA, using the NanoSight NS300 system (Malvern Panalytical, Malvern, UK) equipped with a 488 nm laser and high-sensitivity CMOS camera. Five videos of 60-second duration were captured for all measurements and averaged for each sample. All samples were analysed under constant flow conditions (flow setting 100) and at ambient temperature (~25 °C). Corresponding video capture parameters were set at a camera level of 6, with post-processing analyses being performed at a detection threshold of 4. Data were analysed using the NTA software (v3.4.0.0.3).

**Scanning electron microscopy (SEM).** The morphology of polystyrene latex nanoparticles was analysed using SEM at baseline to confirm particle shape and size distribution. Briefly, nanoparticle suspensions

were sonicated and prepared at 1 mg/mL in DI water. A 20 µL droplet of nanoparticle suspension was deposited on a 5x5 mm silicon wafer chip (Ted Pella, Inc., CA, USA). After drying at ambient temperature for 24 hours, particles were gold sputter coated with a height at 35 mm and coating parameters; 40s, 0.08mb, and 30mA (Agar Scientific Manual Sputter Coater, Agar Scientific Ltd., Essex, UK). All nanoparticle samples were imaged using Field Emission Scanning Electron Microscope (FE-SEM) at 20,000X and 60,000X magnification with a 5kV emission energy (Hitachi SU6600, Hitachi High-Tech Europe GmbH, Krefeld, Germany). All images were analysed in Image J (NIH, Bethesda, USA) for particle size and circularity using the particle analysis function.

### 3.5.3 Analysis of polystyrene latex nanoparticles with AF4-UV-MALS-DLS-fluorescence

Nanoparticles were isolated and analysed using a metal-free AF2000 MultiFlow FFF, which is enabled with in-built software for control and data acquisition. The separation system consists of a solvent organiser (#PN7140), solvent degasser (#PN7520), two isocratic pumps for controlling tip and focus flow ((#PN1130, Postnova Analytics, Landsberg am Lech, Germany), a solvent selector (#PN7310), and a Smart Stream Splitter (#PN1650) prior to entering the AF4 cartridge (Postnova Analytics, Landsberg am Lech, Germany). The separation channel was equipped with a spacer of 350 µm nominal height and a regenerated cellulose membrane with a 10 kDa molecular weight cut-off size as the accumulation wall for all measurements, which were performed at ambient temperature (~22˚C).

For all frit-inlet AF4 experiments, a frit inlet plate was introduced to reduce sample loss, and particle aggregation that could be induced by the focus flow in conventional AF4. The AF4 system was coupled with multiple in-line detectors including a fluorescence detector (FLD) (#RF-20A XS , Postnova Analytics, Landsberg am Lech, Germany), a multiangle light scattering (MALS) detector (#PN3621, Postnova Analytics, Landsberg am Lech, Germany), a refractive index (RI) detector (#PN3150, Postnova Analytics, Landsberg am Lech, Germany), a UV detector (#SPD-M40, Postnova Analytics, Landsberg am Lech, Germany), and a Zetasizer Nano ZS dynamic light scattering (DLS) setup (Malvern Panalytical, Malvern, UK), which was used in combination with the radius of gyration ($R_g$) obtained from MALS analysis to calculate the hydrodynamic ($R_h$) for shape factor measurements using the equation below.

$$SF = \frac{R_g}{R_h} \qquad \text{Equation 3.1}$$

A summary of known $R_g/R_h$ is summarised in (Table 1) below:

**Table 3.1.** A summary of known particle shape factor ranges ($R_g/R_h$) and their corresponding morphologies.

| Shape | $R_g/R_h$ | References |
|---|---|---|
| **Sphere** | 0.775 | 168,169 |
| **Hollow Sphere** | 1 | 168 |
| **Linear Coil Polymer** | 1.5 | 168 |
| **Rod** | 1.87 | 169 |

Fluorescence detector measurements were performed for carboxylate-modified which has a yellow-green dye and a fluorescence excitation/emission ($\lambda_{em}$/ $\lambda_{ex}$) of 505 nm/515 nm. Prior to sample analysis, a system calibration was performed *via* direct injection using 2 mg/mL bovine serum albumin (n=3) to ensure that the sample channel and detectors were operating under optimal conditions.

Run conditions selected for the FI-AF4 separation of polystyrene latex nanoparticles from bulk incubation media are included as follows;

**Table 3.2** Corresponding run parameters used for the FI-AF4-based resolution of polystyrene latex nanoparticles from protein-containing media. *RC: Regenerated Cellulose, MWCO: Molecular weight cutoff size.*

| Parameter | Settings |
|---|---|
| **FFF Configuration** | FI-AF4 |
| **Spacer** | 350 µm |
| **Membrane** | RC (10 kDa MWCO) |
| **Carrier solution** | 0.2% Novachem |
| **Injection volume** | 20 µL |
| **Detector Flow** | 0.3 mL/min |
| **Crossflow** | 2.5 mL/min (0.2) Exponent |

### 3.5.4 Optimization of AF4 flow protocols

**The Development of an AF4-MD pipeline for polymeric nanoparticle characterization**

The impact of cross flow (2-3 mL/min) and detector flow (0.5 mL/min) alteration on the retention time and recovery of polystyrene latex nanoparticles was investigated. The corresponding elution conditions for each method explored during method optimization are detailed below.

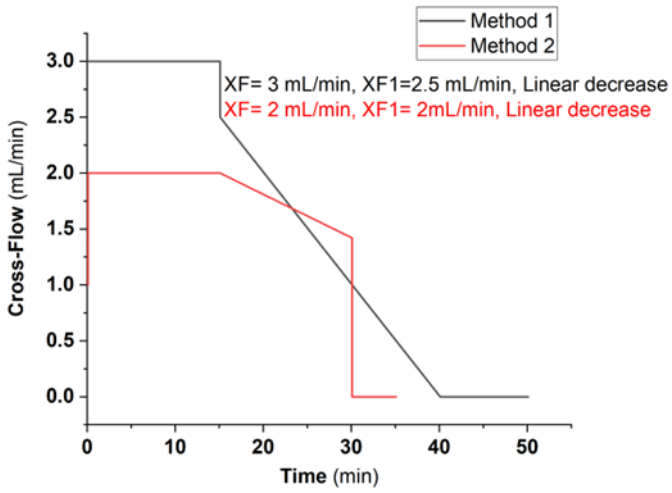


**Figure 3.2.** A summary of the first iteration of AF4-MD method development. Showing AF4-MD method 1 (M1) with an initial constant cross-flow of 3 mL/min, followed by a linear decrease of 2.5 mL/min, and method 2 (M2) showing an initial constant cross-flow of 2 mL/min, followed by a linear decrease of 2 mL/min. XF= cross-flow.

In the first iteration of method development, we compared a linear decrease in cross-flow starting at 3 mL/min, followed by a 2.5 mL/min for method 1 (M1). In method 2 (M2), a lower cross-flow was investigated with an initial constant cross flow of 2 mL/min, followed by a linear decrease at 2 mL/min.

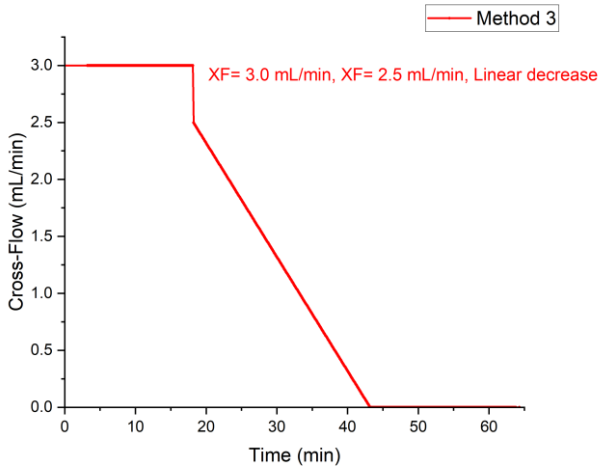


**Figure 3.3**. Summary of the second iteration of AF4-MD method development. Showing AF4-MD method 3 (M3). Showing an initial constant cross-flow of 3 mL/min, followed by a linear decrease of 2.5 mL/min. XF= cross-flow.

In the second iteration of AF4-MD method development, we investigated an initial constant cross-flow of 3 mL/min, followed by a linear decrease at 2.5 mL/min. This method was longer overall when compared to previous methods

### *3.5.5* The Development of a FI-AF4-MD pipeline for polymeric nanoparticle characterization

I investigated the impact of decay cross flow (2.5 mL/min) with a detector flow of 0.3 mL/min on the retention time and recovery of polystyrene latex nanoparticles. The corresponding run parameters beyond flow rates for each method explored during method optimization are detailed in (**Figure 3.4**, and **Figure 3.5**) below.

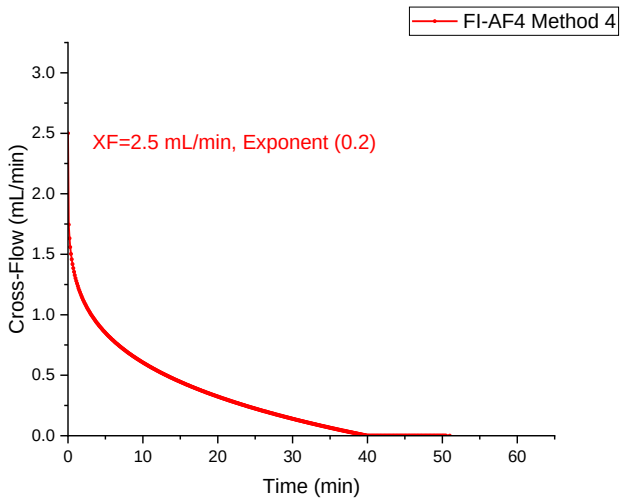


**Figure 3.4**. A summary of the first iteration of FI-AF4-MD method development. Showing a FI-AF4-MD method 4 (M4) which shown a decay cross-flow profile applying a 2.5 mL/min cross-flow over 40 mins with an exponent of (0.2). XF= cross-flow.

In the first iteration of FI-AF4-MD method development we applied a 2.5 mL/min cross-flow (exponent 0.2) for 40 mins with a decay cross-flow profile, followed a constant cross-flow of 0 for 10 min showing method 4 (M4).

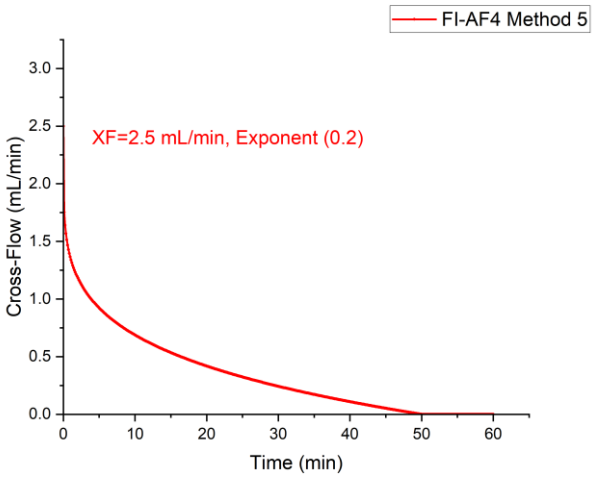


**Figure 3.5**. A summary of the second iteration of FI-AF4-MD method development. Showing a FI-AF4-MD method 5 (M5) which shown a decay cross-flow profile applying a 2.5 mL/min cross-flow over 40 mins with an exponent of (0.2). XF= cross-flow. XF= cross-flow.

In the second iteration of FI-AF4-MD method development we applied a 2.5 mL/min cross-flow (exponent 0.2) for 50 mins with a decay cross-flow profile, followed a constant cross-flow of 0 for 10 min showing method 5 (M5).

### 3.5.6 Calculation of nanoparticle recovery following FI-AF4-based separation

Nanoparticles are known to interact with AF4 membranes during their separation via FFF. Therefore, I determined the (%) nanoparticle recovery using the following equation:

$$\% \, \mathbf{Recovery} = \frac{\mathbf{A}}{\mathbf{A_0}} \times \mathbf{100} \qquad \textbf{(Equation 3.2)}$$

Where, A is the peak area determined for the nanoparticles (in the presence of the corresponding cross flow applied in the optimal separation method, and $A_0$ represents the peak area of NPs with minimal membrane interactions (absence of cross flow).

### Statistical Analysis

All processed data were plotted in Origin (version 2022). Unless otherwise stated, a One-way ANOVA statistical test was performed on all samples to evaluate any statistically significant differences between samples ($P<0.05$). The P-values are defined as *$P<0.05$, **$P<0.01$, ***$P<0.001$.

## 3.6 Results

Polystyrene latex nanoparticles were selected as a model system to optimise and develop AF4-MD methodology for the high-resolution separation and inline analysis of polystyrene latex nanoparticle-protein complexes formed following incubation in 10% vol FBS for 2- and 24-hours.

In Chapter 2, I examined the impact of the centrifugation-resuspension protocol as the industry gold-standard approach used for the routine isolation of nanoparticles from incubation media during protein corona studies. The focus of this chapter is to develop a robust and reproducible AF4 separation method with inline multidetector analysis of nanoparticle and nanoparticle-protein complexes. I explored the impact of different AF4 run parameters on the resolution of nanoparticle-protein complexes from bulk protein media used during the analysis of nanoparticle-protein interactions.

### 3.6.1 Baseline analysis of polystyrene latex nanoparticles

Polystyrene latex nanoparticle physicochemical properties were analysed at baseline (control samples) prior to incubation with media containing 10% vol FBS. FE-SEM imaging was used to measure the morphology of the nanoparticles and confirm the size values obtained from DLS and NTA analyses (**Figure 3.6**).

Image analysis was performed on FE-SEM micrographs using Image J to calculate the mean particle diameter, and circularity for unmodified, amine- and carboxylate-modified polystyrene latex nanoparticles. Overall, FE-SEM images revealed that all nanoparticle types were of predominantly spherical morphology (also confirmed with a measured circularity of ~0.9 for all particles examined). I also confirmed particle size, with a measured mean diameter of 105.7 (±16.9), and 99.2 (±9.6) nm for unmodified, and carboxylate-modified nanoparticles, respectively. These values are roughly all identical to the mean diameter (nm) as measured with DLS (**Table 3.3**).

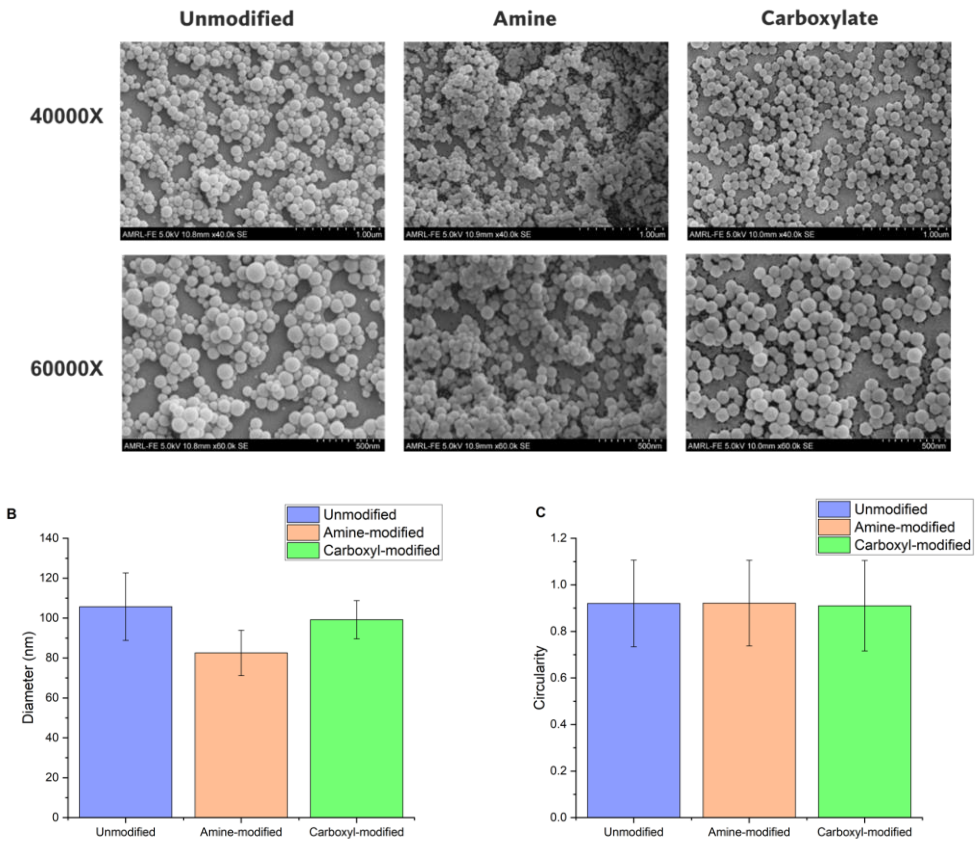


**Figure 3.6**. FE-SEM micrographs for unmodified, amine- and carboxylate-modified polystyrene latex nanoparticles obtained using field emission scanning electron microscopy (FE-SEM) at 40,000X and 60,000X magnifications. Size (N≥ 200) and circularity (N≥2200) analysis of the particles were performed in ImageJ. One-way ANOVA and Dunnett's multiple comparisons test were used for statistical analysis, * denotes $p < 0.05$, ** $p < 0.01$, *** $p < 0.001$, and **** $p < 0.0001$.

Image analysis was performed on FE-SEM micrographs using ImageJ to calculate mean particle diameter, and circularity for each nanoparticle type. Overall, FE-SEM images revealed that all three nanoparticle types were of predominantly spherical in morphology confirmed by measured circularity from SEM, which was ~0.9 for all particles examined. The corresponding particle size measured by SEM, was a mean diameter of 105.7 (±16.9), 82.6 (±11.4), and 99.2 (±9.6) nm for unmodified, amine-modified and carboxylate-modified nanoparticles, respectively.

**Table 3.3.** Corresponding parameters obtained from DLS (PDI and z-average), analysis of FE-SEM micrographs (SEM size and circularity), and electrophoretic light scattering (zeta potential). Values are represented as mean (standard deviation), N=3.

| Parameter | Unmodified | Amine-modified | Carboxylate-modified |
|---|---|---|---|
| **Z-average (nm)** | 118.1 (±0.5) | 82.4 (±0.2) | 94.9 (±0.2) |
| **SEM size (nm)** | 105.7 (±16.9) | 82.6 (±11.4) | 99.2 (±9.6) |
| **PDI** | 0.035 (±0.003) | 0.041 (±0.007) | 0.017 (±0.002) |
| **Circularity** | 0.92 (±0.2) | 0.92 (±0.2) | 0.91 (±0.2) |
| **Zeta potential (mV)** | -34 (±1) | 50 (±1) | -34 (±1) |

All polystyrene latex nanoparticles characterised at baseline were approximately in the 100 nm diameter size range. All nanoparticles analysed were also of low polydispersity (i.e., PDI<0.05). The unmodified and carboxylate modified polystyrene latex nanoparticles carried a negative zeta potential (~ -34 mV). SEM data show that the size measurements obtained by SEM are similar to those measured by DLS analysis.

### 3.7 AF4-MD method development (first iteration: the impact of cross flow)

During the initial iteration of AF4 method development, the impact of cross flow, using methods 1 (3 mL/min cross flow) and 2 (2 mL/min cross flow) was compared using unmodified polystyrene latex nanoparticles (**Figure 3.2, Figure 3.3**). The impact of AF4 cross flow parameters on nanoparticle agglomeration, recovery rate of the analyte, and the resultant signal intensity was also evaluated. Differences in method parameters (i.e., crossflow, method run time duration), and the predicted fractogram peaks for polystyrene latex nanoparticles under baseline conditions, and for unbound bulk proteins (FBS) which were used for all sample incubations for methods 1 and 2 are included as follows:

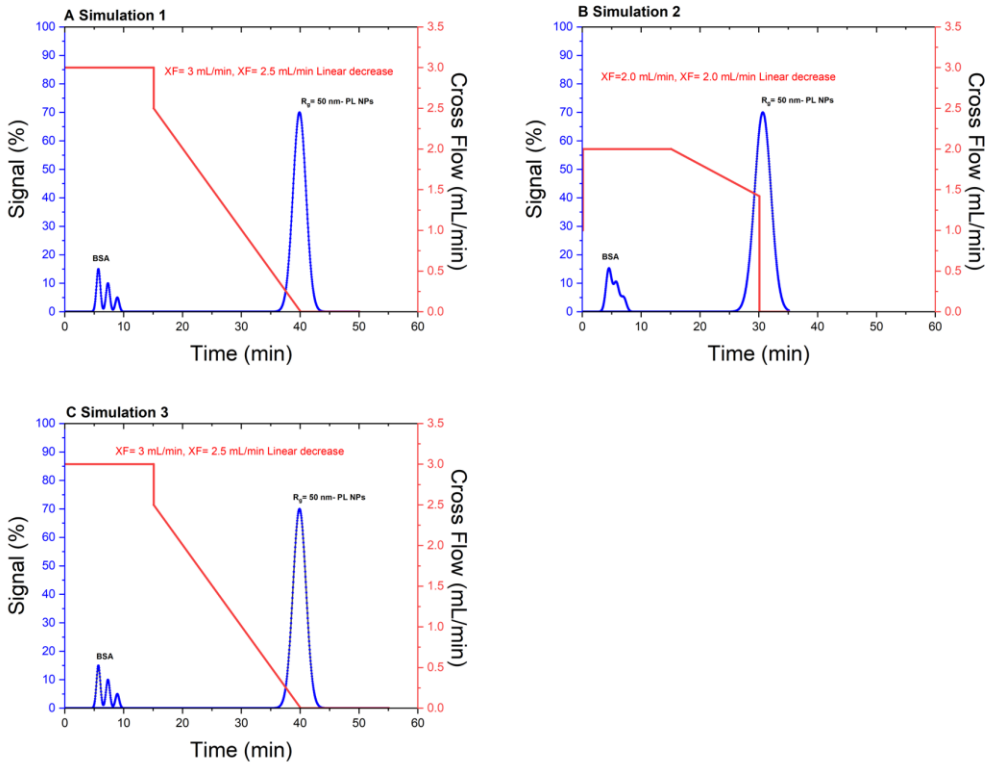


**Figure 3.7.** AF4-UV-MALS method simulations used to predict elution conditions for unmodified, amine-modified, and carboxylate-modified polystyrene latex nanoparticles measurements at 0 hour (baseline control) and following incubation within 10% vol FBS at 2 and 24 hours at 37 ˚C.

Based on the simulation for baseline polystyrene latex nanoparticles with a predicted $R_g$ of 50 nm, it would be expected that these particles elute at ~40 minutes for simulation one, ~31 min for simulation two, and ~40 min for simulation three.

Following incubation in protein-containing medium, a shift in the elution peak resulting from nanoparticle-protein corona formation would be expected, which led to an increase in the mean particle size with unbound proteins being separated from the sample between (4-10 min) based on the method used.

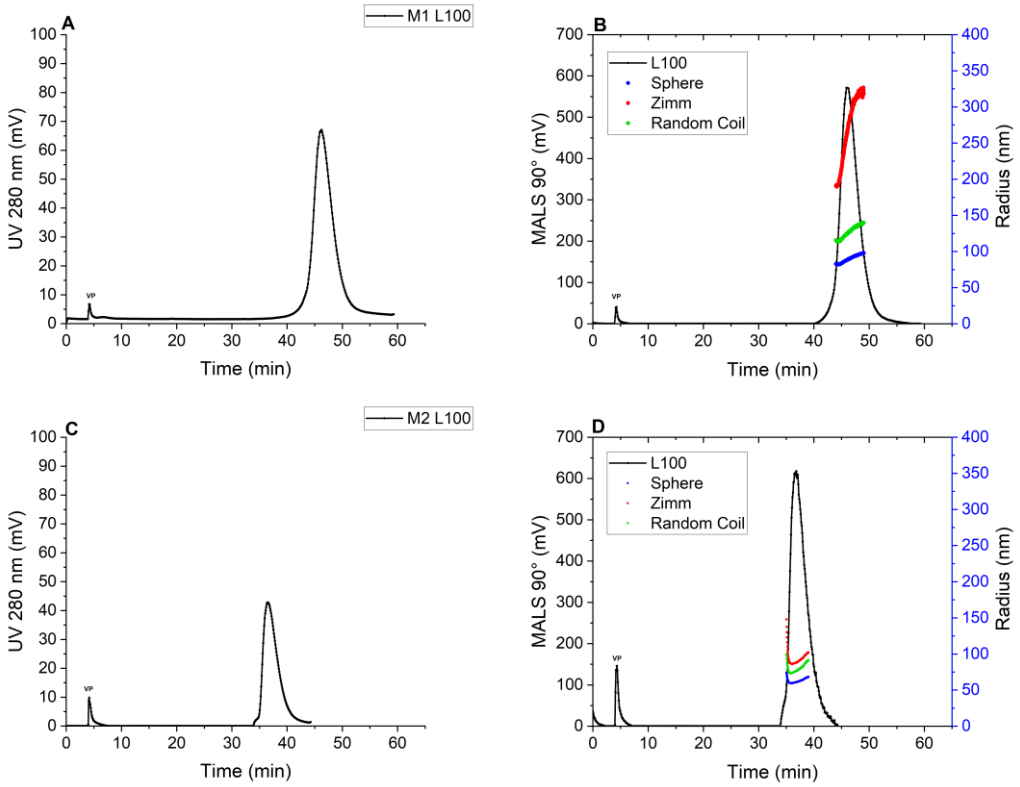


**Figure 3.8.** AF4-UV-MALS fractograms of unmodified polystyrene latex nanoparticles (baseline-0 hours, 100 nm diameter) as detected with UV (280 nm) (A, C), and MALS (90˚) detectors (B, D). Using 10% vol PBS (pH 7.4) as a running buffer. $R_g$ is plotted across the region of interest on the MALS fractograms using multiple models of fit (sphere, Zimm, and random coil). VP: void peak.

Comparing methods 1 and 2, an increase in mean polystyrene latex nanoparticle size was observed with a radius of gyration ($R_g$) of 88.2 nm obtained from method 1, which is higher than the radius measurement obtained using method 2 ($R_g$ 62.4 nm). Overall, both methods 1 and 2 show a unimodal peak in agreement with the run simulations performed (**Figure 3.7.**). However, the observed increase in mean $R_g$ associated with both methods may be a result of agglomeration induced during the focusing step.

Furthermore, with method 2 a lower UV signal intensity (at 280 nm) and tailing was observed, suggesting potential nanoparticle agglomeration. The elution peak for both methods was longer than the predicted simulations, with an increase in elution time from 40 min to 46 min observed with method 1, and from 31 min to 36.5 min observed with method 2 (simulation versus experimental).

Preliminary measurements suggest that a cross flow of (2 mL/min) is more suitable for the AF4-based separation of polystyrene latex nanoparticles. However, both methods 1 and 2 were unsuitable for optimal nanoparticle separation and analysis at baseline, since the mean measured particle radius for unmodified polystyrene nanoparticle is ~50 nm as determined by previous measurements using DLS and PTA (**Table 3.3**). The use of both methods resulted in a much higher reported $R_g$, indicating the formation of aggregates at these cross-flow rates. Therefore, additional AF4 method optimization was required.

### 3.7.1 The impact of a linear decay cross flow profile on isolating nanoparticle-protein complexes from bulk biological media

During the second iteration of method optimisation, I investigated the reproducibility of measured parameters for unmodified, and carboxylate-modified polystyrene latex nanoparticles at baseline and following incubation with 10% vol FBS using AF4-MD method 3 (**Figure 3.3**), with a 10% vol PBS carrier liquid.

**Unmodified polystyrene latex nanoparticles**

Unmodified polystyrene latex nanoparticles eluted between 42-55 min, compared to 2 hour timepoint samples, and subsequently analysed using the same AF4-UV-MALS setup.

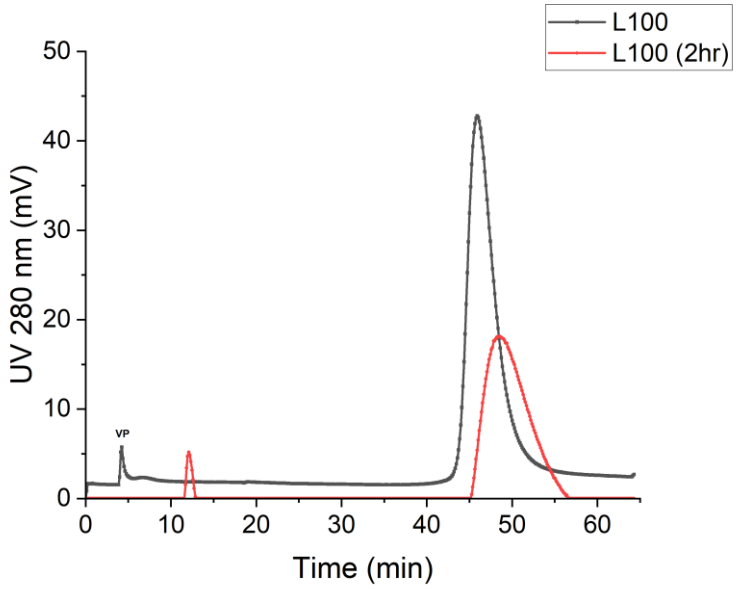


**Figure 3.9.** AF4-UV fractograms for unmodified polystyrene latex nanoparticles (0.1 mg/mL) at 0 hours (black trace) and 2 hours incubation with 10% vol FBS at 37 °C (red trace) detected at 280 nm. L100 (N=3), L100 (2-hrs) (N=1). VP: void peak.

A shift in peak elution was observed in both UV and MALS detector fractogram traces, showing a change from 42 min at 0 hours (absence of protein), to 45 min at the 2-hour timepoint. This change in elution profile was also accompanied by an increase in the measured radius of gyration for the 2-hour samples, consistent with the surface-adsorption of proteins. Furthermore, a small peak occurred at ~11 min

on the UV trace, which corresponds to the separation of the bulk unbound protein from the incubation mixture from nanoparticle-protein complexes. Next, the impacts of incubation with protein were examined using AF4-MALS.

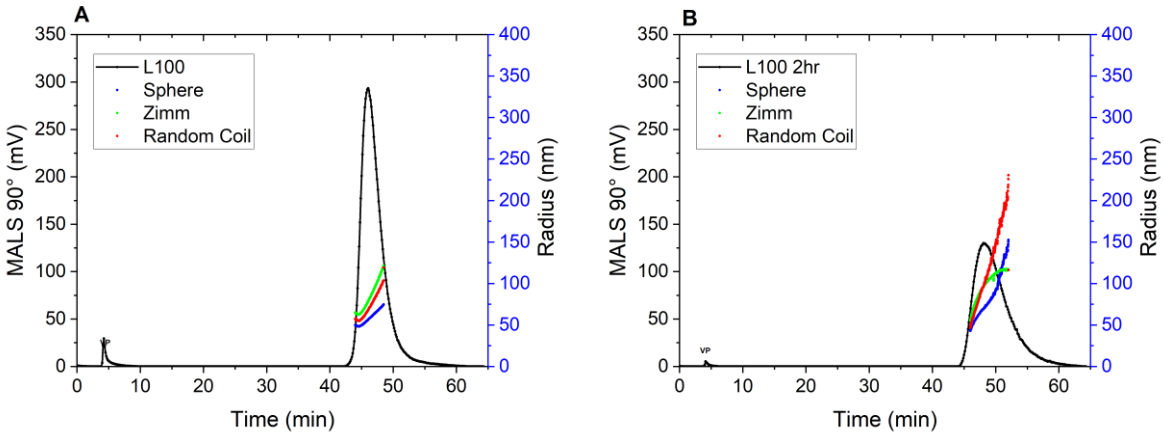


**Figure 3.10** AF4-MALS fractograms for unmodified polystyrene latex nanoparticles (0.1 mg/mL) at 0 hours (A) and 2 hours incubation with 10% vol FBS at 37 °C (B). $R_g$ is plotted across the entire region of interest on the MALS trace using multiple models of fit (sphere, zimm, and random coil). L100 (N=3), L100 (2-hrs) (N=1). VP: void peak.

Unmodified polystyrene latex nanoparticles were characterized using MALS with a mean $R_g$ of 56 nm at baseline using the spherical model of fit. These findings show high correlation with previous hydrodynamic size measurements using DLS, as shown in **Table 3.3**.

Using the spherical model of fit, an increase in the mean $R_g$ was observed to 70.4 nm at the 2 hour timepoint. Peak tailing was observed for unmodified polystyrene latex nanoparticles at baseline, and following incubation with protein-containing media, which suggest the potential presence of multiple nanoparticle-protein and protein-protein sub-species that may not be resolved from each other using method 3. Moreover, the efficiency of the sample fractionation was exceptionally low using this method, giving rise to potential run times ≥60 minutes. Therefore, this method was not further explored for unmodified polystyrene latex nanoparticles.

### Carboxylate-modified polystyrene latex nanoparticles

Method 3 was also used to study the separation of carboxylate-modified polystyrene latex nanoparticles as a different surface chemistry (**Figure 3.11**), to confirm any apparent differences in elution time and resolution of polystyrene latex nanoparticle fractions from protein containing incubation media.

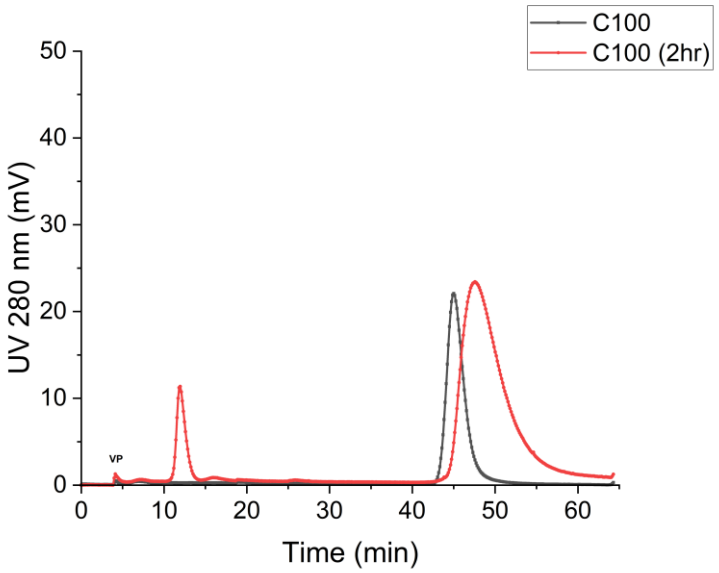


**Figure 3.11.** AF4-UV fractograms for carboxylate-modified polystyrene latex nanoparticles (0.1 mg/mL) at 0 hours (black trace) and 2 hours incubation with 10% vol FBS at 37 °C (red trace) using method 3 with a 10% vol PBS running buffer. UV measurements were obtained at 280 nm, and baseline correction was performed for all UV measurements. C100 (N=3), C100 (2-hr) (N=1). VP: void peak

At 0 hours (baseline control), carboxylate-modified polystyrene latex nanoparticles eluted at 45 min, which increased to 47.5 mins following a 2 hour incubation with 10% vol FBS. This is in comparison to unmodified polystyrene latex nanoparticles, which eluted between 42-55 min. This method wasn't further explored due to the late elution point of baseline nanoparticles, and the severe tailing. Next, the AF4-MALS trace was examined for carboxylate-modified nanoparticles.

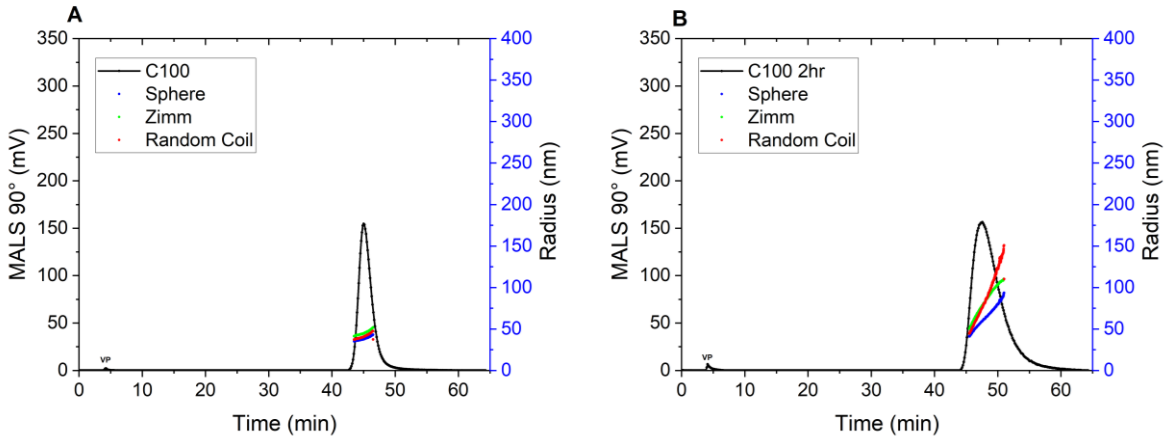


**Figure 3.12.** AF4-MALS fractograms for carboxylate-modified polystyrene latex nanoparticles (0.1 mg/mL) at 0 hours (A) and following 2 hours incubation with 10% vol FBS at 37 °C (B). $R_g$ is plotted across the entire region of interest on the MALS trace using multiple models of fit (sphere, zimm, and random coil). C100 (N=3), C100 (2-hrs) (N=1). VP: void peak.

The MALS signal strength obtained for both 0 and 2 hour samples was acceptable at ~150 mV. Changes in the elution time were accompanied by an increase in the mean particle $R_g$ from 38 nm at baseline to 59 nm following incubation with protein-containing medium when using the spherical model of fit. As seen in previous measurements, a peak occurring at ~11 mins was observed on the UV trace following protein-incubation, suggesting the separation of unbound protein from the incubation mixture.

When using method 3, consistently reproducible fractogram traces were obtained for the unmodified and carboxylate-modified polystyrene latex nanoparticles at baseline and following incubation in protein-containing medium. However, both these nanoparticles eluted at later timepoints (~46 min) at 0 hours, which increased to ~49 min following incubation in 10% vol FBS for 2 hours. Within the AF4 separation and inline measurement period any further separation for nanoparticle-protein sub-populations at higher particle sizes could not be observed, as suggested due to the tailing observed both at baseline and following incubation within protein-containing medium which is further supported by the tailing observed in incubated nanoparticle-protein samples. Therefore, method 3 was not further explored as a viable method.

### Amine-modified nanoparticles

Amine-modified polystyrene latex nanoparticles had a peak maxima that eluted at 45.4 min at baseline, which shifted to 48.1 min at the 2 hour timepoint on both UV and MALS traces.

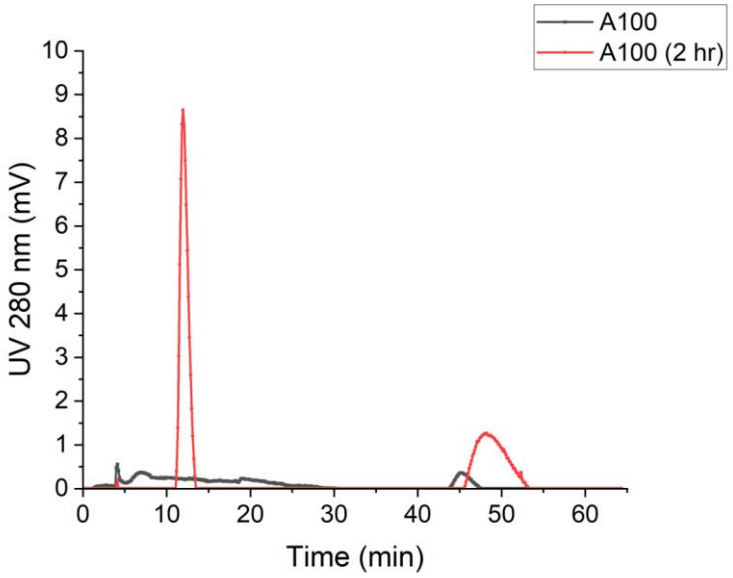


**Figure 3.13** AF4-UV fractograms for amine-modified polystyrene latex nanoparticles (0.1 mg/mL) at 0 hours (black trace) and 2 hours incubation with 10% vol FBS (red trace) using method 3 with a 10% vol PBS (pH 7.4) running buffer. UV measurements were obtained at 280 nm, and baseline correction was performed for all measurements. A100 (N=3), A100 (two-hours) (N=1). VP: void peak

The shift in elution time was attributed to an increase in mean particle size resulting from the nanoparticle protein corona formation. Furthermore, a peak maxima was observed at ~11 min following the two-hour incubation in 10% vol FBS on the UV trace, which indicates the separation of unbound protein from nanoparticle-protein mixtures. However, the intensity of the signal for amine-modified nanoparticles was consistently low at baseline and following incubation with protein-containing media (0.5 versus 2 mV). Consistent with these observations, the MALS signal strength for amine-modified nanoparticles was ~5 mV.

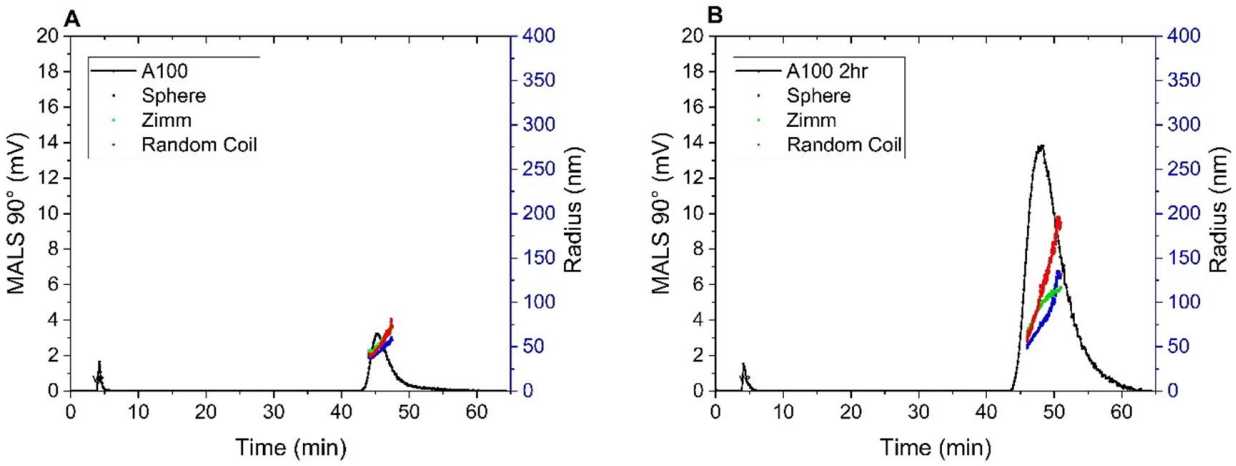


**Figure 3.14** AF4-MALS fractograms for amine-modified polystyrene latex nanoparticles (0.1 mg/mL) at 0 hours (A) and following incubation with 10% v/v FBS at 37 ℃ for 2 hours (B). $R_g$ is plotted across the entire region of interest on the MALS fractograms using multiple models of fit (sphere, zimm, and random coil). A100 (N=3, baseline), A100 (N=1, 2 hours). VP: void peak.

Using the spherical model of fit, an increase in the mean $R_g$ from 42.6 nm at 0 hours, to 70.4 nm following protein corona formation was seen (**Figure 3.14**). As with previous samples, tailing was observed for amine-modified polystyrene latex nanoparticles at baseline and following protein corona formation, which suggests either the presence of additional sub-populations within the measured sample that were not resolved using this AF4 method or inducing particle agglomeration from high cross flow rates during AF4 separation.

### 3.7.2 The impact of decay cross flow on measured nanoparticle parameters using frit inlet (FI-) AF4-MD

Conventional AF4 is associated with inducing nanoparticle agglomeration during the focusing step as a consequence of the focus flow, so I explored the use of a frit-inlet (FI)-AF4 channel to reduce the risk of nanoparticle aggregation during the focusing step.

A simulation of the frit-inlet AF4 (FI-AF4) methods was performed prior to performing sample measurements to predict the elution of polystyrene latex nanoparticles at 0 hours (control samples) and following incubation with protein-containing medium in the Nova Analysis software. Here the differences in AF4 method parameters (i.e., cross flow, method duration), and the predicted elution time for polystyrene latex

nanoparticles under baseline conditions, and for unbound bulk proteins is shown, which was used for all sample incubations.

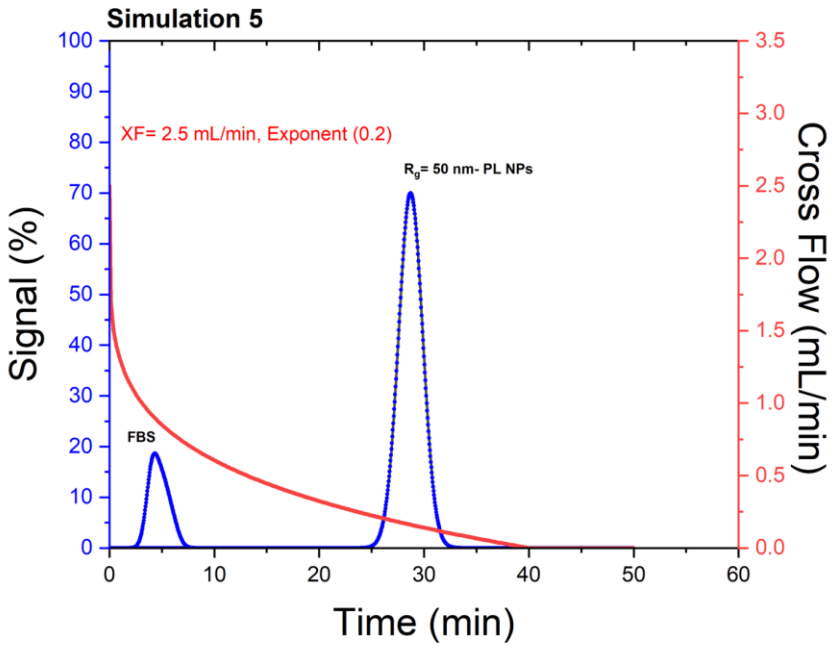


**Figure 3.15** FI-AF4-UV-MALS method simulations used to predict elution conditions for unmodified, amine-modified, and carboxylate-modified polystyrene latex nanoparticles measurements at baseline (control) and following incubation within 10% vol FBS at 2 and 24 hours at 37 ˚C.

Based on the simulations for baseline unmodified, amine-, and carboxylate-modified polystyrene latex nanoparticles ($R_g$ =50 nm), a peak was predicted to elute at ~25 min in method 4, at ~15 min for method 5, and ~29 min for method 6.

Following incubation with 10% vol FBS, a later elution time for all polystyrene latex nanoparticles was expected in response to nanoparticle-protein complex formation, with the unbound protein fraction separation occurring between 5-9 min, and 2-8 min for method 4 and method 5, respectively.

A decay cross flow profile was applied to resolve subpopulations within the samples following incubation in 10% vol FBS medium. This was performed as per method 4 (**Figure 3.4**) using 0.2 *%v/v* Novachem as the carrier liquid.

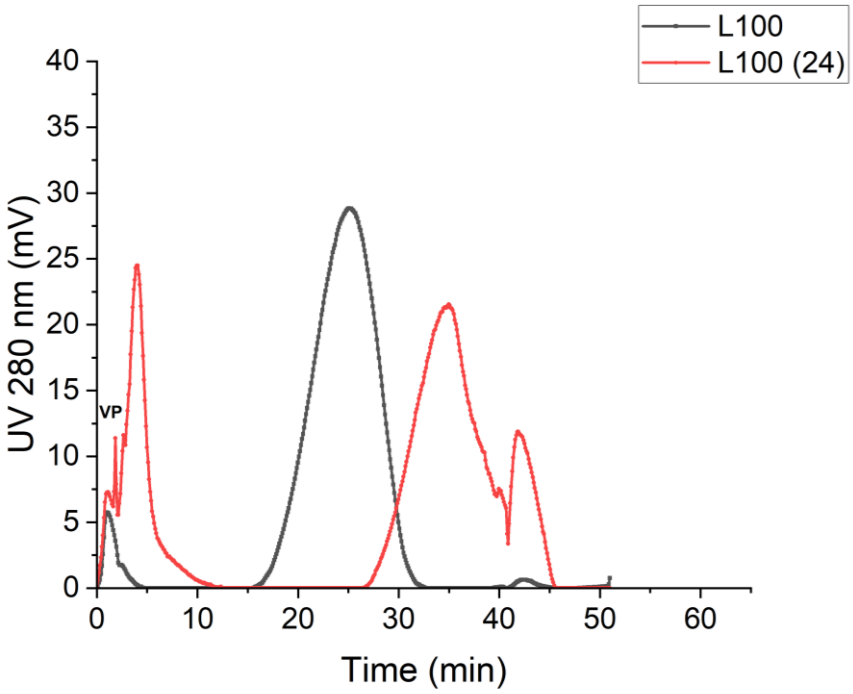


**Figure 3.16.** FI-AF4-UV fractograms for unmodified polystyrene latex nanoparticles (0.1 mg/mL) at baseline (black trace) and following incubation with 10% vol FBS for 24 hours (red trace) using method 4 and 0.2 *%v/v* Novachem running buffer. Measurements (UV) were obtained at 280 nm, and baseline correction was performed for all UV measurements. L100 (N=3, baseline), L100 (N=3, 24 hours). VP: void peak

A narrow unimodal peak (10 min peak width) was observed for the UV (280 nm) fractogram traces at time 0 (baseline conditions), eluting at ~25 min. Following 24 hours incubation in protein-containing medium (10% vol FBS), changes in polystyrene latex nanoparticle elution profiles were seen relative to baseline. Furthermore, various nanoparticle-protein subpopulations were resolved with elution peak maxima emerging at 35 min, 39.8 min, and 42 min, respectively.

Further analysis of nanoparticle parameter changes was performed using the MALS detector (**Figure 3.17**).

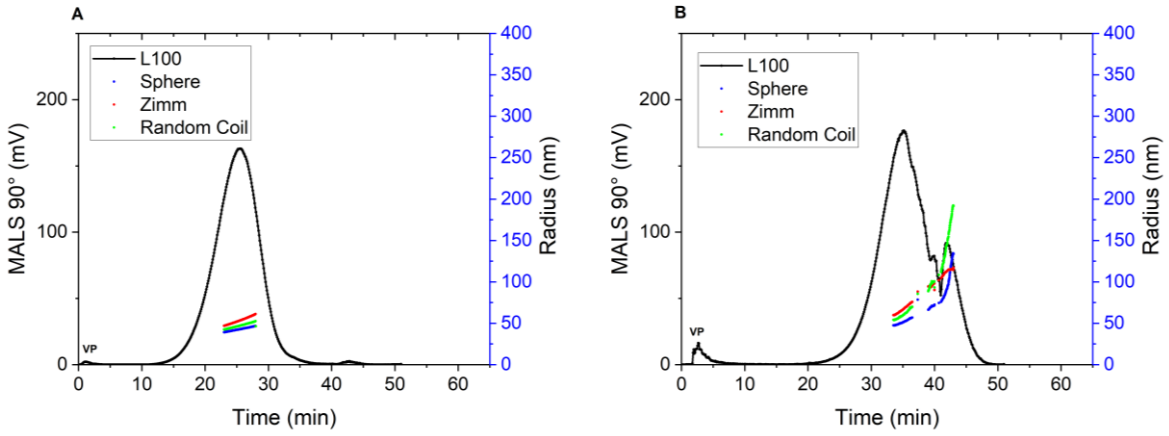


**Figure 3.17.** FI-AF4-MALS fractograms for unmodified polystyrene latex nanoparticles (0.1 mg/mL) at baseline (A) and following incubation with 10% vol FBS at 37 °C for 24 hours (B). $R_g$ is plotted across the entire region of interest on the MALS trace using multiple models of fit (sphere, zimm, and random coil) in method 4. L100 (N=3), L100 (24 hrs) (N=3). VP: void peak.

An increase in the mean $R_g$ was observed for all samples following incubation in 10% vol FBS for 24 hours, with an initial increase in mean $R_g$ from 42.0 nm at baseline, to 50.5 nm for the first region of interest (ROI) when using the spherical model of fit. The measured $R_g$ further increased for later elution peaks with measured $R_g$ of 70.7 and 90.5 nm at 39.8 and 42 min, respectively. Similar trends were seen using the zimm model of fit with an increase in $R_g$ from 53 nm at baseline rising to 66 nm (ROI1), 97 nm (ROI2), and 112 nm (ROI3). Data were also fitted using the random coil model, with a mean $R_g$ of 47 nm at baseline which increased following protein corona formation with a mean increase to 59 nm (ROI 1), 100 nm (ROI 2), and (144 nm ROI 3).

The cross flow was increased in method 5 to allow for the improved resolution of sub-species following incubation with protein-containing media using 0.2 *%v/v* Novachem as the carrier liquid.

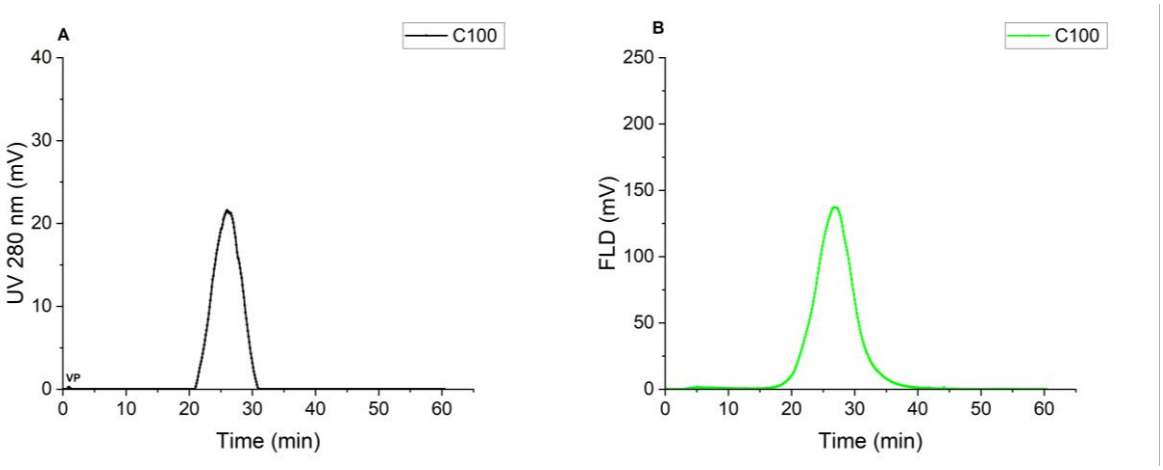


**Figure 3.18.** FI-AF4 fractograms for carboxylate-modified polystyrene latex nanoparticles (0.1 mg/mL) showing (A) UV (280 nm) elution profile, and (B) the FLD elution profile (em/ex 505/515) using method 5 with 0.2 *%v/v* Novachem running buffer. Baseline correction was performed for all measurements. C100 (N=3). VP: void peak

A unimodal peak was observed in the UV and fluorescence traces for carboxylate-modified polystyrene nanoparticles at baseline, with the peak eluting at ~20 min in both UV (21-31 min) and fluorescence (19-36 min) fractograms. This shows a similar elution profile to baseline nanoparticles as seen for the previous iteration of method development. Further analysis was performed using MALS and DLS, which allows the shape factor to be determined as an approach to infer particle morphology (**Figure 3.19**).

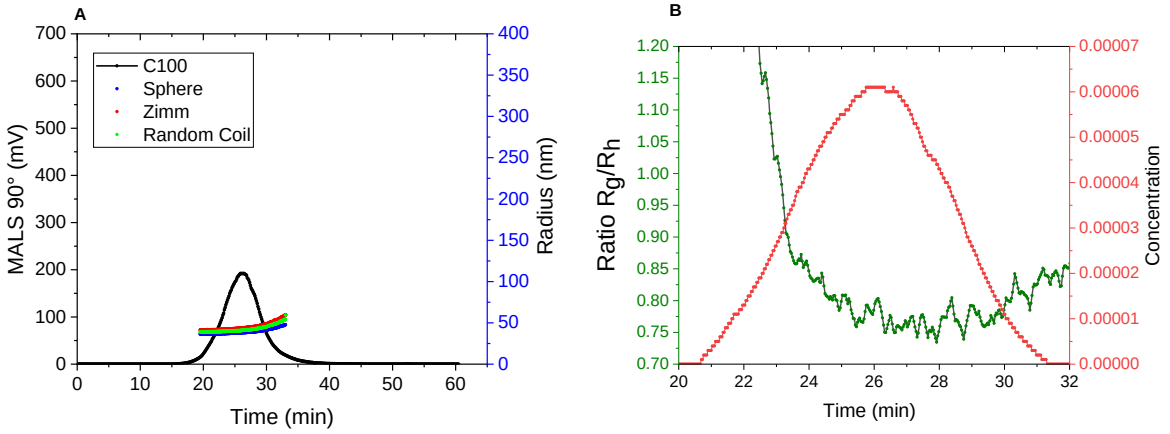


**Figure 3.19.** FI-AF4-MALS fractograms for carboxylate-modified polystyrene latex nanoparticles (0.1 mg/mL) at baseline with (A) showing 90˚ MALS with $R_g$ plotted across the region of interest using multiple models of fit (sphere, zimm, and random coil), and (B) showing the measured shape factor over peak particle elution. C100 (N=3).

The observed mean $R_g$ at baseline for carboxylate nanoparticles was (39 ± 1.6 nm), with a mean shape factor of ~0.8 , which suggests that the nanoparticles characterized are predominantly spherical in shape as shown in previous studies [170] which show a shape factor (~0.78).

### 3.7.3 FI-AF4- MD analysis of polystyrene latex nanoparticles following incubation with protein-containing media.

In this chapter, I explored the difference between different AF4 protocols, investigating the impact of cross flow rates, linear versus exponential decay profiles, and frit-inlet versus conventional AF4 based separation of nanoparticles from bulk protein containing media as an approach for isolating nanoparticle-protein complexes. Overall, these data show that the optimal separation of highly polydisperse samples, including nanoparticle-protein complexes formed following incubation with protein containing media occur with a higher resolution using decay cross flow profiles and with frit-inlet AF4 separation. In this final iteration of method development, I extended the cross flow rate (2.5 mL/min, exponent 0.2) to a 50 min duration run with 0.2% *v/v* Novachem as the carrier liquid.

### Unmodified polystyrene latex nanoparticles

FI-AF4-UV-fluorescence-MALS-DLS was used to measure the properties of polystyrene latex nanoparticles at 0 hours and following incubation with 10% vol FBS at 2 and 24 hours.

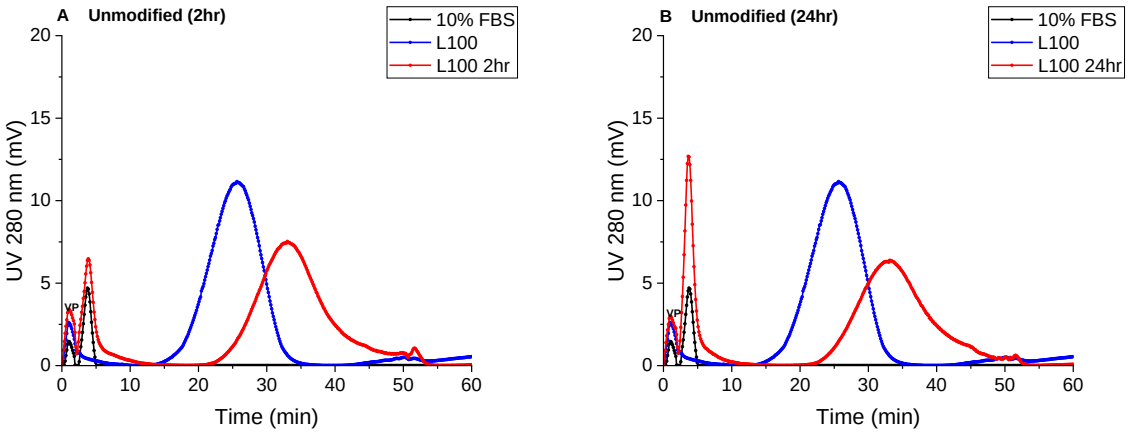


**Figure 3.20.** FI-AF4-UV traces (280 nm) for unmodified polystyrene latex nanoparticles (0.1 mg/mL) at 0 hour (blue trace) and 2 hour (A) and 24 hour (B) incubation with 10% vol FBS at 37 °C. Baseline correction was performed for UV measurements. An injection of (10% vol FBS) was performed to confirm the elution profile of the bulk incubation media (black trace) for comparison with bulk unbound protein fractograms from nanoparticle-protein samples (red trace). All samples (N=3). VP: Void Peak.

A narrow unimodal peak was observed for unmodified polystyrene latex nanoparticles at baseline with UV detection (280 nm), with a peak maximum at 25 min. At 2 hours, a shift in elution time was observed with two peaks occurring at 33.5 min and 52 min. A similar elution profile was observed at 24 hours, with peak eluting at 33.5 min and 51.5 min, respectively. For the 10% vol FBS injections, a narrow peak eluted at ~5 min following the void peak, which was also observed for traces corresponding to nanoparticle-protein samples (i.e., 2- and 24-hours).

A decrease in signal intensity was observed following incubation with protein-containing medium, however this was accompanied by an increase in elution time (22-52 mins for 2- and 24-hours). Furthermore, an increased signal between ~3-5 min was seen, which shows the separation of unbound bulk media protein fractions from nanoparticle-protein complexes. Therefore, the observed changes in elution time can be attributed to protein corona formation following exposure to protein-containing medium.

The percentage sample recovery was calculated using the UV elution traces at 0 hours (86%), 2-hours (85%), and 24-hours (74%) with a significant decrease in recovered samples following 24 hours (which shows a more pronounced unbound protein signal). All measured samples showed a >70% recovery threshold as described in ISO/TS 21362:2021, meeting this method quality criteria.[171]

Nanoparticle size was measured using a combination of in-line MALS-DLS which allowed for the characterization of various parameters including $R_g$ (MALS), $R_h$ (DLS), and the shape factor (MALS-DLS, $R_g/R_h$).

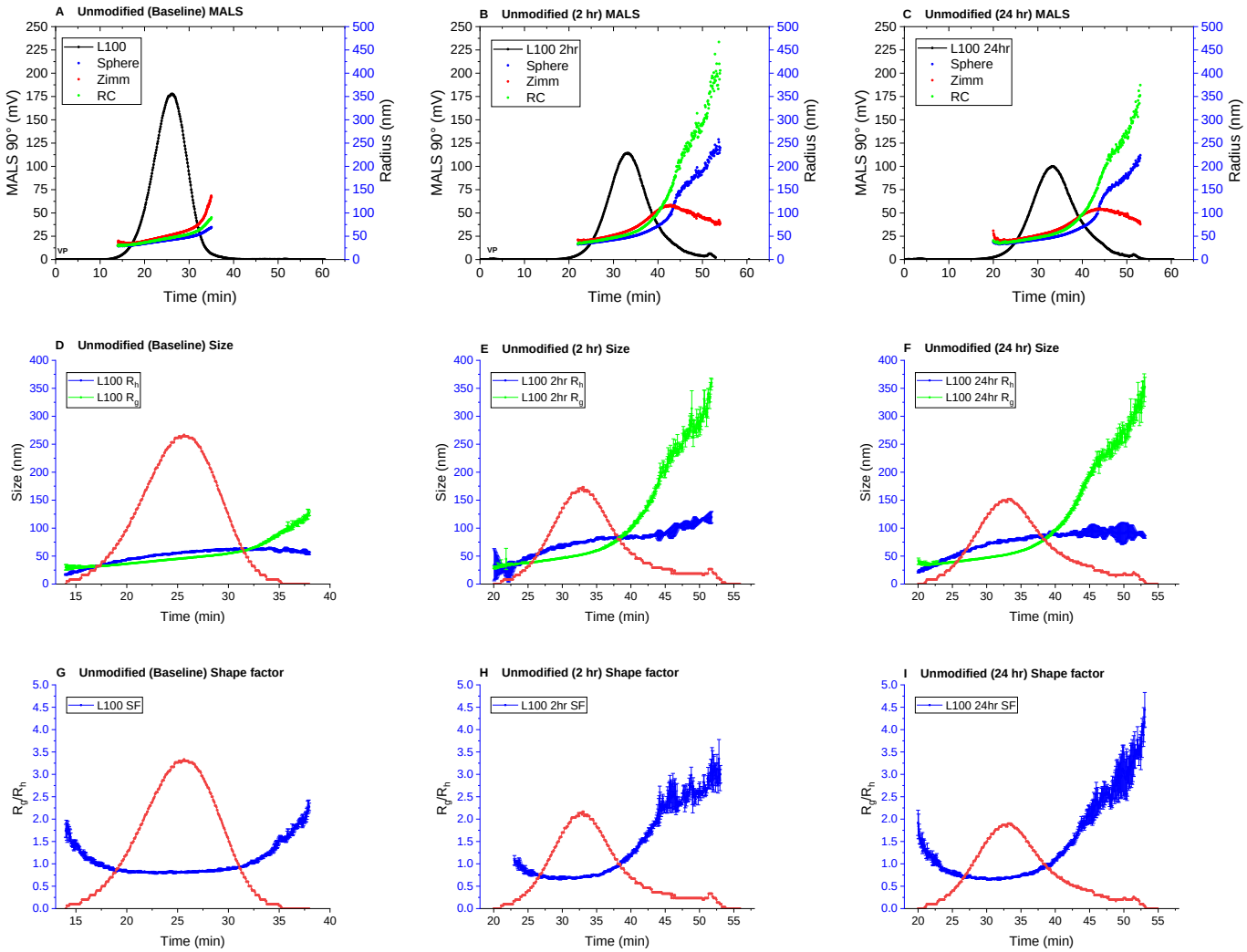


**Figure 3.21.** FI-AF4-MALS-DLS showing unmodified polystyrene latex nanoparticle elution at 0 hours and following, 2 and 24 hour incubation with 10% vol FBS at 37 °C. Showing measured nanoparticle $R_g$ using MALS (A, B, C), mean ($R_g$, $R_h$) as calculated using MALS/DLS (D, E, F), and the shape factor ($R_g/R_h$) (G, H, I). N=3.

The measured $R_g$ was 42.0 nm at baseline for unmodified polystyrene latex nanoparticles, with an increase to 48.0 nm following a two-hour incubation in 10% vol FBS for the initial peak at (33.5 min), which increased further to 219.0 (± 6.5) nm for the second peak that eluted at 52 min when using the spherical model of fit.

A decrease in the measured MALS signal following incubation within protein-containing medium, was accompanied by a broader elution peak profile (~21-52 min) due to the presence of multiple sub-populations in samples containing FBS, polystyrene latex nanoparticles, and nanoparticle-protein complexes. The hydrodynamic radius ($R_h$) calculated from the DLS measurement traces show similar trends to the measured $R_g$ size, with an increase in particle size observed with incubation duration (2- versus 24- hours), and a higher mean size during peak elution at baseline, and for the initial peak following a two-hour incubation when compared to $R_g$ measurements.

Using the inline DLS detector the hydrodynamic radius was determined, which combined with MALS detector radius of gyration measurements were used to calculate the shape factor as a predictor of nanoparticle shape.

The shape factor calculated for unmodified polystyrene latex nanoparticles at 0 hours was 0.77, which suggests a spherical particle morphology. These measurements show high corelation with FE-SEM circularity data (**Figure 3.6**). At the 2-hour timepoint, the shape factor was determined as 0.61, eluting at 33.5 min and an additional calculated shape factor increasing to 2.7 for the peak eluting at 52 min was calculated- suggesting changes in the shape of polystyrene latex nanoparticles from a predominantly spherical morphology to rod shaped particles eluting at later timepoints (i.e., 52 min).

An assumption used in light scattering measurements is often the assumption of a spherical morphology. This approach demonstrates the need for performing multiple models of fit (spherical, zimm, random coil) on MALS data obtained for mixed samples containing protein, nanoparticles, and nanoparticle-protein complexes. In this case, the nanoparticle-protein complexes had a mean $R_g$ of 61.0 nm at 33.5 min, and 85.0 nm at 52 min using the Zimm model for 2-hour samples. Using the random coil fit, $R_g$ was

measured as 47.0 nm at 33.5 min, and 354.0 nm at 52 min (**Figure 3.21**). Further, analysis was performed using FI-AF4-MALS-DLS with polystyrene latex nanoparticles incubated for 24 hours within 10% vol FBS (at 37 °C).

Similar trends were observed following 24 hours incubation in 10%vol FBS, with the mean $R_g$ from 42.0 nm at baseline to 48.0 nm at 33.5 min, further increasing to 197.0 (± 3.4) nm at 51.5 min, when performing the spherical model fit. A decrease in the MALS signal was observed for the 24-hour timepoint, however this was accompanied by an increase in the width of the eluted peaks.

Furthermore, a clear upward trend was observed for the measured mean $R_g$ and $R_h$ across all samples, with a higher mean $R_h$ derived from the initial eluted peak occurring at 33.5 min for baseline samples and following 24 hours incubation. A significantly higher $R_g$ was observed for the peak eluting at 51.5 min, compared to the measured $R_h$. The shape factor determined was 0.68, which suggests a predominantly spherical morphology for the peak eluting at 33.5 min, which increased to 3.5 for peaks eluting at 52 min. This shows that the spherical model of fit is not optimal for the nanoparticle fractions eluting at later times.

### Carboxylate-modified polystyrene latex nanoparticles

Carboxylate-modified polystyrene latex particles were incubated for 2 and 24 hours in 10% vol FBS at 37˚C and characterized using a FI-AF4-MD pipeline. Here we examined the impact of a different surface chemistry on measured nanoparticle parameters, with a general increase in particle size following incubation within protein-containing and the emergence and characterization of multiple sub-populations arising from nanoparticle-protein and protein-protein interactions.

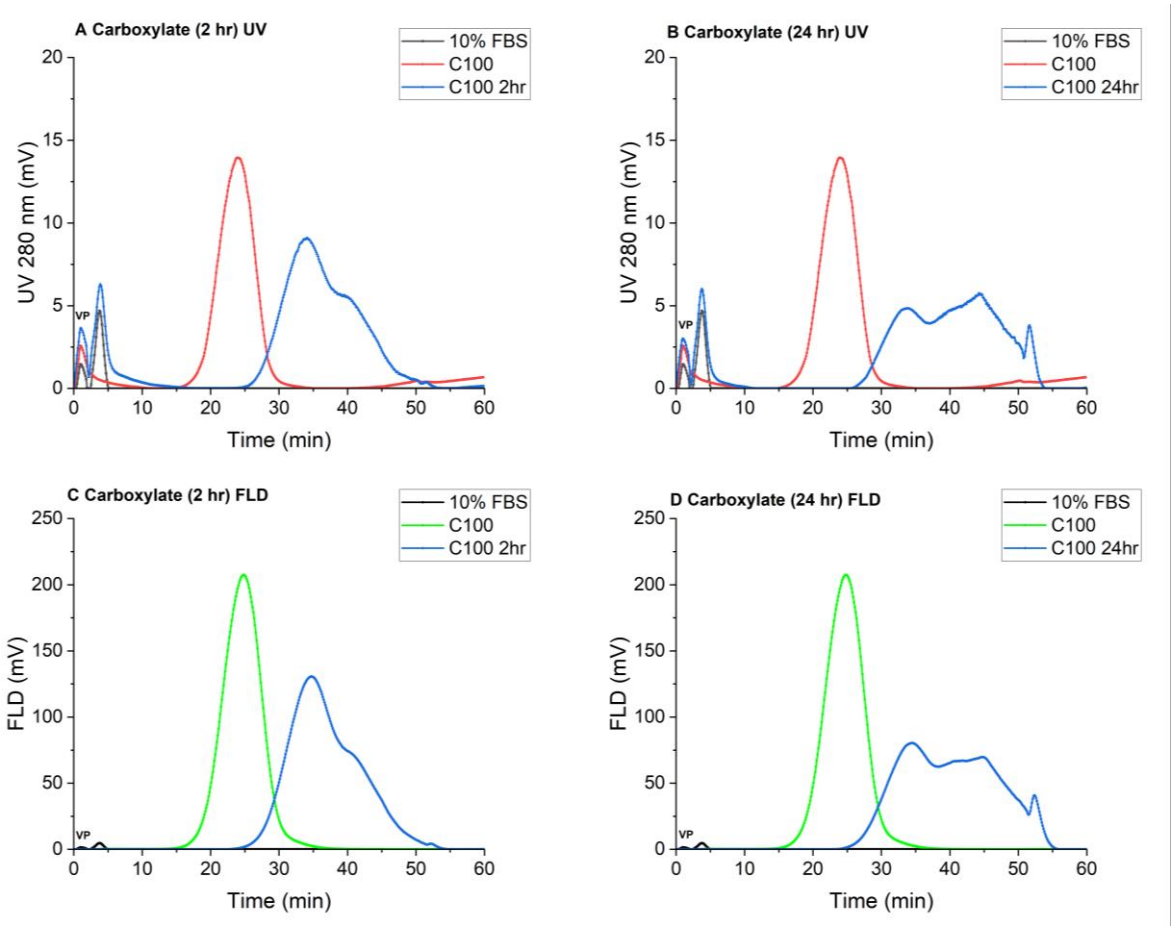


**Figure 3.22**. Corresponding UV (280 nm), and FLD (excitation/emission 505/515 nm) fractograms obtained using a FI-AF4-MD pipeline for carboxylate-modified polystyrene latex nanoparticles (0.1 mg/mL) at 0 hours and following 2- (A, B), and 24- hours incubations in 10% vol FBS at 37 °C (C,D). Baseline correction was performed for UV and FLD measurements. An injection of (10%vol FBS) was performed to confirm the elution profile of the bulk incubation media (black trace) for comparison with the eluted peak corresponding to bulk unbound protein fractions in the presence of nanoparticle-protein complexes (black trace). All measured samples (N=3). VP: Void Peak.

A narrow unimodal peak was observed for carboxylate-modified polystyrene latex nanoparticles at baseline eluting at 24 min, which shows a similar trend to previous runs. A shift in the elution time was observed to ~34 min at 2 hours,

with additional peaks eluting at ~40 and 51 min. Similarly, a shift in elution time was observed for 24 hours, with a peak eluting at ~34 min, and additional peaks eluting at ~40, ~44, and ~51 min.

The UV trace for carboxylate-modified nanoparticles at 0 hours eluted at 24 min (~15 mV), which decreased to ~9 and 6 mV for 2- and 24-hour samples, respectively. Decreases in signal intensity were accompanied by peak width increases, suggesting the emergence of multiple sub-populations for both 2- and 24-hour samples. Furthermore, as seen with the UV traces (**Figure 3.22**), a peak eluted at ~3-5 min corresponding to FBS protein fractions, which was observed in the UV fractograms for 2- and 24-hour samples. These observations along with measurements from the fluorescence detector show the separation of nanoparticle-protein complexes from unbound bulk proteins, where the fluorescence signal corresponding to FITC in the polystyrene latex nanoparticles is absent in the peaks eluting at ~11 min. Similar trends were observed and cross-validated through use of the fluorescence detector as an orthogonal approach to identify sub-populations containing fluorescent nanoparticles.

The percentage of sample recovered from the AF4 separation of carboxylate-modified nanoparticles was calculated using the UV elution profiles with a 95% recovery at 0 hours (control), decreasing to 82% for 2-hour, and 81% for 24-hour timepoints. Size and shape analysis was then performed for carboxylate-modified nanoparticles at 0-, 2- and 24-hours using MALS and DLS detectors with similar trends observed with the unmodified polystyrene latex nanoparticles as shown in (**Figure 3.23**).

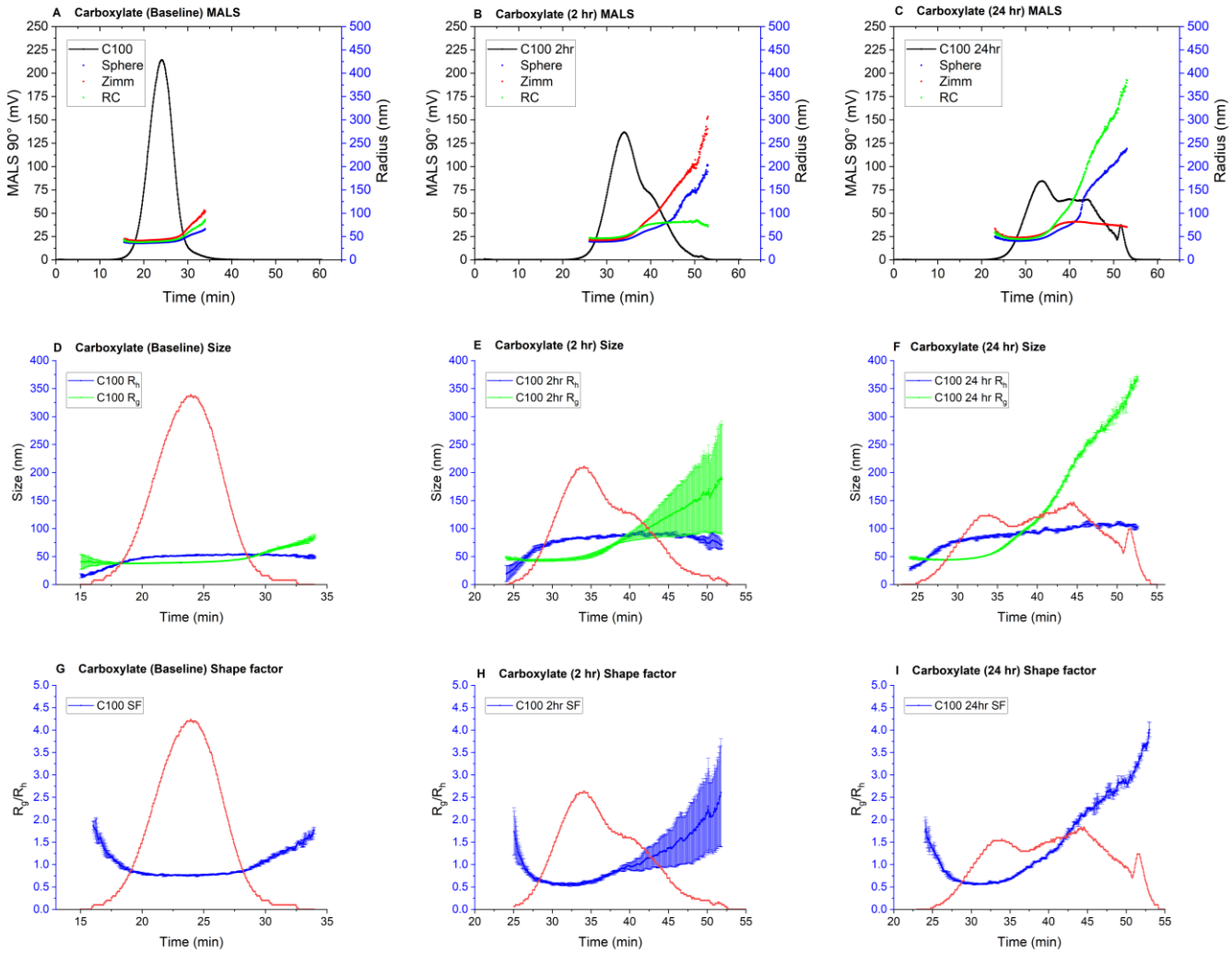


**Figure 3.23.** FI-AF4-MALS-DLS fractograms of carboxylate-modified nanoparticles at 0,2 and 24 hour incubation with 10% vol FBS at 37 °C. Showing measured nanoparticle $R_g$ using MALS (A-C), mean ($R_g$, $R_h$) as calculated using MALS/DLS (D-F), and the shape factor, $R_g/R_h$ (G, H, I). N=3.

An increase in mean nanoparticle size was observed at 2 hours, with a mean $R_g$ of 37 nm at 0 hours, which increased to 43 nm (elution ~34 min), 66 nm (elution ~40 min), and 168 nm (elution ~51 min). Furthermore, multiple models of fit were explored for optimal radius of gyration measurement.

A similar trend was initially observed when applying a zimm model of fit to the fractogram with a mean $R_g$ 44 nm at 0 hours, which increased to 52 nm (elution ~34 min), further increasing to 77 nm (elution ~40 min), and 79 nm (elution ~51 min). The random coil fit was explored, also showing an increase in size over time as with the spherical model of fit, with a mean baseline $R_g$ 40.0 nm, increasing to 47 nm (elution~34 min), 92 nm (elution~40 min), and 242 nm (elution ~51 min) at 2 hours.

Notably, samples eluting > 40 min showed a high degree of polydispersity. Shape characterization was then performed with a mean calculated shape factor of 0.77 at ~24 min for carboxylate-modified polystyrene latex nanoparticles at 0 hours, suggesting the spherical fit is optimal for size measurements. 2-hour samples had a shape factor of 0.59 for peaks eluting at ~34 min, and 0.96 for peaks eluting at ~40 min, and 2.47 for peaks eluting at ~51 min. These results show the formation of multiple sub-populations following 2-hour incubations in protein-containing medium, some of which approach less spherical morphologies at later elution times, which would necessitate the use of multiple models of fit for determining the $R_g$ derived from MALS measurements.

Similar trends were observed at 24 hours, with an increase in mean particle size accompanied by the emergence of multiple subpopulations in comparison to 2-hour samples eluting at ~45 min and ~52 mins. Size analysis using MALS showed an $R_g$ increase from 37.0 nm at 0 hours to 47 nm (elution ~34 min), 75 nm (elution ~40 min), 146 nm (elution ~45 min), and 223 nm (elution ~52 min) with the spherical fit. Notably, an increase in particle size was measured for sub-populations eluting at similar times for 2-hour incubation samples.

A comparison of the shape factor ($R_g/R_h$) trends for carboxylate-modified polystyrene latex nanoparticles at 24 hours showed a higher $R_h$ during initial particle elution, however after ~38 min a sharp increase in the mean $R_g$ was

observed in comparison to $R_h$. Furthermore, samples eluting at ~34 min had a shape factor of ~0.62, which indicates a spherical model of fit is the most optimal for size characterization. However, peaks eluting at ~40 min had a shape factor of 1.26, which increased to 2.23 at ~45 min, and 3.21 for peaks eluting at ~51.5 min. Next amine-modified polystyrene latex nanoparticles were characterized using the FI-UV-MALS-DLS configuration.

### 3.7.4 Amine-modified polystyrene latex nanoparticles

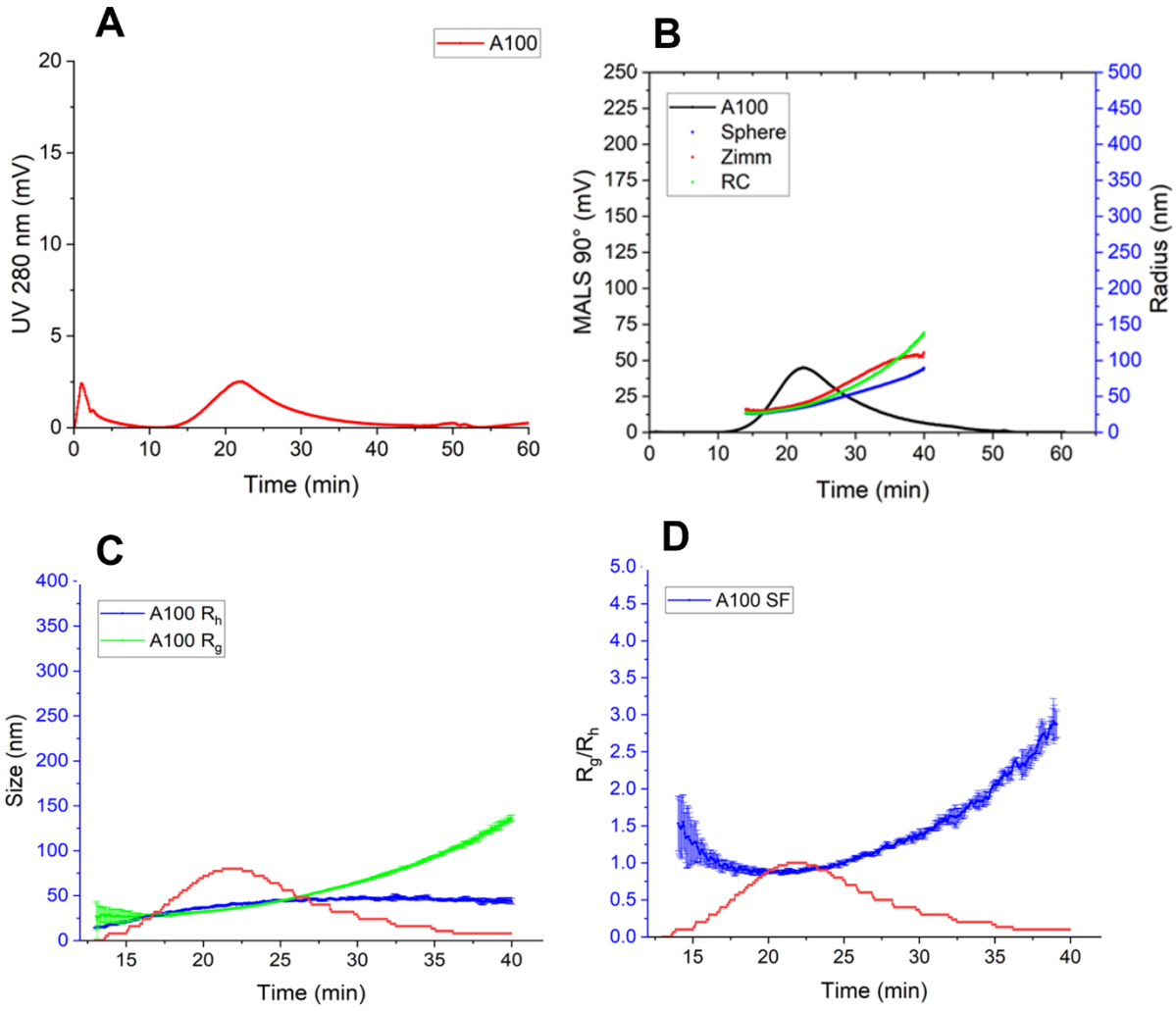


**Figure 3.24.** FI-AF4-MALS-DLS of amine-modified polystyrene latex nanoparticles at 0 hours (baseline). UV trace (A) and MALS trace (B), mean $R_g$ size profile determined over the regions of interest (C) and the shape factor determined using the MALS and DLS traces ($R_g/R_h$) (D).

Amine-modified polystyrene latex nanoparticles were separated and analysed using this pipeline; however, we observed a low peak UV signal intensity ~5 mV in comparison to unmodified, and carboxylate-modified polystyrene latex nanoparticles. Furthermore, we observed peak tailing with sample elution

being between ~12-40 min, which shows particle aggregation and an observed higher sample polydispersity.

This is further supported by size characterization using MALS and DLS. which show an upward trend in mean size over time with mean $R_g$ being higher than $R_h$ after ~25 min elution. The mean $R_g$ for peak elution is 35.0 (± 0.4) nm at ~23 min using the spherical model of fit, which is accompanied by a mean shape factor of 0.94 that increases for nanoparticles eluted after ~25 min. This indicates that polystyrene latex nanoparticles become less spherical at later elution points in the presence of protein-containing medium. Due to the poor signal intensity associated with the amine-modified polystyrene latex nanoparticles, 2- and 24-hour samples were not further investigated.

**Table 3.4.** Summary of shape factor changes following unmodified, and carboxylate-modified nanoparticle incubation within 10%vol FBS for 2 and 24 hours. ROI: Region of interest

| Particle | ROI | Shape Factor |
|---|---|---|
| **Unmodified (0 hours)** | ROI1 (~24 min) | 0.77 |
| **Unmodified (2 hours)** | ROI1(~33.5 min) | 0.61 |
| | ROI2 (~51.5 min) | 2.7 |
| **Unmodified (24 hours)** | ROI1 (~33.5 min) | 0.68 |
| | ROI2 (~52 min) | 3.5 |
| **Carboxylate (0 hours)** | ROI1 (~24 min) | 0.77 |
| **Carboxylate (2 hours)** | ROI1 (~34 min) | 0.59 |
| | ROI2 (~40 min) | 0.96 |
| | ROI3 (~51 min) | 2.47 |
| **Carboxylate (24 hours)** | ROI1 (~34 min) | 0.62 |
| | ROI2 (~40 min) | 1.26 |
| | ROI3 (~45 min) | 2.23 |
| | ROI4 (~51.5 min) | 3.21 |

The trends in shape factor data presented show that following incubation with 10% vol FBS, nanoparticles eluted at later time-points (i.e. 50 min) are not spherical in morphology, with a further increase in measured shape following 24 hours incubation when compared to two hours. This data suggests that alternate models of fit are more appropriate for size analysis of MALS data.

### 3.8 Discussion

In this chapter the use of conventional and frit inlet (FI) AF4 methodology was explored using polystyrene latex nanoparticles a model system, and multiple orthogonal inline analytical detectors hyphenated with AF4 to optimise and comprehensively analyse subpopulations contained in heterogenous mixtures of nanoparticles and protein containing incubation media. Multiple inline analytical detectors were explored as orthogonal analytical techniques, as each detector can contribute different information to the analysis of nanoparticle fate following exposure to protein containing media.

The centrifugation-resuspension technique for the isolation of nanoparticles from biological media remains the gold-standard approach in studying nano-bio interactions, which is associated with significant alterations in the composition of the soft and hard protein corona due to its intrinsically invasive nature and the significant loss of nanoparticles with each centrifugation cycle.[172] Therefore, gentler *in situ* techniques are needed to enable the recovery of nanoparticle-protein complexes for downstream recovery, which I explored in this chapter.

At the time of writing this chapter, there is a lack of literature on the implementation of AF4-based methodology for the isolation of nanoparticle-protein complexes from bulk protein-containing media in mixed species samples. A previous study using AF4 showed that polystyrene latex nanoparticles retained soft corona proteins following separation, and LC-MS analysis.[69] Particularly, there are no studies reporting the impact of flow, cross flow and decay profiles on the resolution of different subspecies within samples containing a mixture of proteins and polymeric nanoparticles.

Therefore, I explored the optimisation and development of AF4 methodology using untreated polystyrene latex nanoparticles at baseline and following

exposure to protein-containing media at physiologically relevant temperatures and different durations (2- and 24-hour incubations), representing early timepoints following introduction to biological media and later timepoints at which equilibration of the surface-adsorbed protein content would be expected.

Polystyrene latex nanoparticles with different surface modifications were selected as a model system representing polymeric nanoparticles for this study, due to their long-term chemical stability (resistance to hydrolytic degradation) in contrast to biodegradable nanoparticle systems (e.g., poly(lactic-co-glycolic) acid). The impact of surface charge functionalisation effects on elution *via* AF4 methodology and nanoparticle-protein interactions was profiled using multiple orthogonal inline detectors to probe changes occurring in nanoparticle characteristics in response to incubation with protein-containing media at physiologically relevant temperature (37 °C) for 2 and 24 hours. I used 10% vol FBS as the incubation medium to mimic the protein content and composition under cell culture conditions.

The ISO standard [171] on the Analysis of nano-objects using asymmetrical-flow and centrifugal field-flow fractionation guidance, outlines the best practices for AF4 method development and data processing to optimise methodology parameters. In this chapter, I used the ISO criteria in the optimisation and selection of AF4 protocol methods using the resolution of sub-populations, the efficiency of subpopulation separation (total run time), the percent area coverage corresponding to the void peak, and percent mass recovery of the sample (an indicator of sample loss due to non-specific interactions with the AF4 membrane) during the AF4 run as the criteria to select for optimal methods. In cases where inefficient resolution was observed (run duration >60 min), other criteria were not assessed.

### 3.8.1 The effect of AF4 flow parameters on the resolution of nanoparticle-protein complexes from bulk protein media

Conventional AF4 methodology uses a combination of cross flow and focus flow to achieve high-resolution separation of different subpopulations in heterogeneous and complex mixtures. Therefore, I investigated the impact of

different AF4 method parameters on the ability of AF4 to resolve nanoparticle-protein complexes from bulk protein-containing media.[160]

Initial measurements in methods 1-2 developed in this chapter were performed using the conventional AF4 channel, with the methods yielding a narrow unimodal peak as expected for unmodified polystyrene latex nanoparticles at baseline. However, the measured radius of gyration obtained from the spherical fit of the MALS trace resulted in a mean measured size of 88.2 nm with method 1, and 60 nm with method 2. Measurements performed with conventional AF4 methods resulted in an increase in the mean measured size of unmodified polystyrene latex nanoparticles. One of the most likely causes for this observation was the presence of a focus flow step at 3.3 mL/min for all measured samples. The shear flow stress to which the samples are subjected during the focusing phase is likely to cause nanoparticle agglomeration, which is a key limitation of using conventional AF4 in the analysis of nanomaterials previously reported in the literature.[173]

Another key aspect of developing methods 1-2 was to better understand the impact of cross flow on nanoparticle samples, with the results suggesting that a lower cross flow rate would be more suited to the samples being studied. Furthermore, the late elution of these nanoparticles shows that neither of these methods would be optimal for polydisperse samples as nanoparticle-protein complexes and nanoparticle agglomerates would be expected to elute at later timepoints beyond the AF4 run duration (beyond 60 minutes).

Using method 3, I explored the incubation of polystyrene latex nanoparticles in protein-containing media at a reduced cross flow rate of 2.5 mL/min following a linear decrease in cross flow. The baseline unmodified polystyrene latex nanoparticles had a measured mean radius of gyration size of 56 nm using the spherical model of fit, which increased to 70 nm following protein corona formation in response to incubation with protein-containing media. Furthermore, I observed a small peak following 10 mins for the UV which indicates the separation of nanoparticle from bulk protein incubation medium; however, as with previous techniques a later elution time was observed, which failed to separate nanoparticle-protein complexes of different sizes indicating

a low efficiency of the method to resolve subpopulations within the nanoparticle-protein sample mixture. While an increase in cross flow may improve overall resolution of the AF4 method in separating different subspecies. This may lead to further issues including sample loss and flow induced aggregation resulting from the shear forces experienced by the sample. Furthermore, in this method I also investigated the elution of amine-modified and carboxylate-modified polystyrene latex nanoparticles (**Figure 3.11**, **Figure 3.12**). One of the main challenges associated with method 3 was a high loss of sample for cationic amine-modified nanoparticles (low sample mass recovery) despite the changes observed in zeta potential following protein corona formation seen in Chapter 2. Therefore, this method was not further explored for amine-modified polystyrene latex nanoparticles.

### 3.8.2 Exploring the use of FI-AF4 methodology for the resolution of nanoparticle-protein complexes

In response to previously obtained data, method 4 (**Figure 3.4**) was developed to optimise polystyrene latex nanoparticle separation from bulk protein-containing media, which applied a power cross flow profile using a FI-AF4 configuration, using a 0.2% v/v Novachem carrier liquid as the mobile phase. A peak eluting at ~26 min was observed for 0 hour samples, corresponding to a mean $R_g$ of 38 nm using the spherical fit for MALS data. Following incubation in protein-containing medium, later elution of all samples was expected across all methods with unbound protein separation occurring between 5-9 min. Optimal separation was achieved using the FI-AF4-MD pipeline with a decay cross flow profile as shown in (**Figure 3.16**) using method 4. This method showed a higher resolution of nanoparticle-protein samples with the identification of multiple sub-populations following protein corona formation.

Method 5 was subsequently developed, introducing a hold time for the cross flow by 10 min to allow for further resolution of nanoparticle-protein complexes from bulk protein media. This method was then used for the final comparison of unmodified and carboxylate-modified polystyrene latex nanoparticles following treatment in 10% vol FBS for 2- and 24-hr incubations.

Unmodified polystyrene nanoparticles were initially investigated, with the UV signal showing an expected shift to later elution times following incubation within protein-containing medium (2 and 24 hours) as observed in previous studies.[69] This shift was accompanied by the emergence of two sub-populations following incubation with protein for 2 and 24 hours. Similar trends were observed with carboxylate-modified particles with the emergence of three sub-populations following 2 hours incubation, further increasing to four following 24 hours incubation.

### 3.8.3 Changes in modelled nanoparticle geometry in response to protein corona formation

The powerful combination of hydrodynamic size measurements from DLS with radius of gyration measurements obtained by the MALS detector can be used to determine the shape factor parameter, which can be used to infer particle geometry.[163] To-date the shape factor from in-line AF4 analysis has not been explored to study mixed sample populations, particularly in the context of nanoparticle-protein complex formation with protein corona samples. Most current studies perform offline analysis of recovered sample fractions using DLS instrumentation, which renders the real-time monitoring of changes in particle morphology challenging.

In this chapter, I explored how the shape factor of unmodified and carboxylate-modified polystyrene latex nanoparticles are altered in response to incubation with protein-containing media for various durations. The introduction of protein-containing media resulted in a high calculated shape factor (>1.5) which suggest a rod-like shape for both unmodified and carboxylate-modified polystyrene latex nanoparticle-protein complexes eluting at later timepoints (after ~45 min) overall indicating a change in the morphology of these nanoparticles. Furthermore, differences were observed between different sub-populations within identical samples (**Table 3.4)**. Previous studies have shown nanoparticle morphology, and size play a key role in determining their biological fate.[174,175] Which suggest that certain sub-populations may show more optimal parameters for cellular uptake.

Despite an accurate measurement of baseline size and unbound protein separation, the UV and MALS signals detected were very low for amine-modified polystyrene latex nanoparticle experiments. This shows that further method optimisation is required including changes to the cross flow, carrier liquid buffer composition (pH, ionic strength, and salt composition), and additional steps may be required when developing methods for positively charged nanoparticle systems (e.g., amine-modified polystyrene latex nanoparticles).

A limitation associated with the application of AF4 methodology is the limited range of AF4 membrane surface chemistries available (e.g., amphiphilic regenerated cellulose, PVDF), which means the potential loss of sample due to non-specific adsorption and interactions that may occur at each stage of sample elution. In the case of amine-modified polystyrene latex nanoparticles and the regenerated cellulose membranes used to develop the AF4 methodology in this chapter, the negative charge of the cellulose membrane at physiologically relevant pH (7.4) and positive surface charge of the amine-modified nanoparticles will result in electrostatic attractions and surface-adsorption of nanoparticles, giving rise to sample loss. These observations are consistent with previous literature efforts in which AF4 methodology has been developed for profiling lipid nanoparticle-based systems. The cationic and lipophilic nature of lipid nanoparticles generally results in poor sample mass recovery and a low signal intensity. Therefore, a common approach that has been adopted to counteract this effect has been the preconditioning of AF4 membranes with protein (e.g., bovine serum albumin- BSA).[176] Multiple injections of BSA have been shown to stabilise reproducibility between individual injections and improved signal. My comparison of the differential AF4 separation profiles across unmodified, amine- and carboxylate-modified nanoparticles highlights the need for individualised optimisation of separation methods according to nanoparticle surface chemistry.

## 3.9 Conclusions

In this chapter, I have explored the development of a robust and reproducible frit-inlet and conventional AF4 configuration protocols for the gentle separation and inline analysis of nanoparticle-protein interactions in media containing protein. Specifically, I showed that use of the frit-inlet configuration leads to a higher mass recovery and a lower incidence of AF4-induced nanoparticle agglomeration in comparison to conventional AF4, which is associated with sample loss during the focusing step. The information provided in this study can guide the initial design and optimisation of methodology for the recovery of nanoparticles from protein-containing media, which can underpin the downstream analysis of the protein corona using offline analytical techniques such as mass spectrometry.

In comparison to the centrifugation-resuspension approach explored in chapter 2, the AF4 method explored was less disruptive to the particles formed with minimal sample loss observed in line with a high percent mass recovery determined in later methods.

Noteworthy also was the emergence of particles deviating from the spherical morphology for polystyrene latex nanoparticles incubated with protein eluting at later timepoints, as determined by the shape factor parameter combining MALS and DLS size measurements. Overall, this finding has implications for applying the spherical model of fit to the analysis of such regions of interest and highlights the complexity of analysing mixed species samples containing both polymer and protein components. At the time of writing this thesis, no models have been developed to enable the analysis of such complex systems, necessitating the need for analysing samples by region of interest and assessing the quality of fit for each model. This finding also highlights the importance of using additional inline detectors as an orthogonal approach to analysis or the downstream recovery of different region of interest fractions for further offline analyses.

Another challenge in implementing AF4 methodology, was using a physiologically relevant buffer system that would lead to fractograms profiles compliant with the AF4 ISO recommendations. I explored the use of

phosphate buffer and phosphate-buffered saline, which overall resulted in significant sample loss and poorer signal intensities using the UV and MALS detectors. Future efforts are required to explore the impact of AF4 carrier liquid composition on the corresponding AF4 fractogram profiles obtained in the context of ionic strength and pH of the buffer to minimise non-specific interactions with the AF4 membrane while not significantly altering the nanoparticle corona composition.

The findings in this chapter indicate that method optimisation is needed on a case-by-case basis for different nanoparticle systems based on the sample composition, and the AF4 methodology that meets the requirements of efficiency, resolution, and mass recovery.

# Chapter 4 Exploring the use of EF4 hyphenated with multiple detectors for studying *in situ* Polymeric Nanoparticle-Protein Interactions

## 4.1 Abstract

Electrical asymmetrical flow field-flow fractionation (EAF4) is a newer modality of flow field flow fractionation that separates particles and proteins based on their size or molecular weight and simultaneously derives the electrical parameters for each population. At the time of writing this thesis, the use of the EAF4 technique for the analysis of nanomaterials in the literature remains underreported. In this chapter, I explored the potential to use EAF4 as an orthogonal method for isolating polystyrene latex nanoparticles from bulk protein containing media based on their surface charge properties, and to determine the electrophoretic mobility and zeta potential of nanoparticle-protein complexes formed using this approach. Subsequently, I compared the electrical parameter values obtained from EAF4 with electrophoretic light scattering results and the changes in particle size in response to incubation with protein containing media against other in situ approaches, frit-inlet flow field flow fractionation and particle tracking analysis.

This chapter shows that EAF4 can present an exciting new approach by which nanoparticle interactions with biological systems may be characterized. However, limitations associated with the maximum current that can be applied for the separation of proteins hinders and limits its applicability for high resolution separation of samples without compromising their integrity. Further optimisation and method development is required for future efforts using EAF4 based separation of nanoparticles in biological matrices.

## 4.2 Introduction

One of the key challenges in the translation of novel nanoparticle formulations, is understanding the role of nano-bio interactions and the formation of the protein corona on the subsequent biological fate of nanomedicines.[107] For this purpose, there is a clear need to develop analytical methods with the ability to resolve nanoparticles from complex biological media containing biomolecules.[177]

In chapters 2 and 3,[172] the limitations of conventional analytical techniques for the analysis of nanoparticles in complex biological media was discussed, highlighting the need for alternative orthogonal approaches for the resolution and simultaneous analysis of nanoparticles incubated in complex biological media.

A separation technique for the analysis of nanomaterials, which is growing in interest is asymmetrical flow field-flow fractionation (AF4), which can be multiplexed with various online detectors for the rapid and efficient separation of components sized in the nanometer to micron size range, contained within a polydisperse system at high resolution.[166] AF4 is a sized-based separation technique, which will separate various species within a polydisperse sample according to their diffusion coefficients.

EAF4 represents a new sub-technique of AF4, and the concept of EAF4 in its current form was first introduced in 2015.[178] It combines AF4 and electrical field-flow fractionation (EIFFF) in a separation channel. This combination of flow and application of a perpendicular electrical field enables the separation of various species in a sample based on both diffusion coefficient (the AF4 component) and the surface charge of species (the EAF4 component). The application of an electrical field in EAF4, causes particles moving in the carrier liquid to move in a vertical direction, and is counterbalanced by the diffusion of the particles. AF4 and EIFFF can be applied separately or simultaneously as in the case of EAF4 to resolve different charged species within a sample.[179] In EAF4, the accumulation wall carries a net surface charge that is induced by the applied electrical field, resulting in a shift in the elution time of a charged

particle based on the strength and directionality of an applied electrical force.[180]

Therefore, EAF4 can simultaneously provide information on the size and electrical parameters of an analyte, such as particle size, colloid stability, electrophoretic mobility and zeta potential.

The zeta potential of suspended biomolecules and nanoparticles with different surface properties reflects the range over which electrostatic interactions occur in dispersions, and is directly related to the effective surface charge of the dispersant in the buffer system, ionic strength of the medium, among other sample properties.[181] Therefore, the zeta potential of a sample can be related to intermolecular electrostatic interactions occurring between different charged species contained within a solution, and consequently their physical stability when dispersed in a solution phase. In the context of the nanoparticle protein corona formed following exposure to protein containing media, changes in zeta potential can be used to infer electrostatic interactions occurring between nanoparticles and biomacromolecules contained within complex biological media, with changes in nanoparticle zeta potential can be attributed to the surface adsorption of biomolecules onto the nanoparticle surface[182].

The benefits of using EAF4 in this context is that the impacts of formulation conditions or incubation in complex biological media can be profiled at high resolution for new nanomaterials under investigation.

In this chapter, I compare the utility of EAF4 and FI-AF4 with the latest Nanosight Pro particle tracking analysis (PTA) system for studying the impacts of nanoparticle protein corona formation in media containing protein on both size and charge characteristics of nanoparticles. In an ideal scenario, EAF4 provides charge- and size- dependent separation of species contained within the analyte that carry different charge or charge density, even with the same size properties (i.e. hydrodynamic radius). It is expected that the charge-based separation of sample components would offer a higher resolution of species and permit the non-destructive *in situ* analysis of changes in nanoparticle surface charge properties in the absence of a need for recovering

nanoparticles from incubation media using more destructive approaches such as centrifugation-resuspension.[183] Analytical separation of the different intermediates formed in response to incubation with biological media involves the resolution of different species ranging from monomeric protein contained in the bulk biological media to nanoparticle-protein agglomerates.[184] While traditional asymmetric flow field flow fractionation separates different species according to their size, in some instances knowledge of the different charged moieties within a sample can play an important role as it impacts intermolecular electrostatic forces impacting the physical and colloid stability of the complexes formed in the dispersion.[172]

The analysis of nanomedicine protein corona characteristics formed in response to nanoparticle exposure to complex biological media remains a challenge, requiring the physical isolation of nanoparticle biomolecular complexes formed from biological incubation media. In this chapter, EAF4 multiplexed with multiple online detectors is used to study the potential role of this approach for the recovery of nanoparticles from protein-containing medium such as 10% *v/v* foetal bovine serum (FBS), mimicking the typical protein content levels to which nanoparticles are exposed under cell culture conditions. As with chapters 2 and 3 in this thesis, polystyrene latex nanoparticles were used as a robust non-degradable model of polymeric nanoparticles used to study the impact of protein corona formation on particle size and zeta potential. The added advantage of using EAF4 for this application, is the ability for simultaneous separation and *in situ* analysis of particle size and surface charge parameters.

## 4.3 Materials and Methods

### 4.4 Materials

Unmodified (Cat #LB1, Merck, Glasgow, UK), carboxylate-modified fluospheres (Cat #F-8803, ThermoFisher, Renfrew, Renfrewshire, UK) and amine-modified (Cat #L9904, Merck, Glasgow, UK) polystyrene latex nanoparticles were used for all the measurements reported in this study. FBS was purchased from Fisher Scientific (Invitrogen, Renfrew, Renfrewshire, UK) and centrifuged to remove any larger aggregates prior to sample preparation.

Phosphate-Buffered Saline (PBS) was purchased from Fisher Scientific (Invitrogen, Renfrew, Renfrewshire, UK). Sodium carbonate was purchased from Merck (Glasgow, UK).

## 4.5 Methods

### 4.5.1 Nanoparticle protein corona sample preparation

Polystyrene latex nanoparticles with a diameter of 100 nm were incubated in 10% *v/v* FBS diluted with PBS at the same polymer concentration (1 mg/mL), equivalent to a particle concentration of ~1.8 x $10^{12}$ particles/mL for all samples.

Nanoparticles with various surface modifications were selected to model positively charged (amine-modified), and negatively-charged (carboxylate-modified) nanoparticles.

Amine- and carboxylate-modified polystyrene latex nanoparticles were incubated under physiologically-relevant temperature conditions (37˚C) for 24 hours. Nanoparticle-protein samples were incubated under gentle end over end rotation agitation to reduce the potential for particle sedimentation effects. Equation 1 was used to estimate the total nanoparticle concentration used for all experiments, to ensure that the nanoparticle-to-protein ratio was maintained constant across the different polystyrene latex nanoparticle surface modifications measured.

$$N = \frac{(6 \times 10^{10}) \times S \times P_L}{\pi \times P_s \times d^3} \qquad \textbf{(Equation 4.1)}$$

Where $S$ represents the concentration of solids (%w/w), d the diameter (μm), $P_s$ the density of the bulk polymer (g/mL), and $P_L$ the density of latex (g/mL). The concentration of fetal bovine serum (FBS) selected was (10 %vol), mimicking cell culture conditions. The same batch of FBS was used for all experiments, corresponding to a total protein concentration of 3.9 mg/mL.

For detailed methodology on the preparation of polystyrene latex nanoparticles in biological media and their centrifugation-resuspension isolation from biological media, see methodology in Chapter 2. The same

method was applied in this chapter to perform a direct comparison between PTA and DLS.

### 4.5.2 Analysis of polystyrene latex nanoparticle properties

**Particle Tracking Analysis (PTA).** The particle size distribution of polystyrene latex nanoparticles suspended in PBS (at baseline and following incubation with media containing protein) were characterized using the NanoSight NS Pro (Malvern Panalytical, Malvern, UK), which was equipped with a 488 nm laser and a high-sensitivity sCMOS camera. An average was taken of three sample videos with all samples analysis being performed at ambient temperature (~25˚C) and under identical flow (1.5 µL/min). All post-processing analysis were automatically performed using the NTA software (NS Xplorer).

**Electrophoretic Light Scattering (ELS).** Zeta potential measurements for all samples was performed using a Malvern Zetasizer Nano ZS (Malvern Panalytical, Malvern, Worcestershire, UK). Zeta potential values were measured for all polystyrene latex nanoparticles at baseline and following incubation with medium containing protein, set at ambient temperature (25 °C) with a two-minute temperature equilibration of sample prior to each measurement. The Smoluchowski approximation was used for data processing and zeta potential calculations.

### 4.5.3 EAF4-MD multiplexed with Orthogonal Inline Detection (UV/MALS/DLS/Fluorescence)

EAF4 isolation, and analysis for nanoparticles, and nanoparticle-protein samples were performed using an AF2000 Asymmetrical Flow FFF system, which was configured with an EAF2000 Electrical Flow FFF channel. This system was multiplexed with two isocratic pumps (#PN1130) for controlling tip and focus flow, respectively. The running buffer was passed through a solvent organiser (#PN7140), solvent degasser (#PN7520), solvent selector (#PN7310), and a smart stream splitter (#PN1650) prior to entering the channel. The system was coupled with an electrical FFF module (#PN2411) to control the electrical field. A 350 µm spacer, and a regenerated cellulose

membrane with a 10 kDa molecular weight cut-off size were used for all measurements reported in this chapter, which were set at ambient temperature (25 °C).

The EAF4 system was coupled with multiple in-line detectors including a UV detector (#SPD-M40), a 21-angle multiangle light scattering (MALS) detector (#PN3621), refractive index (RI) detector (#PN3150), fluorescence detector (FLD) (#RF-20A XS), and a Zetasizer Nano ZS (Malvern Panalytical, Malvern, UK), which was used in combination with the radius of gyration ($R_g$) obtained from MALS analysis to calculate the hydrodynamic ($R_h$) for shape factor (SF) calculations using the equation below.

$$SF = Rg/Rh \quad \text{(Equation 4.2)}$$

**Fluorescence detection:** Particles containing fluorescent dyes were further analysed using the FLD detector, with carboxylate-modified nanoparticles possessing a yellow-green dye which was measured at excitation/emission ($\lambda_{em}$/ $\lambda_{ex}$) of 505 nm/515 nm, and amine-modified polystyrene latex nanoparticles with a fluorescent orange dye with an ($\lambda_{em}$/ $\lambda_{ex}$) of 475 nm/540 nm.

**Performance of system calibration:** System calibration was performed using bovine serum albumin (BSA) prior to sample analysis to perform calibration and verify MALS detector system performance.

Run conditions selected for the EAF4-based separation of polystyrene latex nanoparticles from bulk incubation media are shown in **Table 4.1**:

**Table 4.1** Corresponding run parameters used for the EAF4-MD-based resolution of polystyrene latex nanoparticles from protein-containing media. RC: Regenerated Cellulose, MWCO: Molecular weight cutoff size

| Parameter | |
|---|---|
| **Spacer** | 350 µm |
| **Membrane** | RC (10 kDa MWCO) |
| **Carrier solution** | 0.5 mM $Na_2CO_3$ |
| **Injection volume** | 20 µL of a 0.1 mg/mL sample |
| **Detector Flow** | 0.50 mL/min |
| **Current (+/-)** | 0.2 mA |

### 4.5.4 Selection of electrical field strength and polarity

**Electrical field strength** Optimal electrical field strength used for the resolution of nanoparticles from biological media was selected based on pre-defined parameters as shown in **Table 4.2** for electrical field strength combined with method development.

**Table 4.2** The electrical field strength as a function of the conductivity of the running buffer and applied electrical current.

| Applied Current (mA) | Conductivity (mS/cm) | Electrical Field Strength (V/m) |
|---|---|---|
| **0.1** | **0.1** | **3.05** |
| **0.2** | **0.1** | **6.10** |
| **0.3** | **0.1** | **9.15** |
| **0.4** | **0.1** | **12.20** |
| **0.5** | **0.1** | **15.26** |
| **0.6** | **0.1** | **18.31** |
| **0.7** | **0.1** | **21.36** |

**Polarity** The polarity opposite to the test particle net charge was applied to enable the movement of nanoparticles under the application of a

current/voltage. For example, a negative polarity was applied for positively-charged amine-modified polystyrene latex nanoparticles, and a positive polarity for negatively-charged unmodified and carboxylate- polystyrene latex nanoparticles.

**Selection of flow conditions** Following initial method development, the optimal run conditions were selected to ensure nanoparticle-protein separation from bulk protein medium as shown in **Figure 4.1**.

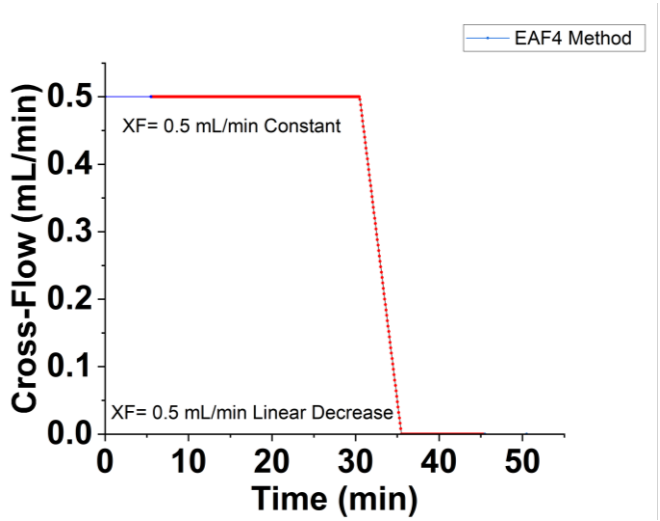


**Figure 4.1** Elution conditions optimized for EAF4-based separation of polystyrene latex nanoparticles from protein-containing incubation media.

### 4.5.5 Estimation of electrophoretic mobility and zeta potential parameters using EAF4

**Electrophoretic mobility** The electrophoretic mobility of samples was estimated by performing a reference measurement for each test polystyrene latex nanoparticle in the absence of an electrical field, and performing measurements in the presence of an electrical field (± 0.2 mA in positive and negative polarity mode).

The ratio of net retention times between measurements in the presence and absence of the electrical field and total drift velocity was used for each measurement with the ratio of crossflow and detector flow.

The electrical field strength (E) was determined by measuring the conductivity during elution, using the following equation:

$$\mathrm{E} = \frac{\mathrm{I}}{\mathrm{A}.\kappa}$$ **(Equation 4.3)**

Where *E* (V/m) represents the electrical field strength, *A* the applied current (mA), and *κ* the conductivity of the carrier liquid (mS/m).

The drift velocity induced by the cross flow, $v_c$, was determined using the following equation: $v = \frac{F_c}{A}$ **(Equation 4.4)**

Where $F_c$ represents the cross flow (mL/min) and A ($m^2$) the channel area. This parameter was estimated at 2.543 x $10^{-6}$ m/s for measurements performed with a current of 0.2 mA.

Subsequently, the drift velocity induced by the electrical field, $v_{em}$, was calculated using the following equation:

$$v_{em} = \left[ e^{\frac{t_{r,i}}{t_r} ln\left(1+\frac{fF_c}{F_{det}}\right)} - \left[1 + \frac{fF_c}{F_{det}}\right] \right] . \frac{F_{det}}{A.f}$$ **(Equation 4.5)**

Where $t_{r,i}$ is the retention time with the applied current, $t_f$ the retention time in the absence of a current/voltage, *f* the focusing parameter, $F_c/F_{det}$ cross flow/detector flow ratio, and *A* the channel area. The sum of both drifts was used as the total drift for determining electrophoretic mobility. A summary of the values for each of these parameters, is represented below:

**Table 4.3** Corresponding parameters used to calculate the drift velocity used for input into electrophoretic mobility calculations:

| Parameter | Value |
|---|---|
| **$F_c$ (mL/min)** | 0.5 |
| **$F_{det}$ (mL/min)** | 0.5 |
| **$F_c/F_{det}$** | 1 |
| **A ($m^2$)** | 0.0032775 |

The total drift velocity was plotted against the electrical field strength, the slope of which was determined using a linear least squared fit, representing the electrophoretic mobility ($\mu_{em}$). The correlation coefficient of the linear

regression was used to determine the quality of fit for each calculation. The following equation was used to estimate electrophoretic mobility:

$$\mu_{em} = \frac{\upsilon}{E} \qquad \text{(Equation 4.6)}$$

Where $\mu_{em}$ represents electrophoretic mobility,[185] $v$ the drift velocity induced by the electrical field, and $E$ the electrical field strength applied.

**Calculation of zeta potential** The Smoluchowski approximation,[186] which is normally used for nanoparticulate systems, was used to determine the zeta potential (ζ) of eluting peaks in mV, using the following equation:

$$\zeta = \frac{3}{2}\frac{\eta.\mu_{em}}{\epsilon_0\epsilon_r f(\kappa_a)}.1000 \qquad \text{(Equation 4.7)}$$

Where $\eta$ is the viscosity of the carrier liquid at 25 °C, $\varepsilon_0$ the vacuum permittivity (physical constant), $\mu_{em}$ the calculated electrophoretic mobility, $\varepsilon_r$ relative permittivity of water at 25 °C, $f(\kappa a)$ the Henry's function, κa=κ $R_h$, κ the reciprocal of the Debye length (thickness of the electrical double layer), $R_h$ the hydrodynamic radius of the particle in solution, $\kappa a$ estimate of the ratio of the particle radius to the electrical double layer. The corresponding values are summarised in **Table 4.4**:

**Table 4.4** Corresponding input parameters used to determine the zeta potential of analysed samples.

| Parameter | Value |
|---|---|
| **$\varepsilon_0$ (A s $V^{-1}$ $m^{-1}$)** | 8.854187 x $10^{-12}$ |
| **$\varepsilon_r$ (-)** | 78.53114 |
| **f(κa)** | 1.5 |
| **$R_h$ (nm)** | 50 |

### 4.5.6 Calculation of nanoparticle recovery following EAF4-based separation

Nanoparticles, and nanoparticle-protein samples are known to interact with the channel membrane during the FFF separation program as such the particle recovery (%) needs to be calculated to ensure the quality of collected data. This is performed using the equation below:

$$\% \text{ Recovery} = \frac{A}{A_0} \times 100$$ **Equation 4.8**

Where, A is the peak area determined for the nanoparticles (in the presence of the corresponding crossflow applied in the optimal separation method, and $A_0$ represents the peak area of NPs with minimal membrane interactions (absence of cross flow).

### 4.5.7 EAF4-multidetector (MD) method quality verification

The EAF4-MD methodology selected below was developed to be in line with the ISO published in 2021,[171] which outlines the standard parameters needed to validate FFF-based methods. This includes a minimum sample recovery threshold of (≥ 70%) and reporting the method of recovery as per equation 4.8.

Furthermore, when using multiple detectors, the void peak should be used as a reference point to align the various measurements. This also allows for the calculations of delay volume, and void peak volume.

### 4.5.8 Statistical Analysis

All data analysis was performed within Origin (version 2022). Unless otherwise stated, a one-way ANOVA statistical test was performed to determine if there were any statistically significant differences in measured sample results ($P<0.05$).

## 4.6 Results

Polystyrene latex nanoparticles were selected in this thesis as a robust and non-degradable model system to investigate the potential of using EAF4 for the resolution of nanoparticles from media containing serum, following a 24-hour incubation at 37 °C to allow for the formation of further nanoparticle-protein sub-populations (i.e., the protein corona). In Chapter 3, we demonstrated that conventional and frit inlet AF4 can gently separate nanoparticle-protein complexes formed from the bulk incubation media and analysed the physical properties of the different fractions formed.

### 4.6.1 *In situ* analysis of nanoparticle-protein complexes using particle tracking analysis in fluorescence and scatter modes

Particle tracking analysis (PTA) was used in both fluorescence and scatter mode to compare both the measured number of particles in each mode prior to and following incubation with media containing 10 %vol FBS at 37 °C. The reason for selecting both modes on the PTA was to contrast the effects of background contributions from the excess protein contained within the incubation media on the number of detected particles and corresponding particle measured particle diameter.

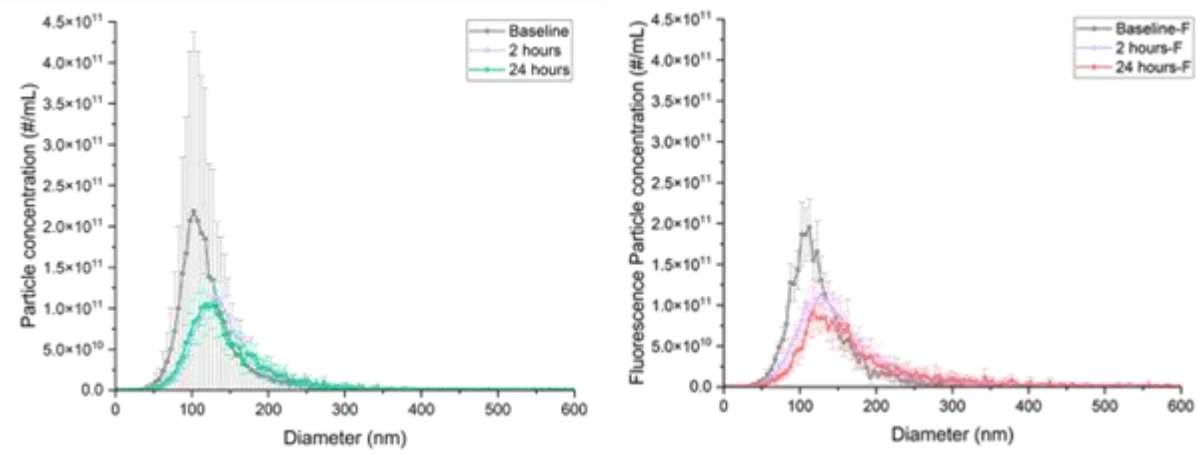


**Figure 4.2.** Carboxylate-modified polystyrene latex nanoparticle particle size distribution as measured by PTA in the light scatter (green) and fluorescence mode (red) at baseline and following (2 and 24 hr) incubations with 10 %vol FBS at 37 ˚C. Error bars represent mean ± standard deviation (n=3

A mean nanoparticle diameter of 123 (±2) nm was measured for baseline carboxylate-modified nanoparticles, which increased to 149 (±3) nm following a two-hour incubation, and 147 (±7) nm following 24-hour incubation when measured in light scattering mode. While similar trends were observed in the PTA fluorescence measurement mode, we observed an increase in mean particle diameter at baseline 131 (±3) nm and following two-hour 160 (±5) nm and 24-hour 178 (±11) nm incubations. The increase in mean particle diameter following incubation in medium containing protein, was accompanied by peak widening for measured carboxylate-modified polystyrene latex nanoparticle-protein samples due to the formation of nanoparticle-protein, and protein-protein aggregates shown in (**Table 4.5**) below. With an increase in particle

size span was observed with a baseline span of (0.70) increasing with incubation time in light scattering modes (0.89) at two-hour and (0.99) 24-hour incubations. A similar trend was observed with the NTA fluorescence mode, where an increase in measured size distribution was span observed from (0.86) at baseline for carboxylate-modified polystyrene latex nanoparticles, to (1.0) following two-hour incubations, and (1.11) following 24-hour incubations. We observed an increase in measured span for nanoparticle, and nanoparticle-protein samples when characterized using fluorescence mode compared to light scattering mode.

**Table 4.5** Corresponding *in situ* particle size and concentration measurements of carboxylate-modified polystyrene latex nanoparticles using PTA in the scatter and fluorescence modes (n=3). Values represented are mean ± standard deviation.

| Mode | Scatter | | | Fluorescence | | |
|---|---|---|---|---|---|---|
| Incubation duration (hour) | 0 | 2 | 24 | 0 | 2 | 24 |
| Mode [nm] | 101 (3) | 133 (9) | 128 (9) | 113 (7) | 128 (13) | 118 (19) |
| Mean [nm] | 114 (3) | 149 (3) | 147 (7) | 131 (3) | 160 (5) | 178 (11) |
| Concentration [#/mL] | 1.36E+12 (2.3E+11) | 1.85E+12 (1.21E+11) | 1.85E+12 (2.50E+11) | 2.69E+12 (1.71E+11) | 2.31E+12 (1.2E+11) | 1.91E+12 (9.32E+10) |
| D10 [nm] | 80 (2) | 98 (2) | 94 (5) | 84 (1) | 93 (2) | 101 (3) |
| D50 [nm] | 106 (1) | 137 (2) | 133 (7) | 118 (3) | 142 (3) | 151 (4) |
| D90 [nm] | 155 (10) | 212 (10) | 217 (13) | 185 (9) | 245 (13) | 282 (26) |
| Span | 0.70 | 0.89 | 0.99 | 0.86 | 1.0 | 1.11 |

The ratio of measured particle numbers by fluorescence and scatter mode was used to determine the labelling efficiency and the ability of the NS Pro system to measure nanoparticle scattering effects over a scattering background containing protein. Overall, the ratio of measured particle concentration was ~ 1 for baseline and 1.25 for particles incubated for 2 hours, indicating that only the contribution of nanoparticles and nanoparticle-protein complexes was being measured as opposed to protein-protein agglomerates.

Another key trend to emerge was a decrease in the mean particle concentration measured by PTA following incubation with medium containing protein, as shown in both light scattering and fluorescence measurement modes (**Table 4.5**). This was likely caused due to nanoparticle-protein aggregation, and the early precipitation of nanoparticle-protein complexes formed.

The measured mode diameter observed for carboxylate-modified polystyrene latex nanoparticles following incubation with media containing protein at both 2 and 24-hour incubation timepoints changed from a baseline of 102.5 (±5) nm at time 0, increasing to 132.5 (±9.0) nm following a two-hour incubation, and 127.5 (±9.0) nm following a 24-hour incubation when measured in the light scattering mode. A similar trend was observed for polystyrene latex nanoparticle samples analysed in the fluorescence mode, with a baseline mode of particle diameter of 112.5 (±7.0) nm, which increased to 127.5 (±13.0) nm following a two-hour incubation, and 117.5 (±19) nm following a 24-hour incubation with medium containing protein. A decrease in the mean mode diameter was observed following a 24-hour incubation when compared to two-hour incubations in both light scattering, and fluorescence mode analysis.

Next, changes in particle size observed with PTA in fluorescence and scatter mode were compared with DLS measurements for carboxylate-modified nanoparticles isolated and recovered from 10% *v/v* FBS. Overall, a similar

trend of increasing z-average diameter was observed with DLS measurements.

**Table 4.6** Parameters measured by DLS for carboxylate-modified polystyrene latex nanoparticles incubated with 10% *v/v* FBS at 37 °C for various durations and recovered by centrifugation-resuspension. All values are reported as mean (± standard deviation), n=3.

| Incubation duration (hours) | Z-average (nm) | PDI |
|---|---|---|
| **0** | 95.5 (0.1) | 0.01 (0.01) |
| **2** | 130.0 (2.0) | 0.04 (0.01) |
| **24** | 139.4 (2.0) | 0.04 (0.00) |

An overlay of the corresponding PTA and DLS intensity-based size distribution is presented in **Figure 4.3** as follows:

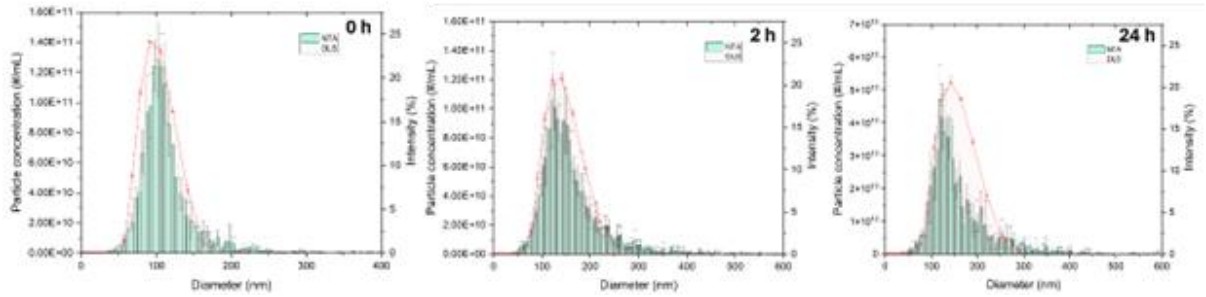


**Figure 4.3** Overlay of corresponding PTA traces in scatter mode and intensity-based size distribution as measured by DLS for carboxylate-modified polystyrene latex nanoparticles incubated with 10 %vol FBS for 0, 2 and 24 hours at 37 °C.

Overall, the overlapping traces corresponding to PTA and DLS data indicate the presence of additional aggregate subpopulations with the PTA traces captured, which were absent in the DLS measured particle size distributions. These differences may be attributed to the physical mode of measurement (ensemble for DLS versus particle-by-particle analysis with PTA) as well as the potential for sample precipitation during the DLS measurements. Therefore, PTA was selected as the method of choice for further investigation in amine-modified polystyrene latex nanoparticles.

Next, the impact of incubation of amine-modified polystyrene latex nanoparticles in media containing 10 %vol FBS was studied using the NS pro PTA setup in fluorescence and scatter mode (**Figure 4.4**).

Amine-modified polystyrene latex nanoparticles were then incubated within 10 %vol FBS for two-, and 24-hours and analysed using PTA in scatter and fluorescence mode.

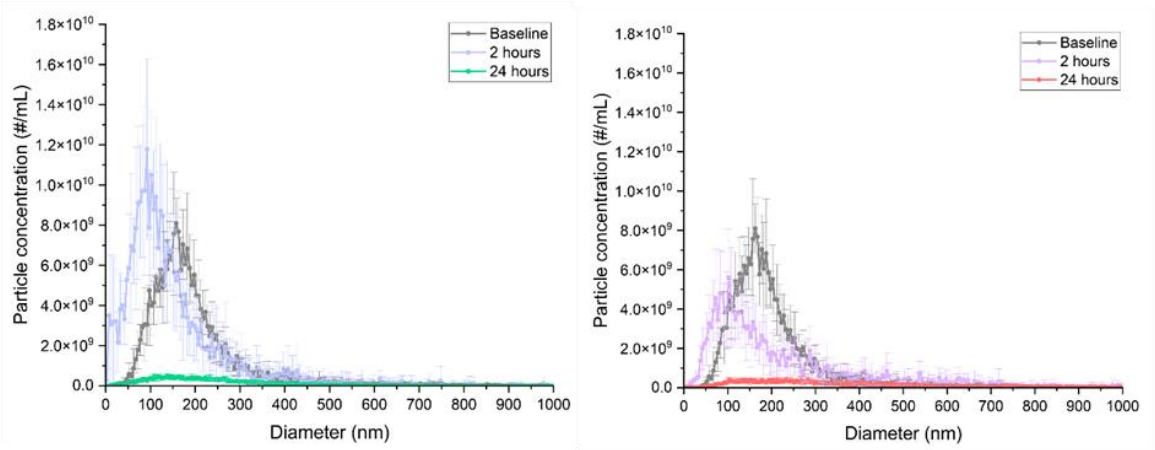


**Figure 4.4** Amine-modified polystyrene latex nanoparticle particle size distribution as measured by PTA in the light scatter (green) and fluorescence mode (red) at baseline and following (2 and 24 hr) incubations with 10 %vol FBS at 37 ˚C. Error bars represent mean ± standard deviation (n=3).

Amine-modified polystyrene latex nanoparticles had a measured mean particle size of 193 (± 9) nm at baseline, and 153 (± 17) nm following 2-hour incubation, and 241 (± 21) nm following a 24-hour incubation when analysed in the scattering mode. A similar trend was observed for samples analysed in the fluorescent mode, with a mean baseline diameter of 314 (± 29) nm at 0 hours, 233 (± 23) nm at 2-hour, and 402 (± 124) nm following a 24-hour incubation in medium containing protein. For amine-modified polystyrene latex nanoparticles, the trend shows an increase in mean particle size following at longer incubation time-points following light scattering, and fluorescent analysis. However, baseline particle analysis has shown high particle agglomeration from the expected particle size (as per previous measurements).

These trends are reflected in the span of the particle distribution with a baseline span of (1.16) at baseline, increasing to (2.0) at 2-hour incubation, and (1.66) following 24-hour incubation for samples analysed using light

scattering mode. A similar trend was observed for particles measured using fluorescence mode with a baseline span of (1.51), which increases to (2.78) following 2-hour incubation, and (2.20) following 24-hour incubation. The increase in particle span was typically accompanied by a decrease in the mean particle concentration as shown in (**Table 4.7**) for samples analysed using both light scattering, and fluorescence mode.

The measured mode diameter observed for amine-modified polystyrene latex nanoparticles following incubation with media containing protein at both 2 and 24-hour incubation timepoints changed from a baseline of 153 (±24) nm at time 0, and then 93 (±36) nm following a two-hour incubation, and 138 (±40) nm following a 24-hour incubation when measured in the light scattering mode. A similar trend was observed for amine-modified polystyrene latex nanoparticle samples analysed in the fluorescence mode, with a baseline mode of particle diameter of 173 (±37) nm, which increased to 103 (±11) nm following a two-hour incubation, and 153 (±39) nm following a 24-hour incubation with medium containing protein. An increase in model diameter was observed when comparing early phase incubation (2-hour), and prolonged intubation (24-hour) with severe particle aggregation occurring at baseline in both light scattering, and fluorescent mode analysis.

**Table 4.7** Corresponding *in situ* particle size and concentration measurements of amine-modified polystyrene latex nanoparticles using PTA (n=3). Values presented represent mean ± standard deviation.

| **Mode** | **Scatter** | | | **Fluorescence** | | |
|---|---|---|---|---|---|---|
| Incubation duration (hours) | 0 | 2 | 24 | 0 | 2 | 24 |
| Mode [nm] | 158 (24) | 93 (36) | 138 (40) | 173 (37) | 103 (11) | 153 (39) |
| Mean [nm] | 193 (9) | 153 (17) | 241 (21) | 314 (29) | 233 (23) | 402 (124) |
| Concentration [#/ml] | 2.09E+11 (1.89E+10) | 2.96E+11 (7.10E+10) | 2.28E+10 (1.75E+09) | 2.23E+11 (2.69E+10) | 1.76E+11 (1.97E+10) | 2.92E+10 (3.17E+09) |
| D10 [nm] | 99 (8) | 50 (14) | 87 (11) | 129 (10) | 67 (7) | 119 (36) |
| D50 [nm] | 170 (8) | 118 (10) | 204 (12) | 264 (23) | 159 (17) | 309 (95) |
| D90 [nm] | 296 (20) | 287 (45) | 425 (32) | 528 (64) | 505 (63) | 798 (250) |
| Span | 1.16 | 2.0 | 1.66 | 1.51 | 2.78 | 2.20 |

The measured labelling efficiency between the scatter and fluorescence mode in the case of amine-modified polystyrene latex nanoparticles overall indicated a highly variable ratio across all conditions tested, with a corresponding ratio of ~1 at baseline, changing to 0.59 following a two-hour incubation in 10 %vol FBS and 1.28 following a 24-hour incubation period. Such significant differences in the particle concentration ratio may be explained by the light scattering properties of the amine-modified nanoparticles and a high background noise resulting from the larger agglomerates formed in response to protein corona formation.

### 4.6.2 Analysis of carboxylate-modified polystyrene latex nanoparticles by EAF4-UV-MALS-DLS-fluorescence

The EAF4-MALS-fluorescence fractograms for carboxylate-modified polystyrene latex nanoparticles are presented in **Figure 4.5**. The corresponding retention time for the peak maximum shifted substantially for the 24-hour samples, from a single peak occurring at ~18.7 min (0 mV) at 0 hours (baseline), to a bimodal peak occurring at ~24 and 35 min (0 mV) for 24 hour samples, indicating a change in nanoparticle size following incubation in protein containing media in both UV and fluorescence traces.

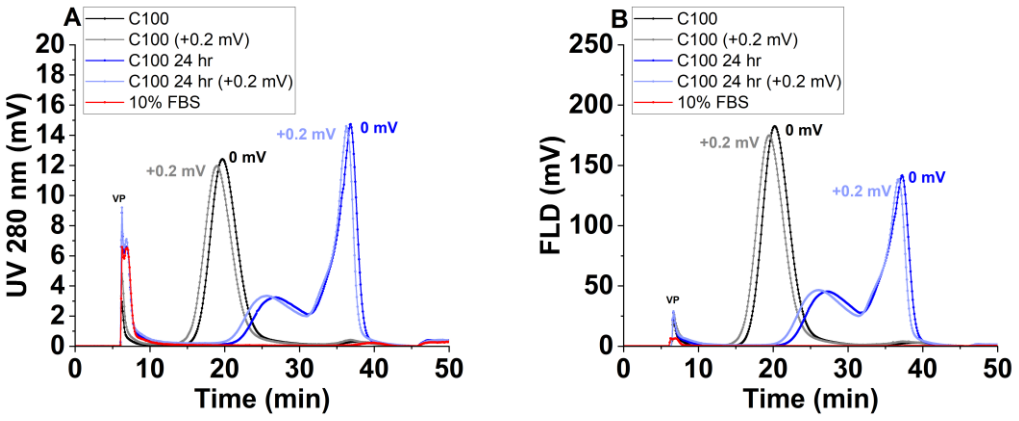


**Figure 4.5** EAF4-UV-fluorescence for carboxylate-modified polystyrene latex nanoparticles (0.1 mg/mL) at 0 and 24 hours (10 %vol FBS at 37˚C). Corresponding fractograms (A) for UV (280 nm), and (B) for fluorescence traces (excitation/emission 505/515 nm). An injection of (10 %vol FBS- red trace) was performed to establish the elution profile of the bulk unbound protein fraction for comparison with nanoparticle-protein elution profiles. All measured samples (N=3). VP: Void Peak.

A summary of the elution times corresponding to different samples in the presence and absence of an electric field is presented as follows:

**Table 4.8** Mean (± standard deviation) AF4-UV peak maxima elution times for carboxylate-modified polystyrene latex nanoparticles in the absence (0 mV) and presence (0.2 mV) of applied current. $R_t$: Retention time, N=3.

| | **0 mV $R_t$ (min)** | | **0.2 mV $R_t$ (min)** | |
|---|---|---|---|---|
| **Sample** | Peak 1 | Peak 2 | Peak 1 | Peak 2 |
| 0 | 19.6 | - | 18.8 | - |
| 24 | 26.3 | 36.8 | 25.3 | 36.3 |
| 10% FBS | 6.8 | - | - | - |

The fluorescence fractogram trace for carboxylate-modified nanoparticles, confirmed all the observed peaks with the UV trace, which could be used to confirm that the eluting peaks correspond to the fluorescent carboxylate-modified polystyrene latex nanoparticles and their complexes with protein.

Peaks eluting for 0 (PBS baseline) and 24 hours (incubated in 10 %vol FBS) had a percent recovery of 89.1% (±0.8) and 80.4% (±1.2), respectively, demonstrating acceptable sample recovery levels.

Next, the impact of the application of a combined cross flow and electrical field strength on the corresponding MALS and DLS traces, and measured radius of gyration and hydrodynamic radius was examined.

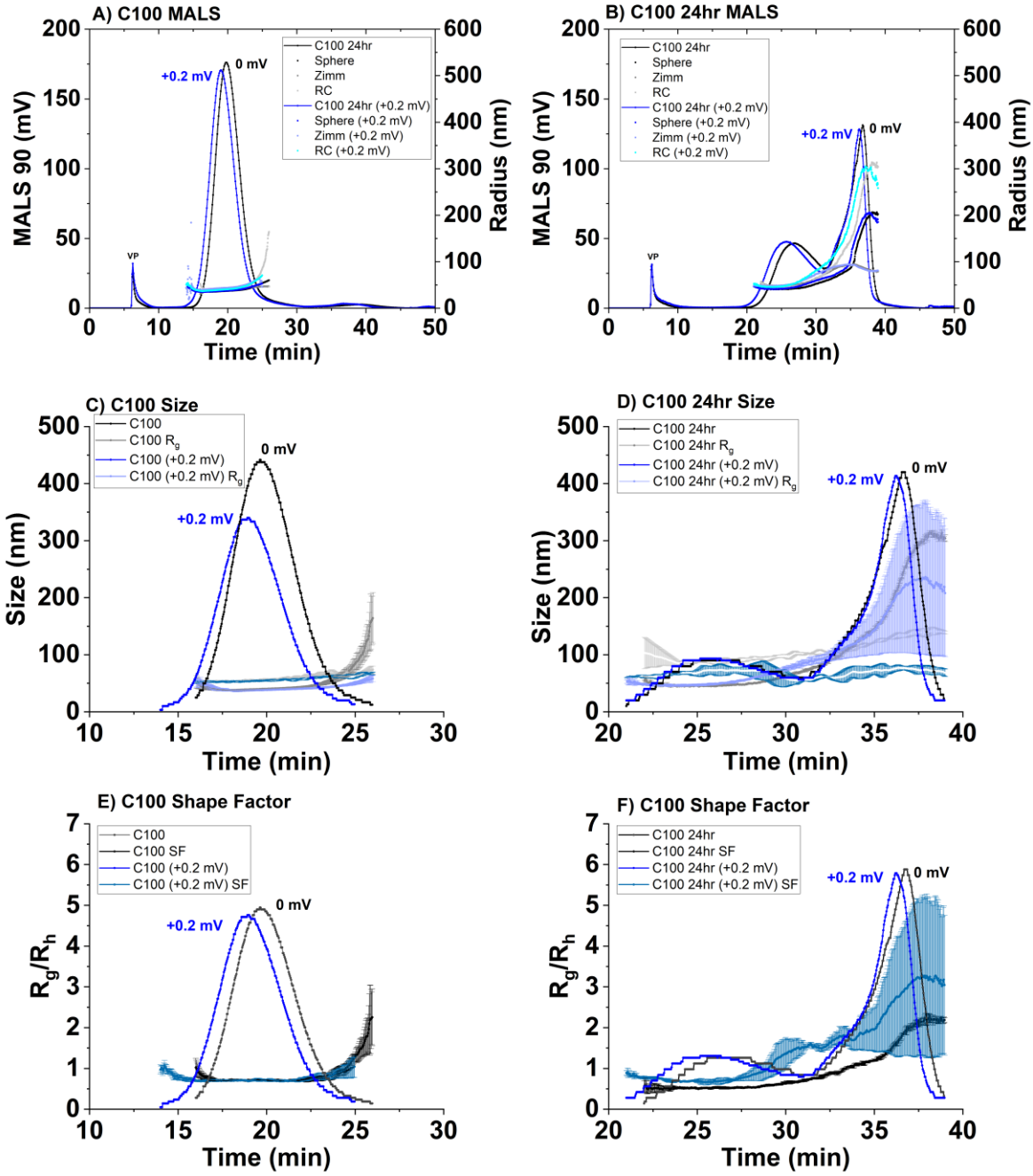


**Figure 4.6** EAF4-MALS for carboxylate-modified polystyrene latex nanoparticles at 0 and 24 hours (10 %vol FBS at 37 °C) (A,B). Corresponding overlay of the elution profile with the radius of gyration profiles of carboxylate-modified polystyrene latex nanoparticles (C-D). Measured shape factor ($R_g/R_h$) (E-F). N=3.

Similar to the UV and fluorescence fractogram traces, the MALS trace for carboxylate-modified nanoparticles was associated with a strong signal (200 mV). A significant change in the MALS profile was observed between 0 hour and 24-hour samples, with a single peak eluting at 18.8 min (0.2 mV), which at 24 hours formed a bimodal elution profile occurring at approximately 18.9 min and 37 min, respectively (**Figure 4.6** A-B). This

change in profile indicates the formation of different nanoparticle-protein complexes, which was also confirmed by shape factor calculations determined from the MALS and DLS traces.

The shape factor determined for carboxylate-modified nanoparticles was ~0.7 in the main eluting peak (15-25 min) at 0 hours, confirming spherical morphology, which following a 24-hour incubation led to the formation of a bimodal distribution, with the first peak having a calculated shape factor of 0.7 (spherical) and the second peak having a shape factor >1 (non-spherical, elongated).

### 4.6.3 Analysis of amine-modified polystyrene latex nanoparticles by EAF4-UV-MALS-DLS-fluorescence detection

Following the successful optimisation of EAF4 methodology for carboxylate-modified polystyrene latex nanoparticles, the same method was applied to the analysis of amine-modified polystyrene latex nanoparticles at 0- and 24-hours incubation.

EAF4-MALS-fluorescence fractograms for amine-modified polystyrene latex nanoparticles, had a much lower signal strength (~20 mV) corresponding retention time for the peak maximum shifted substantially for the 24 hour samples, from a single peak occurring at ~20 min (0 mV) at 0 hours (baseline), to a bimodal peak occurring at ~24 and 35 min (0 mV) for 24 hour samples, indicating a change in nanoparticle size following exposure to the protein containing media in both UV and fluorescence traces. A summary of the elution times corresponding to different samples in the presence and absence of an electric field is presented as follows:

The corresponding UV and fluorescence trace fractograms for these samples are presented as follows:

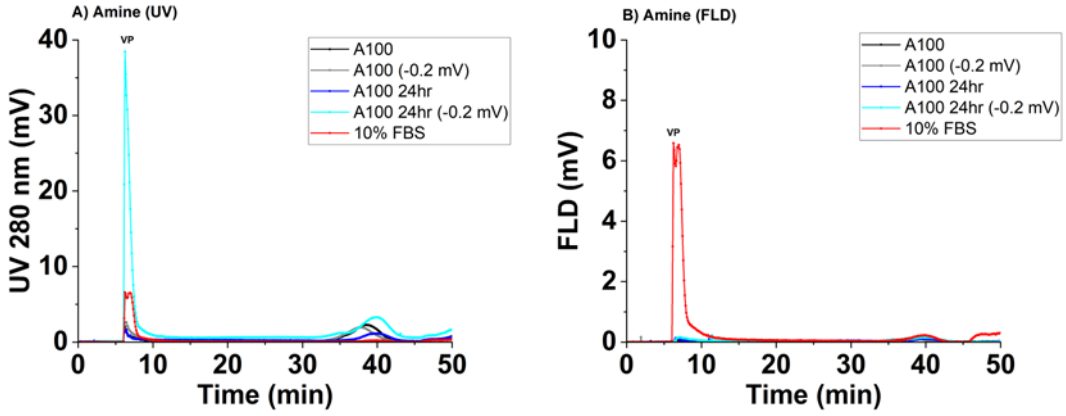


**Figure 4.7** EAF4-UV-fluorescence of amine-modified polystyrene latex nanoparticles (0.1 mg/mL) at 0- and 24-hour incubation in PBS containing 10 %vol FBS at 37˚C. The UV detector was set at 280 nm (left panel), and the fluorescence detector was set at ex/em 475 nm/540 nm (right panel). A 10 %vol FBS injection (red trace) was performed to establish the elution profile of the bulk unbound protein fraction for comparison with nanoparticle-protein samples. N=3. VP: Void Peak

The fluorescence fractogram trace for amine-modified nanoparticles was identical to the elution profile observed with the UV trace, which confirmed that the eluting peaks correspond to the fluorescent amine-modified polystyrene latex nanoparticles and their complexes with protein.

Fractions eluting for 0 (PBS baseline) and 24-hour (10 %vol FBS) had a percent recovery of 17.4% (±1.1) and 19.5% (±33.6), respectively, showing significant loss of amine-modified nanoparticles during the fractionation process and a high degree of variation.

**Table 4.9** Change in peak amine-modified polystyrene latex nanoparticle elution at baseline, and following 24hr incubation within protein-containing media. Mean (± standard deviation) AF4-UV peak elution times for amine-modified polystyrene latex nanoparticles in the absence (0 mV) and presence (0.2 mV) of applied current. $R_t$: Retention time; N=3.

| | **0 mV $R_t$ (min)** | | **0.2 mV $R_t$ (min)** | |
|---|---|---|---|---|
| **Sample** | Peak 1 | Peak 2 | Peak 1 | Peak 2 |
| 0 | 37.8 | - | 38.7 | - |
| 24 | 35.8 | 39.6 | 35.3 | 40.1 |
| 10% FBS | 6.7 | - | - | - |

### 4.6.4 Analysis of unmodified polystyrene latex nanoparticles by EAF4-UV-MALS-DLS

The unmodified polystyrene latex nanoparticles used in this thesis did not contain a fluorophore; therefore, only UV, MALS, and DLS detectors were used for the analyses.

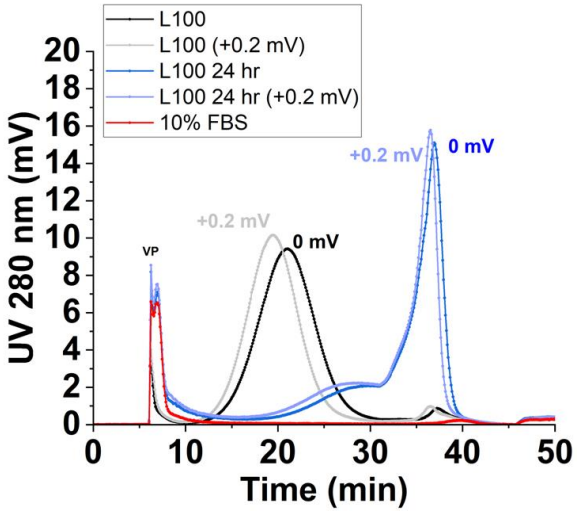


**Figure 4.8** EAF4-UV-fluorescence for unmodified polystyrene latex nanoparticles (0.1 mg/mL) at 0 and 24 hours (10 %vol FBS at 37˚C). Showing an UV (280 nm) fractogram. An injection of (10 %vol FBS- red trace) was performed to establish the elution profile of the bulk unbound protein fraction for comparison with nanoparticle-protein elution profiles. N=3. VP: Void Peak.

The retention time for the peak maxima shifted substantially from 0 hour (baseline) to 24 hours post-incubation, from a predominant peak occurring at ~19.4 min (0.2 mV) at 0 hours (baseline), to a bimodal trace occurring with peak 1 at ~26.2 and 36.4 min (0.2 mV) for 24-hour samples, indicating a change in nanoparticle size following exposure to the protein containing media (UV traces). These results indicate a potential significant change in unmodified latex nanoparticle size and charge following incubation in protein containing media.

Fractions eluting for 0 (PBS baseline) and 24-hour (incubated in 10 %vol FBS) had a percent recovery of 86.2% (±1.6) and 77.6% (±0.3), respectively, with acceptable sample recovery levels.

A summary of the elution times corresponding to different samples in the presence and absence of an electric field is presented as follows:

**Table 4.10**. Change in peak unmodified modified polystyrene latex nanoparticle elution at baseline and following 24hr incubation within protein-containing media. Mean (± standard deviation) AF4-UV peak maxima elution times for unmodified polystyrene latex nanoparticles in the absence (0 mV) and presence (0.2 mV) of applied current. $R_t$: retention time, N=3.

| | **0 mV $R_t$ (min)** | | **0.2 mV $R_t$ (min)** | |
|---|---|---|---|---|
| **Sample** | Peak 1 | Peak 2 | Peak 1 | Peak 2 |
| 0 | 21.1 | 36.9 | 19.4 | 36.3 |
| 24 | 26.3 | 36.7 | 26.2 | 36.4 |
| 10% FBS | 6.7 | - | - | - |

Next, the impact of the application of a combined cross flow and electrical field strength on the corresponding MALS and DLS traces, and measured radius of gyration and hydrodynamic radius was examined.

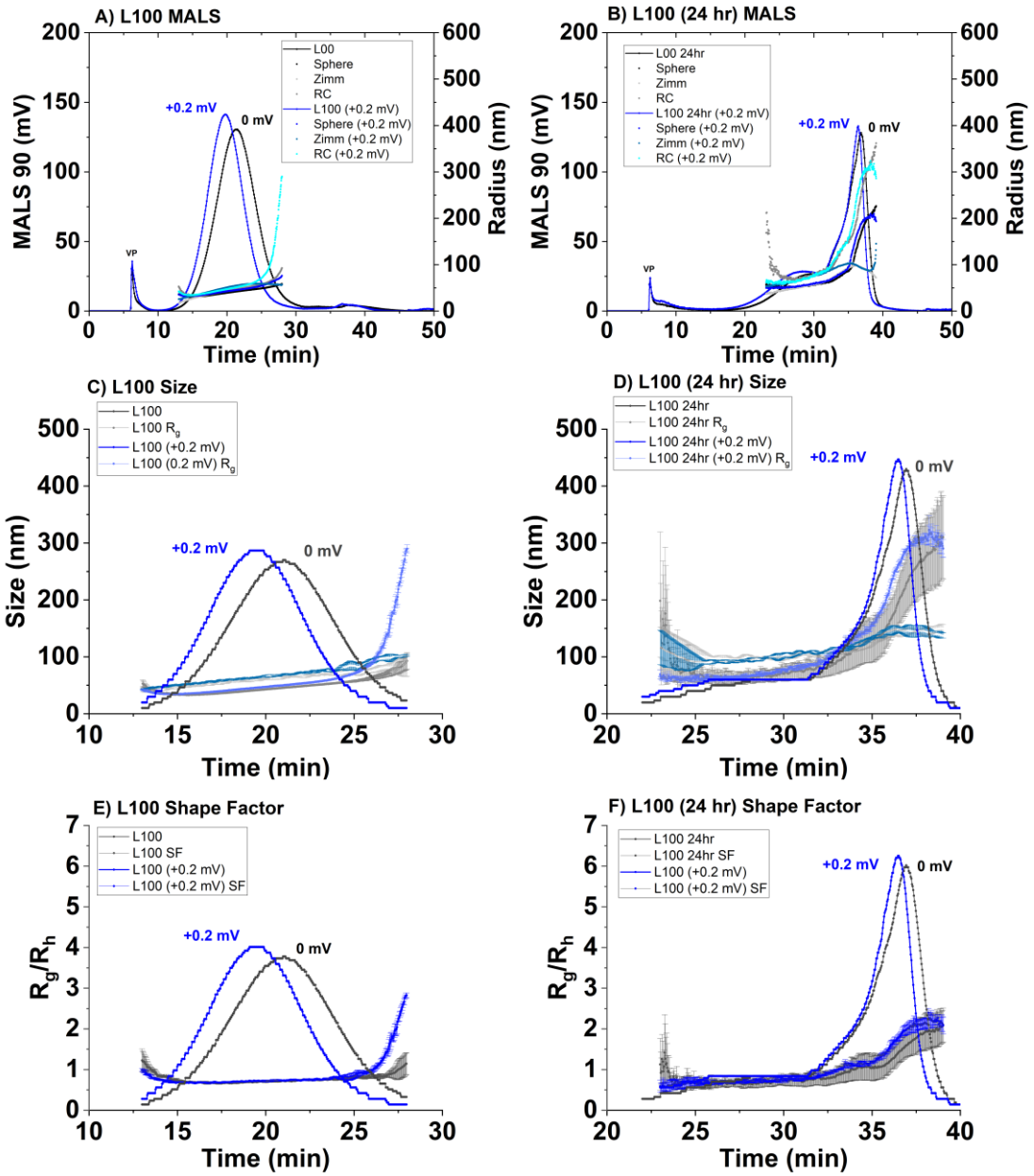


**Figure 4.9** Corresponding EAF4-MALS fractograms for unmodified polystyrene latex nanoparticles at 0 and 24 hours incubated in 10 %vol FBS at 37 °C (B). Corresponding overlay of the elution profile with the radius of gyration profiles of unmodified polystyrene latex nanoparticles (C-D). Measured shape factor ($R_g/R_h$) (E-F). N=3.

The EAF4-MALS elution time for unmodified polystyrene latex nanoparticles, showed a strong signal at baseline, and following 24-hour incubation within protein-containing medium. Furthermore, following incubation we observed a shift in the MALS trace for unmodified nanoparticles with a single peak eluting at 19.7 min (at baseline), increasing to a bimodal elution occurring at 30 min for the first peak, and at 36.8 min for the second peak as shown in (**Figure 4.9A-B**) above. This increase in elution time indicates an increase in mean particle radius and the formation

of various nanoparticle-protein, and protein-protein complexes which were observed using MALS, and DLS data to calculate the shape factor **(Figure 4.9E-F)**.

The calculated shape factor for unmodified particles was ~0.7 at baseline which confirms a spherical morphology for these particles and remains at ~0.7 for the initial peak following incubation (19.7 min), increasing to ~1.5 for the second elution peak (36.8 min) which suggests an elongated, and non-spherical morphology (>1).

### 4.6.5 Comparison of the zeta potential and electrophoretic mobility parameters as measured by EAF4, and ELS.

The corresponding charge-related parameters for amine- and carboxylate-modified nanoparticles derived from EAF4 were compared with equivalent parameters derived from electrophoretic light scattering. A summary of the reported parameters is included as follows:

**Table 4.11** Electrical parameters obtained for 100 nm polystyrene latex nanoparticles (0.1 mg/mL sample concentration) at baseline and following incubation with 10% *v/v* FBS at 37 C for 24 hours. Values represented are mean ± standard deviation. EAF4-MALS: electric asymmetric flow field flow fractionation-multiangle light scattering; EAF4-UV: electric asymmetric flow field flow fractionation-ultraviolet; ELS: Electrophoretic Light Scattering; μ: electrophoretic mobility; ζ: zeta potential, $R^2$: quality of fit (n=3). ND: Not Determined.

| ***Sample*** | ***EAF4-MALS*** | | | ***EAF4-UV*** | | | ***ELS*** |
|---|---|---|---|---|---|---|---|
| | **μ (μm cm $V^{-1}$ $s^{-1}$)** | **ζ (mV** | **$R^2$** | **μ (μm cm $V^{-1}$ $s^{-1}$)** | **ζ (mV)** | **$R^2$** | **ζ (mV)** |
| *Carboxylate* | | | | | | | |
| *Peak 1* | -2.98 | -38.21 | 0.987 | -3.27, | -41.88, | 0.965, | -34.0 ± 0.5 |
| *Peak 2* | | | | -1.15 | -14.68 | 0.995 | |
| *Carboxylate 24h* | | | | | | | |
| *Peak 1* | -2.57, | -32.86, | 0.830, 0.992 | -2.09, | -26.72, | 0.822, | -24.8 ± 0.4 |
| *Peak 2* | -0.89 | -11.42 | | -0.94 | -12.00 | 0.998 | |
| *Amine* | | | | | | | |
| *Peak 1* | -0.36 | -4.57 | 0.0246 | 1.75, | 22.46, | 0.0632, | 50.4 ± 0.8 |
| *Peak 2* | | | | 0.29 | 3.69 | 0.1202 | |
| *Amine 24h* | | | | | | | |
| *Peak 1* | ND, | ND, | ND, | ND, | ND, | ND, | -20.3 ± 0.4 |
| *Peak 2* | ND | ND | ND | ND | ND | ND | |
| *Unmodified* | | | | | | | |
| *Peak 1* | -4.59, | -58.83, | 0.992, | -4.15, | -53.10, | 1, | -33.5 ± 0.8 |
| *Peak 2* | -1.02 | -13.08 | 0.898 | -1.21 | -15.53 | 0.895 | |
| *Unmodified 24h* | | | | | | | |
| *Peak 1* | -1.14, | -14.58, | 0.772, | -2.40 | -30.71, | 0.990, | -31.6 ± 0.6 |
| *Peak 2* | -0.65 | -8.31 | 0.983 | -0.75 | -9.61 | 0.996 | |

The electrophoretic mobility (μ) obtained with the UV and MALS detectors was calculated as the slope of the drift velocity versus the effective electric field strength (see Equation 4.6). Therefore, the $R^2$ parameter reported in **Table 4.11** was used as an estimate of the reliability of electrophoretic mobility (μ) measurement.

For carboxylate-modified nanoparticles, a single peak was observed at 0 hour (baseline), which changed to two peaks following a 24-hour incubation in 10% vol FBS. It was possible to estimate μ and zeta potential values for both timepoints. In the case of both EAF4-MALS and EAF4-UV, a significant change in zeta potential was observed following exposure to protein-containing media, indicating the surface adsorption of proteins from the incubation media.

The $R^2$ quality of fit parameter obtained from both EAF4-MALS (-38.21 and -32.86 mV) and EAF4-UV (-41.88 and -26.72 mV) was >0.8, indicating an acceptable quality of fit, and reliable measured μ and zeta potential, for both 0- and 24-hour measurements, respectively. The zeta potential values obtained from both detectors were comparable to the electrophoretic light scattering (ELS) measurements by DLS (-34.0 mV and -24.8 mV) for both 0- and 24-hour incubation in 10% vol FBS.

Results obtained for the amine-modified nanoparticles were unreliable due to the very low $R^2$ and could not be determined from the 24-hour timepoints due to the poor signal and low recovery rates. Therefore, further conclusions could not be drawn from the amine-modified EAF4 data.

Similar to carboxylate-modified polystyrene latex nanoparticles, unmodified nanoparticles, had a single peak occurring at 0 hour (baseline), which changed to two peaks following a 24-hour incubation in 10% vol FBS, with μ and zeta potential values for both timepoints. In the case of both EAF4-MALS and EAF4-UV, a significant change in zeta potential was observed following exposure to protein-containing media, indicating the surface adsorption of proteins from the incubation media.

The $R^2$ obtained for the unmodified polystyrene latex nanoparticles was >0.9 for all the UV detector estimated values, demonstrating zeta potential values

that accurately mirrored the parameters obtained from ELS. Interestingly, while the ELS data yielded, a single value for zeta potential estimation, using EAF4-UV two zeta potential values were determined (-30.71 and -9.61 for peaks 1 and 2, respectively). Such observations indicate that EAF4 can be used for the *in-situ* measurement of polydisperse samples containing different charged species.

As observed with carboxylate-modified polystyrene latex nanoparticles, unmodified nanoparticles experienced a significant change in zeta potential in response to incubation with 10% vol FBS (- 53.10 and -15.53 mV at 0 hours to -30.71 and -9.61 at 24 hours for peaks 1 and 2, respectively for EAF4-UV).

Overall, the extent of zeta potential change measured by ELS following centrifugation-resuspension of polystyrene latex nanoparticles was less than the measured changes using EAF4-UV and EAF4-MALS.

### 4.7 **Discussion**

In this chapter, I compared the EAF4-based separation and inline analysis of nanoparticles incubated with media containing protein with *in-situ* PTA in the latest Nanosight Pro system, and frit-inlet AF4. I used commercially available amine- and carboxylate-modified polystyrene latex nanoparticles to represent non-degradable polymeric nanoparticles carrying a positive and negative surface charge, respectively.

The EAF4 FFF modality, as a newer approach to separation combines the power of an electric field with asymmetric-flow in flow field-flow fractionation, to achieve charge and size-based separation of fractions contained within samples. Following particle injection into the FFF channel, an equilibrium is reached between particle diffusion and the electrical force applied in the presence of a current.[187]

EAF4 as an approach for high resolution separation requires the fine tuning of multiple run parameters that influence the location of analytes in the FFF channel and, the subsequent fractionation of charged species within a polydisperse sample.

Therefore, the careful selection of carrier liquid composition and diffusion (tip, focus, cross flows) and electrical settings (the applied field current/voltage, conductivity) is critical to its successful application. EAF4 relative to other AF4 modes is in its infancy with a handful of studies having reported the optimization of carrier liquid composition for the determination of electrophoretic mobility and zeta potential in nanomaterial and biomacromolecule samples. Current published reports of EAF4 applications are limited to liposomes, protein-based materials, polystyrene latex nanoparticles and exosomes as examples at the time of this study.[178,188,189]

A challenge remaining within the field of nanomedicine is the ability to perform *in situ* analysis of different nanoscale materials such as nanoparticles of varying composition and exosomes in complex biological matrices without the need to recover them using destructive separation based techniques (e.g., centrifugation-wash based isolation of nanoparticles from biological media).[172]

Therefore, AF4 can provide a strategy for the separation of nanoparticle-protein complexes from complex biological media, which I explored in this chapter.

### 4.7.1 A comparison of *in situ* Nanosight Pro measurements of change in nanoparticle size distribution

In the first step, I performed beta testing of the latest Nanosight Pro technology, which uses machine learning approaches in particle detection to reduce user bias, while simultaneously combining fluorescence and scatter modes to optimise the acquisition of particle size distributions for nanosized analytes.[190] Using the PTA, I compared the effects of 2- and 24-hour incubations in media containing 10% *v/v* FBS at 37 °C for amine- and carboxylate-modified nanoparticles relative to baseline. Overall, in both cases the combined use of the fluorescence and scatter modes led to the generation of the labelling efficiency parameter, which can be used as a surrogate for signal to noise ratio on the Nanosight system. With both nanoparticles examined, an increase in both size and span was observed following exposure to protein, consistent with the formation of the protein corona (**Table 4.5** and **Table 4.7**). When performing an overlay of the particle size distribution

measured for carboxylate-modified polystyrene latex nanoparticles by PTA onto the corresponding DLS data obtained from centrifugation-resuspension fractions, a significant overlap in size distribution profile was observed between the two techniques. However, the equivalent DLS intensity-based size distribution data lacked the resolution to detect subpopulations present within the nanoparticle protein corona samples, particularly at higher particle size ranges (>1 micron) (**Figure 4.3**).

Overall, these observations were consistent with findings in Chapter 2 of this thesis using older versions of the Nanosight technology platform (NS300). A limitation of the NS300 system is the reliance on operator judgment for optimising particle acquisition videos. However, this aspect is eliminated by the new approaches used in the Nanosight Pro system. This was demonstrated overall by a high labelling efficiency determined as the ratio of the particle concentration acquired from the scatter and fluorescence modes for carboxylate-modified nanoparticles, which were ~1 (**Figure 4.2**). Using this approach, I was also able to determine the presence of significant background contributions from the protein media or particle agglomeration effects, which was observed in the case of amine-modified polystyrene latex nanoparticles (**Figure 4.4**).

At the time of writing this thesis, there are no reports on the use of the Nanosight Pro to compare the findings of this work. However, the Nanosight Pro offers significant promise as an initial tool for the triage of changes occurring in nanoparticle size in response to incubation media.

### 4.7.2 Analysis of polystyrene latex nanoparticle sample changes in response to incubation with protein containing media by EAF4-MALS-UV-fluorescence

Next, I investigated the use of EAF4 to fractionate nanoparticle-protein complexes from incubation media containing excess protein. The selection of an appropriate carrier liquid in EAF4 method development reduces the probability of loss of nanoparticle and protein-based materials through electrostatic attraction between the analytes and the flow field flow fractionation channel membrane. At the time of writing this thesis, only a

handful of ionic carrier liquids including sodium carbonate (0.5-1mM), phosphate buffer (4mM), sodium dodecyl sulphate (SDS), and potassium chloride (4 mM) are recommended by the vendor (PostNova Analytics) for EAF4.

Therefore, based on guidance from the vendor on recommended carrier liquid compatibility with polystyrene latex nanoparticles, sodium carbonate (0.5 mM, pH 7.5) was selected for the EAF4 based separation of polystyrene latex nanoparticles from 10% *v/v* FBS media.

The percent recovery rate (%) was calculated to estimate the amount of nanoparticle sample loss occurring during fractionation following peak integration. The percent recovery for unmodified (86.2% and 77.6% for 0 and 24-hour timepoints, respectively) and carboxylate-modified (89.1% and 80.4% for 0 and 24-hour timepoints, respectively) nanoparticles were within acceptable ranges, though trending to a reduction in recovery post-incubation with protein. The recovery rates obtained for carboxylate and unmodified nanoparticles were comparable; however, recovery rates for amine-modified nanoparticles were significantly lower (17.4% ±1.1 and 19.5% ±33.6 for 0 and 24 hours, respectively). My findings for amine-modified nanoparticles in this chapter, are consistent with observations in Chapter 3 of this thesis, where I observed poor percentage recovery rates for amine-modified polystyrene latex nanoparticles using frit-inlet AF4.

These observations overall can be explained by the net positive charge of the amine-modified nanoparticles, which potentially promotes electrostatic attraction to the negatively-charged regenerated cellulose membrane. Also, the amine-modified nanoparticles are more prone to a loss of colloid stability in the presence of protein as demonstrated by the PTA data. Therefore, the observed poor signal intensity and recovery rates can be explained by these factors. To overcome the poor recovery rate and signal intensity for positively-charged materials in the future, various strategies such as the use of a different ionic carrier liquid (e.g., phosphate buffer) or the use of membrane pre-conditioning effects may be explored to maximise the signal quality and

recovery rates. Such strategies have been investigated for optimisation AF4-based separation of lipid nanoparticles in previous work.[191]

Next, I examined the resolution of the bulk FBS media from the nanoparticle-protein complexes formed following polystyrene latex nanoparticle incubation for 24 hours. While the protein fraction was resolved adequately from the nanoparticle peaks occurring at ~6-7 min in all samples, the bulk protein fraction corresponding to the FBS injection eluted at approximately the same time as the void peak. While the focus of this study was to not resolve and fingerprint different protein fractions, future studies planning on investigating the contribution of protein fractions or performing mass balance calculations of nanoparticles isolated from binary mixtures require further optimisation of elution conditions.

The combined use of the fluorescence detector at the corresponding excitation and emission wavelengths of the amine- and carboxylate-modified polystyrene latex nanoparticles enabled the verification of the nanoparticle peaks to confirm that the peaks eluting beyond 20 minutes were indeed corresponding to polystyrene latex nanoparticles and not resulting from protein-protein aggregates formed during the 24-hour incubation period.

In chapter 3 of this thesis, I explored the use of conventional and frit-inlet multidetector AF4 for resolving nanoparticle-protein complexes from bulk protein contained in the media. The findings in this chapter indicated some degree of resolution of nanoparticle-protein subpopulations at 2- and 24-hour timepoints. However, using both these approaches, adequate resolution of subpopulations could not be performed within the confines of efficient AF4-based separations. However, using EAF4 in this chapter, I demonstrated a more efficient approach to the resolution of different subpopulations formed using EAF4. The ability of EAF4 to perform higher resolution separation and analysis is an attractive feature, which should be explored further in the future.

While the benefits of using EAF4 with multiple inline channels has been demonstrated for resolving and simultaneously studying the nanoparticle protein corona in this chapter, additional work is required to further establish EAF4 utility in this field of research. For example, additional investigations into

different applied electrical fields and ionic carrier liquids are needed, to investigate the dependence of resolution and measured electrical parameters on these parameters. Moreover, the impact of applying an electric field strength on the integrity of proteins contained within the analyte is needed through use of the fraction collector and downstream analysis of protein content, and subsequent SDS-PAGE and mass spectrometry-based proteomics fingerprinting of the protein corona.

For example, in **Table 4.11** no reliable measurements of electrophoretic mobility and zeta potential could be obtained for amine-modified nanoparticles, which was a consequence of poor recovery and signal to noise in the fractogram traces obtained. This was further evidenced by a low $R^2$ value obtained for the amine-modified nanoparticles at 0 hours. Therefore, further method development is required to optimise the application of EAF4 for amine-modified and potentially more generally for positively-charged analytes. Previous work has shown that carrier liquid composition can significantly alter the quality of fit for EAF4-measured electrical parameters.[192] Moreover, the zeta potential of a dispersant is also dependent on its surrounding environment, including parameters such as ionic strength and pH, with zeta potential reduction observed with increasing ionic strength.

Differences were also observed between EAF4-MALS and EAF4-UV measurements, which have previously been reported in the literature. These observed differences can be reduced by using a high ionic strength carrier liquid and have been attributed to a number of factors.[184,193] For example, interaction of the ions with the electrodes and the AF4 channel, and the delay time between the detectors may mean that a pH change occurs during the measurement, leading to different measured values.[192] In the case of the setup used in this study, the UV detector was positioned as the first detector in the online setup. Further investigations are required to better understand and mitigate for such changes, while minimising the impacts of the ionic carrier liquid on the analyte physicochemical properties.

Overall, in this chapter the relative merits of EAF4 in comparison with PTA and frit-inlet AF4 has been demonstrated showing the potential for future use of

EAF4 in studying nanoparticle bio-nano interactions. The research conducted in this study, is the first of its type, with no points of reference for comparison in the literature at the time of writing this thesis.

## 4.8 Conclusions

EAF4 represents a useful technique for the resolution and analysis of nanoscale materials from complex biological media, based on their combined size and surface charge profiles. At the time of writing this thesis, there are very limited reports of EAF4 applications to the analysis of nanomaterials, indicating that further research and optimization of EAF4 is required to achieve the best separation for determining both size and electrical charge parameters. Overall, a major limitation of using EAF4 relates to the composition of the ionic carrier liquid and associated limitations with the current applied electric field range that can be used with this FFF modality.

In this chapter, I compared the use of EAF4-MALS-UV-FLD with conventional flow field-flow fractionation for the resolution and recovery of polystyrene latex nanoparticles carrying different surface charges from media containing protein and compared this with *in-situ* PTA analysis in the fluorescence and scatter modes. Overall, with the *in-situ* analysis of model carboxylate-modified polystyrene latex nanoparticles representing negatively charged particles, I found an overlap between the measured nanoparticle size profiles for those particles recorded *in situ* by PTA, and the nanoparticles recovered by centrifugation-resuspension and analyzed by DLS. However, the particle size distribution profile of DLS-measured data missed the degree of resolution of sub-populations that were observed with PTA. Moreover, with the PTA setup in scatter mode, all recorded observations could be attributed to signal contributions from polystyrene latex nanoparticles, as demonstrated by the high signal-to-noise ratio achieved by the labelling efficiency. However, the low labelling efficiency seen with amine-modified nanoparticles in the presence of protein highlighted the need to assess the signal-to-noise ratio of PTA systems for performing *in situ* measurements in complex biological media.

My findings from the collective comparison of different approaches for nanoparticle isolation overall show the relative benefits of using different flow

field-flow fractionation modes in recovering nanoparticles from biological media, with the most convenient approach being EAF4. This is because it can simultaneously profile changes in size and nanoparticle surface charge characteristics. The additional ability to measure *in situ* zeta potential and electrophoretic mobility by EAF4 can provide insights into the impacts of the nanoparticle protein corona on surface charge characteristics and size distribution profiles following exposure to biological media.

Overall, EAF4 as a technique remains understudied. In the context of studying nanomedicines in complex biological matrices, it requires additional optimization of carrier liquid composition for future work. Further work, including the downstream isolation and recovery of separated fractions, is required in the future to examine the impact of EAF4-based separation on the integrity of recovered proteins for downstream compositional analyses.

# Chapter 5 General Discussion, Conclusions & Future Directions

This chapter summarises the research findings from this thesis, including i) an evaluation of the role of centrifugation resuspension recovery and shear flow on nanoparticle parameters following exposure to protein containing media (chapter 2), ii) assessing the impact of flow and cross flow parameters, and optimisation of AF4 methodology for nanoparticle isolation from biological media (chapter 3), and iii) examining the impact of the new nanoparticle tracking analysis technology (Nanosight Pro) and EAF4 multidetector setups for simultaneously probing changes in nanoparticle electrical and size-related parameters following exposure to media containing protein at physiologically-relevant temperature.

## 5.1 Thesis Conclusions

The content of this thesis was underpinned by the work of Rattray, researching the performance of nanomedicines and biologicals in the context of their biological interactions in complex biological media at biorelevant conditions and the EPSRC Multiscale Metrology Suite for Next-Generation Health Nanotechnologies, a facility based on the use of multimodal flow field flow fractionation hyphenated with orthogonal physical and chemical detectors for comprehensive analysis of Bionanotechnology prototypes to be used as diagnostics and therapeutics.

As discussed earlier in this thesis, analysis of the protein corona for nanomedicines remains a challenge in the context of the nanoparticle protein corona composition, and the nanoparticle colloid stability being very much prone to sample handling conditions and the subsequent handling of incubated samples. Current analytical technologies used for profiling the nanoparticle protein corona, lack the signal to noise ratio to accurately resolve the bulk proteins and biomolecules contained within the experimental incubation media the from surface-adsorbed molecules contained in the nanoparticle corona. Therefore, there is an acute need to perform resolution of the nanoparticle-biomolecular complexes from bulk biological media, with

the field predominantly using centrifugation-resuspension or buffer exchange approaches to recover these complexes.

Moreover, most of the reported literature on the protein corona perform these experiments under static conditions, where it is widely known that any injected nanomedicine will be subject to shear stress and oncotic pressure when administered to a biological system.

Therefore, the first objective of this thesis was to examine how experimental parameters used in nanoparticle protein corona experiments, such as the physical separation of nanoparticles from protein containing media, and shear flow mimicking venous and arterial blood pressure will subsequently impact the colloid stability and composition of surface-adsorbed proteins.

In the first instance, I used poly(lactic)-co-glycolic acid nanoparticles as a system to study protein corona formation. However, there were inherent challenges associated with particle swelling and hydrolytic degradation, beyond protein adsorption (the phenomenon of interest in this thesis), which led me to consider a non-degradable system to primarily study the impact of the protein corona in polystyrene latex nanoparticles as a model system.

In addressing the objectives of chapter 2, I demonstrated that both shear flow and surface charge for nanoparticles of the same diameter significantly altered the composition of the proteins bound, and also the colloid stability of such systems in biological media.

The second objective of this thesis in chapter 3 was to explore flow field flow fractionation, and different detector hyphenations to study the feasibility of AF4 for recovering nanoparticle-protein complexes from biological media. While the concept of flow field flow fractionation modalities were first reported in 1966,[194] its adoption as a separation and analytical method by the field of nanomedicine and biotechnology remains within its infancy.

In this chapter, I demonstrated that frit-inlet AF4 can be used as a feasible approach for isolating and recovering nanoparticles from biological media. Moreover, I showed that while separating and recovering nanoparticles from biological media, their size and geometry can be profiled simultaneously. The

conclusions from this chapter were that conventional AF4 channels are unsuitable for recovering nanoparticle-protein complexes due to the cross-flow effects. Also, in the case of the amine-modified nanoparticles carrying a positive surface charge, poor recovery was observed due to the AF4 regenerated cellulose membrane carrying a negative charge and also extensive precipitation of the amine-modified nanoparticles following exposure to protein-containing media.

The final objective of this thesis was to explore electrical AF4 as an orthogonal AF4 mode for the separation of nanoparticle-protein complexes based on the different charged species contained in a polydisperse sample (chapter 4). Electric AF4 is a lesser reported method in the literature for the separation and analysis of nanomedicines. Overall, with this approach in the case of differently charged materials, I found this approach to be very useful. However, a limitation of this approach was the limited range of ionic carrier liquids and currents/voltages that could be applied, which could alter the resolution of different charged species in a sample.

## 5.2 Future Work

### 5.2.1 Investigating additional nanomaterial properties

In Chapter 1, I highlighted that parameters such as surface charge will have a significant impact on the range and type of proteins adsorbing onto the nanoparticle surface.[195,196] Therefore, I also compared amine- and carboxylate- functionalised nanoparticles in this context as they carry positive and negative charges, respectively.

This comparison is significant since some of the nanomedicines developed within our research team carry a small positive net charge in the case of lipid nanoparticles with cationic lipids, and silk nanoparticles carrying a negative net charge.

Findings from chapters 2-4 overall demonstrated a significant difference between the positively- and negatively-charged polystyrene latex nanoparticles, both in the context of their colloidal stability following exposure to protein-containing media and recovery rates from AF4 methods developed.

However, caution must be exercised in applying the findings from my work in a single system to nanomaterials manufactured from different material types.

While I have only explored the impact of charge in a single nanoparticle system, some other parameters such as nanoparticle size, hydrophobicity and morphology could be investigated in the future. This could be done by comparing polystyrene latex nanoparticle with different morphologies, and sizes with similar surface functionalisation.

### *5.2.2* Optimising the conditions for performing nanoparticle protein corona formation *in vitro*

As highlighted in the introduction and chapter 2 of this thesis, it is critical that the conditions under which protein corona studies are conducted adequately represent biologically and physiologically relevant events that take place following nanomedicine administration. In chapter 2, I briefly investigated the impact of flow rates in larger vasculature. However, nanomedicines will predominantly encounter capillaries and microvasculature within target and off-target organs. Therefore, there is a critical need to understand the biomechanical and compositional elements that these particles will be exposed to *in vivo*. Future work exploring the formation of the nanoparticle protein corona should ideally explore these conditions, which can be achieved using microfluidics-based lab on a chip or organoid based devices to mimic such conditions. At the time of writing this thesis, there are a number of new commercial technologies on the market that can be used for this purpose.

Beyond shear flow conditions experienced by nanomaterials, it is also important to consider the composition of media which are studied. In this thesis, my goal was to examine equivalent protein concentrations to cell culture experiments *in vitro*. However, future work could further explore this in detail using human serum in target patient therapeutic groups, further facilitating the achievement of precision medicine and understanding interindividual differences in the formation of the nanoparticle protein corona. Furthermore, studies have shown an increase in nanoparticle uptake due to the binding of certain proteins,[197] and this could be a strategy for personalised medicine with nanoparticles designed to adsorb certain proteins or a ‘’smart

corona''. In the long term this could inform the selection of the appropriate delivery system for the right patient.

### 5.2.3 Optimisation of AF4 for nanomaterials with different surface charges

While I was able to optimise the AF4 methodologies in both chapters 3 and 4 for carboxylate-modified nanoparticles, in the case of amine-modified nanoparticles a poor signal intensity and recovery was noted. These observations were consistent with other findings from our lab with DOTAP lipid nanoparticles (unpublished data). Strategies that have been explored include pre-conditioning the AF4 membrane with nanoparticle or bovine serum albumin injections.[191]

Future work could explore alternative AF4 membrane surface functionalization's that are more compatible with positively-charged nanomaterials or exploring calibration of the carrier liquid ionic strength and pH. However, a caveat of altering the carrier liquid would be alteration of nanoparticle stability.

### 5.2.4 Further investigation of the protein corona

In this thesis, I predominantly investigated the inline separation of the different species within the sample (nanoparticle and nanoparticle-protein complexes), without downstream analysis of the protein corona composition or its cellular fate. Using the configuration in the multiscale metrology suite, it is possible to isolate and recover the different fractions and analyse these further using additional analytical technologies or study the impact of cellular exposure to these fractions more closely.

Future work could explore the composition of the protein corona by liquid-chromatography mass-spectrometry based proteomics analysis,[149] and correlate the composition and abundance of different corona proteins with both the inline measurements and cellular fate. This would provide a more detailed mechanistic insight into whether the biological effects observed *in vivo*, are a consequence of protein abundance or the physical impact of the protein corona on nanoparticle fate.

### 5.3 Conclusion

Overall, this thesis demonstrates that the conditions to which nanomedicines are exposed during protein corona incubation experiments, have a profound impact on the subsequent experimental readout. The outcome of such experiments beyond the incubation and recovery parameters, is largely dependent on the physicochemical properties of nanomedicines.

## References


1 Daramy, K. *et al.* Nanoparticle Isolation from Biological Media for Protein Corona Analysis: The Impact of Incubation and Recovery Protocols on Nanoparticle Properties. *J Pharm Sci* (2023). https://doi.org/10.1016/j.xphs.2023.12.021

2 Milane, L. & Amiji, M. Clinical approval of nanotechnology-based SARS-CoV-2 mRNA vaccines: impact on translational nanomedicine. *Drug Deliv Transl Res*, 1-7 (2021). https://doi.org/10.1007/s13346-021-00911-y

3 Ventola, C. L. Progress in Nanomedicine: Approved and Investigational Nanodrugs. *P & T : a peer-reviewed journal for formulary management* **42**, 742-755 (2017).

4 Germain, M. *et al.* Delivering the power of nanomedicine to patients today. *J Control Release* **326**, 164-171 (2020). https://doi.org/10.1016/j.jconrel.2020.07.007

5 Flühmann, B., Ntai, I., Borchard, G., Simoens, S. & Mühlebach, S. Nanomedicines: The magic bullets reaching their target? *Eur J Pharm Sci* **128**, 73-80 (2019). https://doi.org/10.1016/j.ejps.2018.11.019

6 Soares, S., Sousa, J., Pais, A. & Vitorino, C. Nanomedicine: Principles, Properties, and Regulatory Issues. *Frontiers in chemistry* **6**, 360 (2018). https://doi.org/10.3389/fchem.2018.00360

7 De Jong, W. H. & Borm, P. J. Drug delivery and nanoparticles:applications and hazards. *Int J Nanomedicine* **3**, 133-149 (2008). https://doi.org/10.2147/ijn.s596

8 Zhu, M. *et al.* Physicochemical properties determine nanomaterial cellular uptake, transport, and fate. *Acc Chem Res* **46**, 622-631 (2013). https://doi.org/10.1021/ar300031y

9 Pita, R., Ehmann, F. & Papaluca, M. Nanomedicines in the EU-Regulatory Overview. *Aaps j* **18**, 1576-1582 (2016). https://doi.org/10.1208/s12248-016-9967-1

10 Augustine, R. *et al.* Cellular uptake and retention of nanoparticles: Insights on particle properties and interaction with cellular components. *Materials Today Communications* **25**, 101692 (2020). https://doi.org/https://doi.org/10.1016/j.mtcomm.2020.101692

11 Hoshyar, N., Gray, S., Han, H. & Bao, G. The effect of nanoparticle size on in vivo pharmacokinetics and cellular interaction. *Nanomedicine (Lond)* **11**, 673-692 (2016). https://doi.org/10.2217/nnm.16.5

12 Miao, C. *et al.* The size-dependent in vivo toxicity of amorphous silica nanoparticles: A systematic review. *Ecotoxicology and Environmental Safety* **271**, 115910 (2024). https://doi.org/https://doi.org/10.1016/j.ecoenv.2023.115910

13 Doherty, G. J. & McMahon, H. T. Mechanisms of endocytosis. *Annual review of biochemistry* **78**, 857-902 (2009). https://doi.org/10.1146/annurev.biochem.78.081307.110540

14 Salatin, S. & Yari Khosroushahi, A. Overviews on the cellular uptake mechanism of polysaccharide colloidal nanoparticles. *Journal of cellular and molecular medicine* **21**, 1668-1686 (2017). https://doi.org/10.1111/jcmm.13110

15 Khan, I. & Steeg, P. S. Endocytosis: a pivotal pathway for regulating metastasis. *Br J Cancer* **124**, 66-75 (2021). https://doi.org/10.1038/s41416-020-01179-8

16 Choi, J.-S. *et al.* Size-controlled biodegradable nanoparticles: Preparation and size-dependent cellular uptake and tumor cell growth inhibition. *Colloids and Surfaces B: Biointerfaces* **122**, 545-551 (2014). https://doi.org/https://doi.org/10.1016/j.colsurfb.2014.07.030

17 Zhao, J. & Stenzel, M. H. Entry of nanoparticles into cells: the importance of nanoparticle properties. *Polymer Chemistry* **9**, 259-272 (2018). https://doi.org/10.1039/C7PY01603D

18 Banerjee, A., Berezhkovskii, A. & Nossal, R. Kinetics of cellular uptake of viruses and nanoparticles via clathrin-mediated endocytosis. *Phys Biol* **13**, 016005 (2016). https://doi.org/10.1088/1478-3975/13/1/016005

19 Rennick, J. J., Johnston, A. P. R. & Parton, R. G. Key principles and methods for studying the endocytosis of biological and nanoparticle therapeutics. *Nature Nanotechnology* **16**, 266-276 (2021). https://doi.org/10.1038/s41565-021-00858-8

20 Zhang, J. *et al.* Systematic investigation on the intracellular trafficking network of polymeric nanoparticles. *Nanoscale* **9**, 3269-3282 (2017). https://doi.org/10.1039/C7NR00532F
21 Sun, X.-Y., Gan, Q.-Z. & Ouyang, J.-M. Size-dependent cellular uptake mechanism and cytotoxicity toward calcium oxalate on Vero cells. *Scientific Reports* **7**, 41949 (2017). https://doi.org/10.1038/srep41949
22 Capriotti, A. L. *et al.* Analytical Methods for Characterizing the Nanoparticle–Protein Corona. *Chromatographia* **77**, 755-769 (2014). https://doi.org/10.1007/s10337-014-2677-x
23 Patra, J. K. *et al.* Nano based drug delivery systems: recent developments and future prospects. *J Nanobiotechnology* **16**, 71 (2018). https://doi.org/10.1186/s12951-018-0392-8
24 Tavakol, M., Hajipour, M. J., Ferdousi, M., Zanganeh, S. & Maurizi, L. Competition of opsonins and dysopsonins on the nanoparticle surface. *Nanoscale* **15**, 17342-17349 (2023). https://doi.org/10.1039/D3NR03823H
25 Du, B. *et al.* Glomerular barrier behaves as an atomically precise bandpass filter in a sub-nanometre regime. *Nat Nanotechnol* **12**, 1096-1102 (2017). https://doi.org/10.1038/nnano.2017.170
26 Hadji, H. & Bouchemal, K. Effect of micro- and nanoparticle shape on biological processes. *Journal of Controlled Release* **342**, 93-110 (2022). https://doi.org/https://doi.org/10.1016/j.jconrel.2021.12.032
27 Caldorera-Moore, M., Guimard, N., Shi, L. & Roy, K. Designer nanoparticles: incorporating size, shape and triggered release into nanoscale drug carriers. *Expert Opin Drug Deliv* **7**, 479-495 (2010). https://doi.org/10.1517/17425240903579971
28 Albanese, A., Tang, P. S. & Chan, W. C. The effect of nanoparticle size, shape, and surface chemistry on biological systems. *Annu Rev Biomed Eng* **14**, 1-16 (2012). https://doi.org/10.1146/annurev-bioeng-071811-150124
29 Bilardo, R., Traldi, F., Vdovchenko, A. & Resmini, M. Influence of surface chemistry and morphology of nanoparticles on protein corona formation. *Wiley interdisciplinary reviews. Nanomedicine and nanobiotechnology* **14**, e1788 (2022). https://doi.org/10.1002/wnan.1788
30 Mitchell, M. J. *et al.* Engineering precision nanoparticles for drug delivery. *Nature Reviews Drug Discovery* **20**, 101-124 (2021). https://doi.org/10.1038/s41573-020-0090-8
31 Boselli, L. *et al.* Classification and biological identity of complex nano shapes.
32 Gonzalez Solveyra, E. & Szleifer, I. What is the role of curvature on the properties of nanomaterials for biomedical applications? *Wiley interdisciplinary reviews. Nanomedicine and nanobiotechnology* **8**, 334-354 (2016). https://doi.org/10.1002/wnan.1365
33 La-Beck, N. M., Islam, M. R. & Markiewski, M. M. Nanoparticle-Induced Complement Activation: Implications for Cancer Nanomedicine. *Front Immunol* **11**, 603039 (2020). https://doi.org/10.3389/fimmu.2020.603039
34 Xie, X., Liao, J., Shao, X., Li, Q. & Lin, Y. The Effect of shape on Cellular Uptake of Gold Nanoparticles in the forms of Stars, Rods, and Triangles. *Scientific Reports* **7**, 3827 (2017). https://doi.org/10.1038/s41598-017-04229-z
35 Sun, Q., Zhou, Z., Qiu, N. & Shen, Y. Rational Design of Cancer Nanomedicine: Nanoproperty Integration and Synchronization. *Advanced Materials* **29**, 1606628 (2017). https://doi.org/https://doi.org/10.1002/adma.201606628
36 Shah, S., Rangaraj, N., Singh, S. B. & Srivastava, S. Exploring the unexplored avenues of surface charge in nano-medicine. *Colloid and Interface Science Communications* **42**, 100406 (2021). https://doi.org/https://doi.org/10.1016/j.colcom.2021.100406
37 Moore, T. L. *et al.* Nanoparticle colloidal stability in cell culture media and impact on cellular interactions. *Chemical Society Reviews* **44**, 6287-6305 (2015). https://doi.org/10.1039/C4CS00487F

38 Németh, Z. *et al.* Quality by Design-Driven Zeta Potential Optimisation Study of Liposomes with Charge Imparting Membrane Additives. *Pharmaceutics* **14** (2022). https://doi.org/10.3390/pharmaceutics14091798
39 Gunawan, C., Lim, M., Marquis, C. P. & Amal, R. Nanoparticle-protein corona complexes govern the biological fates and functions of nanoparticles. *J Mater Chem B* **2**, 2060-2083 (2014). https://doi.org/10.1039/c3tb21526a
40 Jo, D. H., Kim, J. H. & Lee, T. G. Size, surface charge, and shape determine therapeutic effects of nanoparticles on brain and retinal diseases. *Nanomedicine* **11**, 1603-1611 (2015). https://doi.org/10.1016/j.nano.2015.04.015
41 Kim, B. *et al.* Tuning payload delivery in tumour cylindroids using gold nanoparticles. *Nat Nanotechnol* **5**, 465-472 (2010). https://doi.org/10.1038/nnano.2010.58
42 Gessner, A., Lieske, A., Paulke, B. & Müller, R. Influence of surface charge density on protein adsorption on polymeric nanoparticles: analysis by two-dimensional electrophoresis. *Eur J Pharm Biopharm* **54**, 165-170 (2002). https://doi.org/10.1016/s0939-6411(02)00081-4
43 Foroozandeh, P. & Aziz, A. A. Insight into Cellular Uptake and Intracellular Trafficking of Nanoparticles. *Nanoscale Res Lett* **13**, 339 (2018). https://doi.org/10.1186/s11671-018-2728-6
44 Cedervall, T. *et al.* Understanding the nanoparticle–protein corona using methods to quantify exchange rates and affinities of proteins for nanoparticles. *Proceedings of the National Academy of Sciences* **104**, 2050-2055 (2007). https://doi.org/doi:10.1073/pnas.0608582104
45 Walkey, C. D., Olsen, J. B., Guo, H., Emili, A. & Chan, W. C. Nanoparticle size and surface chemistry determine serum protein adsorption and macrophage uptake. *Journal of the American Chemical Society* **134**, 2139-2147 (2012). https://doi.org/10.1021/ja2084338
46 Boles, M. A., Ling, D., Hyeon, T. & Talapin, D. V. The surface science of nanocrystals. *Nature materials* **15**, 141-153 (2016). https://doi.org/10.1038/nmat4526
47 Mahmoudi, M. & Serpooshan, V. Large Protein Absorptions from Small Changes on the Surface of Nanoparticles. *The Journal of Physical Chemistry C* **115**, 18275-18283 (2011). https://doi.org/10.1021/jp2056255
48 Piloni, A. *et al.* Surface roughness influences the protein corona formation of glycosylated nanoparticles and alter their cellular uptake. *Nanoscale* **11**, 23259-23267 (2019). https://doi.org/10.1039/C9NR06835J
49 Cedervall, T. *et al.* Understanding the nanoparticle-protein corona using methods to quantify exchange rates and affinities of proteins for nanoparticles. *Proc Natl Acad Sci U S A* **104**, 2050-2055 (2007). https://doi.org/10.1073/pnas.0608582104
50 Böhmert, L. *et al.* Isolation methods for particle protein corona complexes from protein-rich matrices. *Nanoscale Advances* **2**, 563-582 (2020). https://doi.org/10.1039/C9NA00537D
51 Barrán-Berdón, A. L. *et al.* Time evolution of nanoparticle-protein corona in human plasma: relevance for targeted drug delivery. *Langmuir* **29**, 6485-6494 (2013). https://doi.org/10.1021/la401192x
52 Noh, H. & Vogler, E. A. Volumetric interpretation of protein adsorption: Competition from mixtures and the Vroman effect. *Biomaterials* **28**, 405-422 (2007). https://doi.org/https://doi.org/10.1016/j.biomaterials.2006.09.006
53 Ke, P. C., Lin, S., Parak, W. J., Davis, T. P. & Caruso, F. A Decade of the Protein Corona. *ACS Nano* **11**, 11773-11776 (2017). https://doi.org/10.1021/acsnano.7b08008
54 Barbero, F. *et al.* Formation of the Protein Corona: The Interface between Nanoparticles and the Immune System. *Semin Immunol* **34**, 52-60 (2017). https://doi.org/10.1016/j.smim.2017.10.001
55 Corbo, C. *et al.* The impact of nanoparticle protein corona on cytotoxicity, immunotoxicity and target drug delivery. *Nanomedicine (Lond)* **11**, 81-100 (2016). https://doi.org/10.2217/nnm.15.188

56 Gabe, I. T. *et al.* Measurement of instantaneous blood flow velocity and pressure in conscious man with a catheter-tip velocity probe. *Circulation* **40**, 603-614 (1969). https://doi.org/10.1161/01.cir.40.5.603
57 in *Encyclopedic Dictionary of Polymers* (ed Jan W. Gooch) 477-477 (Springer New York, 2007).
58 Potters, W. V., Marquering, H. A., VanBavel, E. & Nederveen, A. J. Measuring Wall Shear Stress Using Velocity-Encoded MRI. *Current Cardiovascular Imaging Reports* **7**, 9257 (2014). https://doi.org/10.1007/s12410-014-9257-1
59 Jayaram, D. T., Pustulka, S. M., Mannino, R. G., Lam, W. A. & Payne, C. K. Protein Corona in Response to Flow: Effect on Protein Concentration and Structure. *Biophysical journal* **115**, 209-216 (2018). https://doi.org/10.1016/j.bpj.2018.02.036
60 Marques, C. *et al.* Identification of the Proteins Determining the Blood Circulation Time of Nanoparticles. *ACS nano* **17**, 12458-12470 (2023). https://doi.org/10.1021/acsnano.3c02041
61 Singh, N. *et al.* In vivo protein corona on nanoparticles: does the control of all material parameters orient the biological behavior? *Nanoscale Advances* **3**, 1209-1229 (2021). https://doi.org/10.1039/D0NA00863J
62 Tekie, F. S. M. *et al.* Controlling evolution of protein corona: a prosperous approach to improve chitosan-based nanoparticle biodistribution and half-life. *Scientific Reports* **10**, 9664 (2020). https://doi.org/10.1038/s41598-020-66572-y
63 Partikel, K., Korte, R., Mulac, D., Humpf, H.-U. & Langer, K. Serum type and concentration both affect the protein-corona composition of PLGA nanoparticles. *Beilstein Journal of Nanotechnology* **10**, 1002-1015 (2019). https://doi.org/10.3762/bjnano.10.101
64 Galdino, F. E., Picco, A. S., Sforca, M. L., Cardoso, M. B. & Loh, W. Effect of particle functionalization and solution properties on the adsorption of bovine serum albumin and lysozyme onto silica nanoparticles. *Colloids and Surfaces B: Biointerfaces* **186**, 110677 (2020). https://doi.org/https://doi.org/10.1016/j.colsurfb.2019.110677
65 Sebak, A. A. *et al.* Distinct Proteins in Protein Corona of Nanoparticles Represent a Promising Venue for Endogenous Targeting - Part I: In vitro Release and Intracellular Uptake Perspective. *International journal of nanomedicine* **15**, 8845-8862 (2020). https://doi.org/10.2147/ijn.S273713
66 Gorshkov, V., Bubis, J. A., Solovyeva, E. M., Gorshkov, M. V. & Kjeldsen, F. Protein corona formed on silver nanoparticles in blood plasma is highly selective and resistant to physicochemical changes of the solution. *Environmental Science: Nano* **6**, 1089-1098 (2019). https://doi.org/10.1039/C8EN01054D
67 Hajipour, M. J. *et al.* An Overview of Nanoparticle Protein Corona Literature. *Small (Weinheim an der Bergstrasse, Germany)* **19**, e2301838 (2023). https://doi.org/10.1002/smll.202301838
68 Bonvin, D., Chiappe, D., Moniatte, M., Hofmann, H. & Mionić Ebersold, M. Methods of protein corona isolation for magnetic nanoparticles. *Analyst* **142**, 3805-3815 (2017). https://doi.org/10.1039/c7an00646b

10.1039/c7an00646b.
69 Weber, C., Simon, J., Mailänder, V., Morsbach, S. & Landfester, K. Preservation of the soft protein corona in distinct flow allows identification of weakly bound proteins. *Acta Biomater* **76**, 217-224 (2018). https://doi.org/10.1016/j.actbio.2018.05.057
70 Kari, O. K. *et al.* In situ analysis of liposome hard and soft protein corona structure and composition in a single label-free workflow. *Nanoscale* **12**, 1728-1741 (2020). https://doi.org/10.1039/C9NR08186K
71 Wagner, M., Holzschuh, S., Traeger, A., Fahr, A. & Schubert, U. S. Asymmetric flow field-flow fractionation in the field of nanomedicine. *Anal Chem* **86**, 5201-5210 (2014). https://doi.org/10.1021/ac501664t

72 Zhang, H. *et al.* A nano-bio interfacial protein corona on silica nanoparticle. *Colloids and Surfaces B: Biointerfaces* **167**, 220-228 (2018). https://doi.org/https://doi.org/10.1016/j.colsurfb.2018.04.021
73 González-García, L. E. *et al.* Nanoparticles Surface Chemistry Influence on Protein Corona Composition and Inflammatory Responses. *Nanomaterials (Basel)* **12** (2022). https://doi.org/10.3390/nano12040682
74 Lima, T., Bernfur, K., Vilanova, M. & Cedervall, T. Understanding the Lipid and Protein Corona Formation on Different Sized Polymeric Nanoparticles. *Scientific Reports* **10**, 1129 (2020). https://doi.org/10.1038/s41598-020-57943-6
75 Fleischer, C. C. & Payne, C. K. Secondary structure of corona proteins determines the cell surface receptors used by nanoparticles. *J Phys Chem B* **118**, 14017-14026 (2014). https://doi.org/10.1021/jp502624n
76 Carrillo-Carrion, C., Carril, M. & Parak, W. J. Techniques for the experimental investigation of the protein corona. *Curr Opin Biotechnol* **46**, 106-113 (2017). https://doi.org/10.1016/j.copbio.2017.02.009
77 Olson, B. Assays for Determination of Protein Concentration. *Curr Protoc Pharmacol* **73**, A.3a.1-a.3a.32 (2016). https://doi.org/10.1002/cpph.3
78 Mishra, R. K. *et al.* Biological effects of formation of protein corona onto nanoparticles. *International journal of biological macromolecules* **175**, 1-18 (2021). https://doi.org/10.1016/j.ijbiomac.2021.01.152
79 Costa-Fernández, J. M., Menéndez-Miranda, M., Bouzas-Ramos, D., Encinar, J. R. & Sanz-Medel, A. Mass spectrometry for the characterization and quantification of engineered inorganic nanoparticles. *TrAC Trends in Analytical Chemistry* **84**, 139-148 (2016). https://doi.org/https://doi.org/10.1016/j.trac.2016.06.001
80 Docter, D. *et al.* The nanoparticle biomolecule corona: lessons learned - challenge accepted? *Chem Soc Rev* **44**, 6094-6121 (2015). https://doi.org/10.1039/c5cs00217f
81 Partikel, K. *et al.* Effect of nanoparticle size and PEGylation on the protein corona of PLGA nanoparticles. *Eur J Pharm Biopharm* **141**, 70-80 (2019). https://doi.org/10.1016/j.ejpb.2019.05.006
82 Amoozgar, Z. & Yeo, Y. Recent advances in stealth coating of nanoparticle drug delivery systems. *Wiley Interdiscip Rev Nanomed Nanobiotechnol* **4**, 219-233 (2012). https://doi.org/10.1002/wnan.1157
83 Yu, Q., Zhao, L., Guo, C., Yan, B. & Su, G. Regulating Protein Corona Formation and Dynamic Protein Exchange by Controlling Nanoparticle Hydrophobicity. *Front Bioeng Biotechnol* **8**, 210 (2020). https://doi.org/10.3389/fbioe.2020.00210
84 Madathiparambil Visalakshan, R. *et al.* The Influence of Nanoparticle Shape on Protein Corona Formation. *Small* **16**, e2000285 (2020). https://doi.org/10.1002/smll.202000285
85 Bewersdorff, T. *et al.* The influence of shape and charge on protein corona composition in common gold nanostructures. *Mater Sci Eng C Mater Biol Appl* **117**, 111270 (2020). https://doi.org/10.1016/j.msec.2020.111270
86 Gräfe, C. *et al.* Intentional formation of a protein corona on nanoparticles: Serum concentration affects protein corona mass, surface charge, and nanoparticle-cell interaction. *Int J Biochem Cell Biol* **75**, 196-202 (2016). https://doi.org/10.1016/j.biocel.2015.11.005
87 Lesniak, A. *et al.* Effects of the Presence or Absence of a Protein Corona on Silica Nanoparticle Uptake and Impact on Cells. *ACS Nano* **6**, 5845-5857 (2012). https://doi.org/10.1021/nn300223w
88 Nierenberg, D., Khaled, A. R. & Flores, O. Formation of a protein corona influences the biological identity of nanomaterials. *Rep Pract Oncol Radiother* **23**, 300-308 (2018). https://doi.org/10.1016/j.rpor.2018.05.005
89 Kim, W. *et al.* Protein corona: Friend or foe? Co-opting serum proteins for nanoparticle delivery. *Advanced Drug Delivery Reviews* **192**, 114635 (2023). https://doi.org/https://doi.org/10.1016/j.addr.2022.114635

90 Cai, R. & Chen, C. The Crown and the Scepter: Roles of the Protein Corona in Nanomedicine. *Adv Mater* **31**, e1805740 (2019). https://doi.org/10.1002/adma.201805740
91 Falahati, M. *et al.* A health concern regarding the protein corona, aggregation and disaggregation. *Biochim Biophys Acta Gen Subj* **1863**, 971-991 (2019). https://doi.org/10.1016/j.bbagen.2019.02.012
92 Stetefeld, J., McKenna, S. A. & Patel, T. R. Dynamic light scattering: a practical guide and applications in biomedical sciences. *Biophysical Reviews* **8**, 409-427 (2016). https://doi.org/10.1007/s12551-016-0218-6
93 Harding, S. E. & Jumel, K. Light Scattering. *Current Protocols in Protein Science* **11**, 7.8.1-7.8.14 (1998). https://doi.org/https://doi.org/10.1002/0471140864.ps0708s11
94 Filipe, V., Hawe, A. & Jiskoot, W. Critical evaluation of Nanoparticle Tracking Analysis (NTA) by NanoSight for the measurement of nanoparticles and protein aggregates. *Pharm Res* **27**, 796-810 (2010). https://doi.org/10.1007/s11095-010-0073-2
95 Modena, M. M., Rühle, B., Burg, T. P. & Wuttke, S. Nanoparticle Characterization: What to Measure? *Adv Mater* **31**, e1901556 (2019). https://doi.org/10.1002/adma.201901556
96 Gollwitzer, C. *et al.* A comparison of techniques for size measurement of nanoparticles in cell culture medium. *Analytical Methods* **8**, 5272-5282 (2016). https://doi.org/10.1039/C6AY00419A
97 Ehrhart, J., Mingotaud, A. F. & Violleau, F. Asymmetrical flow field-flow fractionation with multi-angle light scattering and quasi elastic light scattering for characterization of poly(ethyleneglycol-b-ε-caprolactone) block copolymer self-assemblies used as drug carriers for photodynamic therapy. *J Chromatogr A* **1218**, 4249-4256 (2011). https://doi.org/10.1016/j.chroma.2011.01.048
98 Generalova, A. N., Asharchuk, I. M. & Zubov, V. P. Multifunctional polymer dispersions for biomedical assays obtained by heterophase radical polymerization. *Russian Chemical Bulletin* **67**, 1759-1780 (2018). https://doi.org/10.1007/s11172-018-2289-y
99 Gorsd, M. N., Blanco, M. N. & Pizzio, L. R. Synthesis of Polystyrene Microspheres to be Used as Template in the Preparation of Hollow Spherical Materials: Study of the Operative Variables. *Procedia Materials Science* **1**, 432-438 (2012). https://doi.org/https://doi.org/10.1016/j.mspro.2012.06.058
100 Sigma-Aldrich. *Polystyrene Latex Beads* <https://www.sigmaaldrich.com/deepweb/assets/sigmaaldrich/product/documents/116/984/lb1pis.pdf> (2016).
101 Lundqvist, M. *et al.* Nanoparticle size and surface properties determine the protein corona with possible implications for biological impacts. *Proceedings of the National Academy of Sciences* **105**, 14265-14270 (2008). https://doi.org/10.1073/pnas.0805135105
102 Wolfram, J. *et al.* Safety of Nanoparticles in Medicine. *Current drug targets* **16**, 1671-1681 (2015). https://doi.org/10.2174/1389450115666140804124808
103 Lima, T., Bernfur, K., Vilanova, M. & Cedervall, T. Understanding the Lipid and Protein Corona Formation on Different Sized Polymeric Nanoparticles. *Sci Rep* **10**, 1129 (2020). https://doi.org/10.1038/s41598-020-57943-6
104 Gupta, M. N. & Roy, I. How Corona Formation Impacts Nanomaterials as Drug Carriers. *Molecular pharmaceutics* **17**, 725-737 (2020). https://doi.org/10.1021/acs.molpharmaceut.9b01111
105 Tedja, R., Lim, M., Amal, R. & Marquis, C. Effects of serum adsorption on cellular uptake profile and consequent impact of titanium dioxide nanoparticles on human lung cell lines. *ACS nano* **6**, 4083-4093 (2012). https://doi.org/10.1021/nn3004845
106 Griffith, D. M., Jayaram, D. T., Spencer, D. M., Pisetsky, D. S. & Payne, C. K. DNA-nanoparticle interactions: Formation of a DNA corona and its effects on a protein corona. *Biointerphases* **15**, 051006 (2020). https://doi.org/10.1116/6.0000439

107 Mahmoudi, M., Landry, M. P., Moore, A. & Coreas, R. The protein corona from nanomedicine to environmental science. *Nature Reviews Materials* **8**, 422-438 (2023). https://doi.org/10.1038/s41578-023-00552-2

108 Anselmo, A. C. & Mitragotri, S. Nanoparticles in the clinic. *Bioengineering & translational medicine* **1**, 10-29 (2016). https://doi.org/10.1002/btm2.10003

109 Bashiri, G. *et al.* Nanoparticle protein corona: from structure and function to therapeutic targeting. *Lab on a chip* **23**, 1432-1466 (2023). https://doi.org/10.1039/d2lc00799a

110 Hadjidemetriou, M., Al-Ahmady, Z. & Kostarelos, K. Time-evolution of in vivo protein corona onto blood-circulating PEGylated liposomal doxorubicin (DOXIL) nanoparticles. *Nanoscale* **8**, 6948-6957 (2016). https://doi.org/10.1039/c5nr09158f

111 Tirumala, M. G., Anchi, P., Raja, S., Rachamalla, M. & Godugu, C. Novel Methods and Approaches for Safety Evaluation of Nanoparticle Formulations: A Focus Towards In Vitro Models and Adverse Outcome Pathways. *Frontiers in pharmacology* **12**, 612659 (2021). https://doi.org/10.3389/fphar.2021.612659

112 Behzadi, S. *et al.* Cellular uptake of nanoparticles: journey inside the cell. *Chemical Society reviews* **46**, 4218-4244 (2017). https://doi.org/10.1039/c6cs00636a

113 Petros, R. A. & DeSimone, J. M. Strategies in the design of nanoparticles for therapeutic applications. *Nature reviews. Drug discovery* **9**, 615-627 (2010). https://doi.org/10.1038/nrd2591

114 Malewicz, N. M. *et al.* Topical Capsaicin in Poly(lactic-co-glycolic)acid (PLGA) Nanoparticles Decreases Acute Itch and Heat Pain. *Int J Mol Sci* **23** (2022). https://doi.org/10.3390/ijms23095275

115 Patterson, C., Murphy, D., Irvine, S., Connor, L. & Rattray, Z. Novel application of synchrotron x-ray computed tomography for ex-vivo imaging of subcutaneously injected polymeric microsphere suspension formulations. *Pharmaceutical Research* **37**, 97 (2020). https://doi.org/10.1007/s11095-020-02825-9

116 Klarhöfer, M., Csapo, B., Balassy, C., Szeles, J. C. & Moser, E. High-resolution blood flow velocity measurements in the human finger. *Magn Reson Med* **45**, 716-719 (2001). https://doi.org/10.1002/mrm.1096

117 Partikel, K., Korte, R., Mulac, D., Humpf, H. U. & Langer, K. Serum type and concentration both affect the protein-corona composition of PLGA nanoparticles. *Beilstein J Nanotechnol* **10**, 1002-1015 (2019). https://doi.org/10.3762/bjnano.10.101

118 Beragoui, M. *et al.* Bovine serum albumin adsorption onto functionalized polystyrene lattices: A theoretical modeling approach and error analysis. *Progress of Theoretical and Experimental Physics* **2015** (2015). https://doi.org/10.1093/ptep/ptv026

119 González-Gálvez, D., Janer, G., Vilar, G., Vílchez, A. & Vázquez-Campos, S. The Life Cycle of Engineered Nanoparticles. *Advances in experimental medicine and biology* **947**, 41-69 (2017). https://doi.org/10.1007/978-3-319-47754-1_3

120 Kopac, T. Protein corona, understanding the nanoparticle-protein interactions and future perspectives: A critical review. *International journal of biological macromolecules* **169**, 290-301 (2021). https://doi.org/10.1016/j.ijbiomac.2020.12.108

121 Pustulka, S. M., Ling, K., Pish, S. L. & Champion, J. A. Protein Nanoparticle Charge and Hydrophobicity Govern Protein Corona and Macrophage Uptake. *ACS applied materials & interfaces* **12**, 48284-48295 (2020). https://doi.org/10.1021/acsami.0c12341

122 Casals, E., Pfaller, T., Duschl, A., Oostingh, G. J. & Puntes, V. Time evolution of the nanoparticle protein corona. *ACS nano* **4**, 3623-3632 (2010). https://doi.org/10.1021/nn901372t

123 Bernhard, C., van Zadel, M. J., Bunn, A., Bonn, M. & Gonella, G. In Situ Label-Free Study of Protein Adsorption on Nanoparticles. *The journal of physical chemistry. B* **125**, 9019-9026 (2021). https://doi.org/10.1021/acs.jpcb.1c04775

124 Lundqvist, M. *et al.* Nanoparticle size and surface properties determine the protein corona with possible implications for biological impacts. *Proceedings of the National Academy of Sciences of the United States of America* **105**, 14265-14270 (2008). https://doi.org/10.1073/pnas.0805135105

125 Böhmert, L. *et al.* Isolation methods for particle protein corona complexes from protein-rich matrices. *Nanoscale Adv* **2**, 563-582 (2020). https://doi.org/10.1039/c9na00537d
126 Linares, R., Tan, S., Gounou, C., Arraud, N. & Brisson, A. R. High-speed centrifugation induces aggregation of extracellular vesicles. *Journal of extracellular vesicles* **4**, 29509 (2015). https://doi.org/10.3402/jev.v4.29509
127 García-Álvarez, R. & Vallet-Regí, M. Hard and Soft Protein Corona of Nanomaterials: Analysis and Relevance. *Nanomaterials (Basel, Switzerland)* **11** (2021). https://doi.org/10.3390/nano11040888
128 Quattrini, F., Berrecoso, G., Crecente-Campo, J. & Alonso, M. J. Asymmetric flow field-flow fractionation as a multifunctional technique for the characterization of polymeric nanocarriers. *Drug delivery and translational research* **11**, 373-395 (2021). https://doi.org/10.1007/s13346-021-00918-5
129 Chenthamara, D. *et al.* Therapeutic efficacy of nanoparticles and routes of administration. *Biomaterials research* **23**, 20 (2019). https://doi.org/10.1186/s40824-019-0166-x
130 Ferrari, R., Sponchioni, M., Morbidelli, M. & Moscatelli, D. Polymer nanoparticles for the intravenous delivery of anticancer drugs: the checkpoints on the road from the synthesis to clinical translation. *Nanoscale* **10**, 22701-22719 (2018). https://doi.org/10.1039/c8nr05933k
131 Dell'Orco, D., Lundqvist, M., Oslakovic, C., Cedervall, T. & Linse, S. Modeling the time evolution of the nanoparticle-protein corona in a body fluid. *PLoS One* **5**, e10949 (2010). https://doi.org/10.1371/journal.pone.0010949
132 Chinen, A. B., Guan, C. M., Ko, C. H. & Mirkin, C. A. The Impact of Protein Corona Formation on the Macrophage Cellular Uptake and Biodistribution of Spherical Nucleic Acids. *Small (Weinheim an der Bergstrasse, Germany)* **13** (2017). https://doi.org/10.1002/smll.201603847
133 Syed, Y. Y. Nonacog Beta Pegol: A Review in Haemophilia B. *Drugs* **77**, 2003-2012 (2017). https://doi.org/10.1007/s40265-017-0836-8
134 Namiot, E. D., Sokolov, A. V., Chubarev, V. N., Tarasov, V. V. & Schiöth, H. B. Nanoparticles in Clinical Trials: Analysis of Clinical Trials, FDA Approvals and Use for COVID-19 Vaccines. *Int J Mol Sci* **24** (2023). https://doi.org/10.3390/ijms24010787
135 Kamaly, N., Yameen, B., Wu, J. & Farokhzad, O. C. Degradable Controlled-Release Polymers and Polymeric Nanoparticles: Mechanisms of Controlling Drug Release. *Chemical Reviews* **116**, 2602-2663 (2016). https://doi.org/10.1021/acs.chemrev.5b00346
136 Elmowafy, M. *et al.* Polymeric Nanoparticles for Delivery of Natural Bioactive Agents: Recent Advances and Challenges. *Polymers* **15** (2023).
137 Zielińska, A. *et al.* Polymeric Nanoparticles: Production, Characterization, Toxicology and Ecotoxicology. *Molecules* **25** (2020). https://doi.org/10.3390/molecules25163731
138 Shan, X. *et al.* Current approaches of nanomedicines in the market and various stage of clinical translation. *Acta Pharmaceutica Sinica B* **12**, 3028-3048 (2022). https://doi.org/https://doi.org/10.1016/j.apsb.2022.02.025
139 He, H., Liu, L., Morin, E. E., Liu, M. & Schwendeman, A. Survey of Clinical Translation of Cancer Nanomedicines—Lessons Learned from Successes and Failures. *Accounts of Chemical Research* **52**, 2445-2461 (2019). https://doi.org/10.1021/acs.accounts.9b00228
140 Tian, X., Chong, Y. & Ge, C. Understanding the Nano-Bio Interactions and the Corresponding Biological Responses. *Front Chem* **8**, 446 (2020). https://doi.org/10.3389/fchem.2020.00446
141 Hua, S., de Matos, M. B. C., Metselaar, J. M. & Storm, G. Current Trends and Challenges in the Clinical Translation of Nanoparticulate Nanomedicines: Pathways for Translational Development and Commercialization. *Front Pharmacol* **9**, 790 (2018). https://doi.org/10.3389/fphar.2018.00790

142 Brennan, K. *et al.* A comparison of methods for the isolation and separation of extracellular vesicles from protein and lipid particles in human serum. *Scientific Reports* **10**, 1039 (2020). https://doi.org/10.1038/s41598-020-57497-7
143 Ali, A. *et al.* Review on Recent Progress in Magnetic Nanoparticles: Synthesis, Characterization, and Diverse Applications. *Frontiers in Chemistry* **9** (2021).
144 Tan, X. & Welsher, K. Particle-by-Particle In Situ Characterization of the Protein Corona via Real-Time 3D Single-Particle-Tracking Spectroscopy*. *Angew Chem Int Ed Engl* **60**, 22359-22367 (2021). https://doi.org/10.1002/anie.202105741
145 Hajipour, M. J. *et al.* An Overview of Nanoparticle Protein Corona Literature. *Small (Weinheim an der Bergstrasse, Germany)* **19**, e2301838 (2023). https://doi.org/10.1002/smll.202301838
146 Bertrand, N. *et al.* Mechanistic understanding of in vivo protein corona formation on polymeric nanoparticles and impact on pharmacokinetics. *Nature Communications* **8**, 777 (2017). https://doi.org/10.1038/s41467-017-00600-w
147 Ndumiso, M. *et al.* Comparative whole corona fingerprinting and protein adsorption thermodynamics of PLGA and PCL nanoparticles in human serum. *Colloids and Surfaces B: Biointerfaces* **188**, 110816 (2020). https://doi.org/https://doi.org/10.1016/j.colsurfb.2020.110816
148 Konduru, N. V. *et al.* Protein corona: implications for nanoparticle interactions with pulmonary cells. *Particle and Fibre Toxicology* **14**, 42 (2017). https://doi.org/10.1186/s12989-017-0223-3
149 Blume, J. E. *et al.* Rapid, deep and precise profiling of the plasma proteome with multi-nanoparticle protein corona. *Nature Communications* **11**, 3662 (2020). https://doi.org/10.1038/s41467-020-17033-7
150 Pourali, P., Neuhöferová, E., Dzmitruk, V. & Benson, V. Investigation of Protein Corona Formed around Biologically Produced Gold Nanoparticles. *Materials* **15** (2022).
151 Winzen, S. *et al.* Complementary analysis of the hard and soft protein corona: sample preparation critically effects corona composition. *Nanoscale* **7**, 2992-3001 (2015). https://doi.org/10.1039/C4NR05982D
152 Baimanov, D. *et al.* In situ analysis of nanoparticle soft corona and dynamic evolution. *Nat Commun* **13**, 5389 (2022). https://doi.org/10.1038/s41467-022-33044-y
153 Quattrini, F., Berrecoso, G., Crecente-Campo, J. & Alonso, M. J. Asymmetric flow field-flow fractionation as a multifunctional technique for the characterization of polymeric nanocarriers. *Drug Delivery and Translational Research* **11**, 373-395 (2021). https://doi.org/10.1007/s13346-021-00918-5
154 Bian, J., Gobalasingham, N., Purchel, A. & Lin, J. The Power of Field-Flow Fractionation in Characterization of Nanoparticles in Drug Delivery. *Molecules* **28** (2023).
155 Kammer, F. v. d., Legros, S., Hofmann, T., Larsen, E. H. & Loeschner, K. Separation and characterization of nanoparticles in complex food and environmental samples by field-flow fractionation. *TrAC Trends in Analytical Chemistry* **30**, 425-436 (2011). https://doi.org/https://doi.org/10.1016/j.trac.2010.11.012
156 Eskelin, K., Poranen, M. M. & Oksanen, H. M. Asymmetrical Flow Field-Flow Fractionation on Virus and Virus-Like Particle Applications. *Microorganisms* **7** (2019).
157 Fuentes, C. *et al.* Comparison between conventional and frit-inlet channels in separation of biopolymers by asymmetric flow field-flow fractionation. *Analyst* **144**, 4559-4568 (2019). https://doi.org/10.1039/C9AN00466A
158 Ramirez, L. M. F., Rihouey, C., Chaubet, F., Le Cerf, D. & Picton, L. Characterization of dextran particle size: How frit-inlet asymmetrical flow field-flow fractionation (FI-AF4) coupled online with dynamic light scattering (DLS) leads to enhanced size distribution. *Journal of Chromatography A* **1653**, 462404 (2021). https://doi.org/https://doi.org/10.1016/j.chroma.2021.462404
159 Bayart, C. *et al.* Comparison of SEC and AF4 analytical tools for size estimation of typhoid Vi polysaccharides. *Analytical Methods* **11**, 4851-4858 (2019). https://doi.org/10.1039/C9AY00145J

160 Ventouri, I. K., Loeber, S., Somsen, G. W., Schoenmakers, P. J. & Astefanei, A. Field-flow fractionation for molecular-interaction studies of labile and complex systems: A critical review. *Analytica Chimica Acta* **1193**, 339396 (2022). https://doi.org/https://doi.org/10.1016/j.aca.2021.339396
161 Shakiba, S. *et al.* Asymmetric flow field-flow fractionation (AF4) with fluorescence and multi-detector analysis for direct, real-time, size-resolved measurements of drug release from polymeric nanoparticles. *Journal of Controlled Release* **338**, 410-421 (2021). https://doi.org/https://doi.org/10.1016/j.jconrel.2021.08.041
162 Otte, T. *et al.* Characterization of branched ultrahigh molar mass polymers by asymmetrical flow field-flow fractionation and size exclusion chromatography. *Journal of chromatography. A* **1218**, 4257-4267 (2010).
163 Caputo, F. *et al.* Asymmetric-flow field-flow fractionation for measuring particle size, drug loading and (in)stability of nanopharmaceuticals. The joint view of European Union Nanomedicine Characterization Laboratory and National Cancer Institute - Nanotechnology Characterization Laboratory. *Journal of Chromatography A* **1635**, 461767 (2021). https://doi.org/https://doi.org/10.1016/j.chroma.2020.461767
164 Mönkäre, J. *et al.* IgG-loaded hyaluronan-based dissolving microneedles for intradermal protein delivery. *Journal of Controlled Release* **218**, 53-62 (2015). https://doi.org/https://doi.org/10.1016/j.jconrel.2015.10.002
165 Giordani, S. *et al.* Field-Flow Fractionation in Molecular Biology and Biotechnology. *Molecules* **28** (2023). https://doi.org/10.3390/molecules28176201
166 Contado, C. Field flow fractionation techniques to explore the “nano-world”. *Analytical and Bioanalytical Chemistry* **409**, 2501-2518 (2017). https://doi.org/10.1007/s00216-017-0180-6
167 Graewert, M. A. *et al.* Quantitative size-resolved characterization of mRNA nanoparticles by in-line coupling of asymmetrical-flow field-flow fractionation with small angle X-ray scattering. *Scientific Reports* **13**, 15764 (2023). https://doi.org/10.1038/s41598-023-42274-z
168 de la Calle, I., Soto-Gómez, D., Pérez-Rodríguez, P. & López-Periago, J. E. Particle Size Characterization of Sepia Ink Eumelanin Biopolymers by SEM, DLS, and AF4-MALLS: a Comparative Study. *Food Analytical Methods* **12**, 1140-1151 (2019). https://doi.org/10.1007/s12161-019-01448-0
169 Loscalzo, J., Slayter, H., Handin, R. I. & Farber, D. Subunit structure and assembly of von Willebrand factor polymer: complementary analysis by electron microscopy and quasielastic light scattering. *Biophys J* **49**, 49-50 (1986). https://doi.org/10.1016/s0006-3495(86)83588-3
170 Baalousha, M., Kammer Fv Fau - Motelica-Heino, M., Motelica-Heino M Fau - Hilal, H. S., Hilal Hs Fau - Le Coustumer, P. & Le Coustumer, P. Size fractionation and characterization of natural colloids by flow-field flow fractionation coupled to multi-angle laser light scattering.
171
172 Daramy, K. *et al.* Nanoparticle Isolation from Biological Media for Protein Corona Analysis: The Impact of Incubation and Recovery Protocols on Nanoparticle Properties. *Journal of Pharmaceutical Sciences* (2023). https://doi.org/https://doi.org/10.1016/j.xphs.2023.12.021
173 Caputo, F. *et al.* Measuring Particle Size Distribution by Asymmetric Flow Field Flow Fractionation: A Powerful Method for the Preclinical Characterization of Lipid-Based Nanoparticles. *Molecular Pharmaceutics* **16**, 756-767 (2019). https://doi.org/10.1021/acs.molpharmaceut.8b01033
174 Chu, Z. *et al.* Unambiguous observation of shape effects on cellular fate of nanoparticles. *Scientific Reports* **4**, 4495 (2014). https://doi.org/10.1038/srep04495
175 Behzadi, S. *et al.* Cellular uptake of nanoparticles: journey inside the cell. *Chemical Society Reviews* **46**, 4218-4244 (2017). https://doi.org/10.1039/C6CS00636A
176 Mildner, R. *et al.* Improved multidetector asymmetrical-flow field-flow fractionation method for particle sizing and concentration measurements of lipid-based nanocarriers

for RNA delivery. *European Journal of Pharmaceutics and Biopharmaceutics* **163**, 252-265 (2021). https://doi.org/https://doi.org/10.1016/j.ejpb.2021.03.004
177 Hajipour, M. J. *et al.* An Overview of Nanoparticle Protein Corona Literature. *Small* **19**, 2301838 (2023). https://doi.org/https://doi.org/10.1002/smll.202301838
178 Johann, C., Elsenberg, S., Schuch, H. & Rösch, U. Instrument and Method to Determine the Electrophoretic Mobility of Nanoparticles and Proteins by Combining Electrical and Flow Field-Flow Fractionation. *Analytical Chemistry* **87**, 4292-4298 (2015). https://doi.org/10.1021/ac504712n
179 Tri, N., Caldwell, K. & Beckett, R. Development of electrical field-flow fractionation. *Analytical chemistry* **72**, 1823-1829 (2000). https://doi.org/10.1021/ac990822i
180 Meier, F. *Examining the exciting potential of electrical asymmetrical feld-fow fractionatation*, 2019).
181 Shrestha, S., Wang, B. & Dutta, P. Nanoparticle processing: Understanding and controlling aggregation. *Advances in Colloid and Interface Science* **279**, 102162 (2020). https://doi.org/https://doi.org/10.1016/j.cis.2020.102162
182 Kopac, T. Protein corona, understanding the nanoparticle–protein interactions and future perspectives: A critical review. *International Journal of Biological Macromolecules* **169**, 290-301 (2021). https://doi.org/https://doi.org/10.1016/j.ijbiomac.2020.12.108
183 Choi, J., Fuentes, C., Fransson, J., Wahlgren, M. & Nilsson, L. Separation and zeta-potential determination of proteins and their oligomers using electrical asymmetrical flow field-flow fractionation (EAF4). *Journal of Chromatography A* **1633**, 461625 (2020). https://doi.org/https://doi.org/10.1016/j.chroma.2020.461625
184 Drexel, R. *et al.* Fast and Purification-Free Characterization of Bio-Nanoparticles in Biological Media by Electrical Asymmetrical Flow Field-Flow Fractionation Hyphenated with Multi-Angle Light Scattering and Nanoparticle Tracking Analysis Detection. *Molecules* **25**, 4703 (2020).
185 Shallan, A., Guijt, R. & Breadmore, M. in *Encyclopedia of Forensic Sciences (Second Edition)* (eds Jay A. Siegel, Pekka J. Saukko, & Max M. Houck) 549-559 (Academic Press, 2013).
186 Sze, A., Erickson, D., Ren, L. & Li, D. Zeta-potential measurement using the Smoluchowski equation and the slope of the current–time relationship in electroosmotic flow. *Journal of Colloid and Interface Science* **261**, 402-410 (2003). https://doi.org/https://doi.org/10.1016/S0021-9797(03)00142-5
187 Fernández-Trujillo, S. *et al.* Electrical asymmetric-flow field-flow fractionation with a multi-detector array platform for the characterization of metallic nanoparticles with different coatings. *Analytical and bioanalytical chemistry* **415**, 2113-2120 (2023). https://doi.org/10.1007/s00216-022-04506-5
188 Choi, J., Fuentes, C., Fransson, J., Wahlgren, M. & Nilsson, L. Separation and zeta-potential determination of proteins and their oligomers using electrical asymmetrical flow field-flow fractionation (EAF4). *J Chromatogr A* **1633**, 461625 (2020). https://doi.org/10.1016/j.chroma.2020.461625
189 Velimirovic, M. *et al.* Characterization of Gold Nanorods Conjugated with Synthetic Glycopolymers Using an Analytical Approach Based on spICP-SFMS and EAF4-MALS. *Nanomaterials (Basel)* **11** (2021). https://doi.org/10.3390/nano11102720
190 Panalytical, M. *NanoSight Pro*, <https://www.malvernpanalytical.com/en/products/product-range/nanosight-range/nanosight-pro?utm_source=google&utm_medium=cpc&utm_campaign=EN%20-%20WESEU%20-%20Search%20-%20Experiment&utm_term=nanosight%20pro&utm_content=EN%20-%20Product%20-%20NanoSight%20Pro&gad_source=1&gclid=CjwKCAjwgdayBhBQEiwAXhMxtiN2tzYkpThdE5s0ctb8Un6FRcSCnzUsJ8c_fwL9TnU2y-HH9OO_aRoCMxwQAvD_BwE> (

191 Mildner, R. *et al.* Improved multidetector asymmetrical-flow field-flow fractionation method for particle sizing and concentration measurements of lipid-based nanocarriers for RNA delivery. *Eur J Pharm Biopharm* **163**, 252-265 (2021). https://doi.org/10.1016/j.ejpb.2021.03.004

192 Fernández-Trujillo, S. *et al.* Electrical asymmetric-flow field-flow fractionation with a multi-detector array platform for the characterization of metallic nanoparticles with different coatings. *Analytical and Bioanalytical Chemistry* **415**, 2113-2120 (2023). https://doi.org/10.1007/s00216-022-04506-5

193 Techarang, T. & Siripinyanond, A. Use of electrical field-flow fractionation for gold nanoparticles after improving separation efficiency by carrier liquid optimization. *Analytica Chimica Acta* **1144**, 102-110 (2021). https://doi.org/https://doi.org/10.1016/j.aca.2020.12.006

194 Giddings, J. C., Yang, F. J. & Myers, M. N. Flow-field-flow fractionation: a versatile new separation method. *Science (New York, N.Y.)* **193**, 1244-1245 (1976). https://doi.org/10.1126/science.959835

195 Fröhlich, E. The role of surface charge in cellular uptake and cytotoxicity of medical nanoparticles. *International journal of nanomedicine* **7**, 5577-5591 (2012). https://doi.org/10.2147/ijn.S36111

196 Rasmussen, M. K., Pedersen, J. N. & Marie, R. Size and surface charge characterization of nanoparticles with a salt gradient. *Nature Communications* **11**, 2337 (2020). https://doi.org/10.1038/s41467-020-15889-3

197 Aliyandi, A., Reker-Smit, C., Bron, R., Zuhorn, I. S. & Salvati, A. Correlating Corona Composition and Cell Uptake to Identify Proteins Affecting Nanoparticle Entry into Endothelial Cells. *ACS Biomater Sci Eng* **7**, 5573-5584 (2021). https://doi.org/10.1021/acsbiomaterials.1c00804